SURFACE CONDITIONS IN GAS ABSORPTION

An experimental and theoretical study of the effect of surface active materials on the absorption of a gas in films of liquid flowing over the outside of a solid sphere

by

GORDON STEWART, B.Sc.

Thesis presented for the degree of
Doctor of Philosophy

UNIVERSITY of EDINBURGH

August 1962

Contents

SUMMARY

An apparatus is described with which it is possible to measure the rate of absorption of carbon dioxide into a film of liquid flowing over the outside of a solid sphere. Measurements are reported of the absorption rate to films of water and aqueous solutions of Lissapol and n-Hexanol flowing over all or part of the sphere and the effect of the concentration of these surfactants on the absorption rate is examined. The stagnant layer end effect obtained with films of tap water or of aqueous Hexanol is examined in detail with respect to its effect on the hydrodynamics and gas absorption behaviour of a hemispherical falling film. It is found that the type of end effect obtained with Lissapol solutions is different to that with tap water or Hexanol solutions.

The apparatus is modified to allow measurement with a micrometer of the thickness of the liquid film at various points on the sphere and results are reported for films of water and aqueous solutions of the surfactants. The film thickness of Lissapol solutions is found to be greater than the theoretical prediction over a range of latitude on the sphere and an explanation for this is advanced on the basis of the surface ageing of the solution. Assuming that surface shear is produced by surface tension gradients on the film a modified velocity profile is derived. Dynamic surface tension values for Lissapol solutions are calculated from this profile and the film thickness measurements. Some simple measurements of the times of exposure of the liquid film are reported and are close to the predictions of the modified velocity profile.

The effect of the altered velocity profile on the gas absorption is analysed theoretically and the predictions are shown to be in reasonable agreement with the experimental results for the effect of Lissapol concentration on the absorption rate. The results and conclusions from the work are compared with the results of other workers and the theory developed here is shown to be in sympathy with most of the published work.

CHAPTER I

INTRODUCTION

Research in the Field of Gas Absorption.

Although gas absorption is an old and familiar chemical engineering operation a considerable amount of research is being conducted in this field. In general this research can be divided into three broad sections, viz. -

Fundamental research into the mechanism of mass transfer between gas and liquid.

Evaluation of Diffusion Coefficients and Solubilities.

Applied research involving the application of fundamental concepts to industrial systems.

The present research is essentially concerned with the mechanism involved in gas-liquid transfer in the hope that better understanding of this will assist the development of laboratory models of industrial absorbers. Probably the most common type of laboratory model employed to study gas-liquid mass transfer has been the wetted-wall column although in recent years several other methods of contacting liquid and gas have been used. Ever since Higbie (32) pointed out the importance of gas-liquid contact time in the absorption process as carried out in packed columns for example, the tendency has been for laboratory apparatus to approximate more closely to the type of contacter encountered in practice. Higbie's method consisted of releasing bubbles of gas into a narrow tube so that, in effect, the method of contacting approximated to a short wetted wall column and many more recent investigations have been carried out using short wetted wall columns in which contact times less than one second can be obtained (e.g. 22, 36, 50). The main difficulty encountered with such short columns is the significance of end effects relative to the total absorption obtained. An examination of these end effects occupies part of the present work.

Short contact times between liquid and gas have also been achieved using a liquid jet although special precautions must be taken to avoid entry and end effects (e.g. 10, 43, 46). Using specially designed nozzles Scriven and Pigford (46) obtained a jet with a flat velocity profile which considerably simplifies the mathematical analysis of the liquid side diffusion and by taking careful precautions with the collection of the jet liquid they were able to carry out some accurate measurements of gas absorption rates.

In addition to shortening the contact time between gas and liquid, industrial apparatus can be more closely simulated by exposing the liquid to the gas for a series of short

times, as occurs in a packed column. Danckwerts and Kennedy (14) attempted this with their rotating drum apparatus with which films of liquid were exposed for short times on the surface of a rotating cylinder half immersed in the liquid and half exposed to the gas. Again, however, end effects are extremely difficult to analyse. Stephens and Morris (47) used a column of discs over which liquid flowed being mixed at the junctions of the discs. The main difficulty encountered appears to be in achieving even distribution of the liquid over the discs. This difficulty is partly eliminated in the case of columns of spheres as used by Lynn et al (37) and by Davidson et al (16) in which liquid is allowed to flow over a series of table tennis balls. Besides exposing the liquid to the gas for a series of short times, the disc and the sphere columns approximate more closely in geometry to columns of packing pieces. In the present work the single sphere with contact times of the order of one to two seconds has been used for reasons to be discussed later. The importance of contact time when surface active agents are present in the liquid is revealed by the experimental measurements made on the system.

Theoretical analysis of gas absorption generally involves splitting the total resistance to transfer into individual resistances viz. the gas-side, the liquid-side and the interfacial resistance about which there has been some controversy. In the present case the gas-side resistance is removed by using a pure gas although even in this case there is a small resistance due to the presence of the vapour of the absorbing liquid. The liquid side resistance is evaluated by mathematical analysis of the diffusion away from the surface assuming saturation of the interface. This is not strictly correct since there must always be a small interfacial resistance due to the finite rate at which molecules strike the liquid surface. However at normal pressures this is completely negligible compared to the diffusive resistance within the liquid phase so that the interface can be assumed saturated with gas. However many cases in which total resistances have been found to be higher than those predicted theoretically have been explained by assuming a departure from saturation at the interface i.e. by postulating some significant interfacial resistance. As a result, the effect of interfacial conditions on mass transfer between phases has become a topic of considerable interest and a number of important surface phenomena have come to light. A few of these will be discussed in the next section.

Surface Conditions and Interfacial Resistance in Gas Absorption.

The importance of surfaces in chemical engineering generally has been well reviewed in a paper by Davies (17) in which the effect of interfacial phenomena in a number of

unit operations is discussed. In gas absorption the important surface effects so far studied include rippling, interfacial contamination and interfacial resistance, all of which have a direct bearing on the present work and must be studied in some detail.

It is well established that the presence of rippling in a falling film greatly enhances gas absorption to the film but no satisfactory analysis of this improvement in transfer exists. Explanations have been put forward on the basis of increased interfacial area in the rippling film, of increased turbulence in the important surface layers and it has been suggested that the velocity profile is considerably altered in the rippling regime. However, although there have been several examinations of the fluid mechanics of rippling (4, 5, 21, 48), there exists no theoretical analysis of absorption into a rippling film and consequently fundamental experimental investigations into the mechanism of gas absorption must, in general, be carried out under ripple free conditions. In the case of wetted-wall, or sphere columns using pure liquids, the experimenter is restricted to low flow rates or to very short lengths of column if rippling is to be avoided. However it has been found that the addition to water of small amounts of wetting agents successfully eliminates rippling in falling films (12, 13, 15, 16, 22, 48) and this has frequently been the course adopted in gas absorption work. Unfortunately this has led to some confusion in establishing whether interfacial resistance is significant in commonly occurring systems since the resistance could be due, in such cases, to the presence of the wetting agents. Consequently a considerable amount of research has been directed at examination of the effect of surface active agents on mass transfer and a few of the investigations which have a direct bearing on the present work are discussed below.

It has been noted that small quantities of surface active agents considerably reduce mass transfer from liquid droplets or gas bubbles and this has been attributed to the inhibition of circulation within drops or bubbles as a result of poor transfer of shear across an interface contaminated with surface active molecules. However, Garner and Skelland (25), in an examination of transfer from drops in liquid-liquid extraction, found that, in a particular range of surface active agent concentration, the mass transfer rate fell below that for solid spheres in liquid. Consequently they postulated that a surface active film introduces a barrier to absorption. In subsequent work on liquid-liquid transfer it has been found to be extremely difficult completely to remove small quantities of stray surface active material. Also, even although the bulk concentration of the agents may be very small, their effect can be comparatively large when the molecules accummulate at the interface.

In the case of gas absorption in falling films the influence of stray surface active agents is not so marked since the transfer of shear across the interface is not an important effect in promoting mass transfer. However stray materials can introduce a considerable end effect at the point where a falling film or jet enters a pool of liquid. This topic will be examined more thoroughly later as a consequence of experimental results. On the other hand, in the case in which surface active agents are added to the absorbing liquid, it appears that the presence of these agents can introduce a resistance to gas absorption.

Emmert and Pigford (22) used Petrowet to eliminate rippling in a wetted wall column and found that the mass transfer was at a minimum at 0.3% (weight) of the wetting agent. They suggest that this is due to the fact that there exists an optimum concentration for the elimination of rippling but they go on to show that, in a short wetted-wall column in which no rippling exists even in the absence of Petrowet, there is an 11% decrease in the transfer when Petrowet is present. They claim that the agent introduces a barrier to absorption but end effects of the type encountered in the present work with Lissapol were probably important in the short column. Ternovskaya and Belopolskii (49), also using a wetted-wall column, examined the effect of three surface active agents on the absorption of sulphur dioxide in water. Two of the agents showed a minimum in the curve of absorption (at a fixed flow rate) versus surface active agent concentration whereas in the third case the absorption decreased continuously as the concentration of the agent was increased up to 0.5 wt.%. These workers also examined the systems CO_2/H_2O and NH_3/H_2O and found that surface active agents affect the former but not the latter. They conclude that the agents have an effect on the hydrodynamics of the liquid film and can consequently have little effect on a gas film controlled absorption such as ammonia in water. As a result, they also suggest that the effect of surface active agents can be used to differentiate between gas-film and liquid-film controlled absorptions.

Cullen and Davidson (12) carried out an extensive examination of the effect of agents such as Lissapol, Teepol, Petrowet, Sodium dodecyl sulphate on the absorption of CO_2 in water flowing over a sphere. They report that, in the cases of Lissapol, Teepol and slightly impure sodium dodecyl sulphate, the curve of absorption versus concentration of the agent passes through a minimum at low concentrations and thereafter returns to the theoretically predicted rate. In the case of carefully purified sodium dodecyl sulphate however the concentration of the agent appears to have no effect on the absorption. They point out that the region of depressed absorption corresponds with the region of changing surface tension and conductivity and that the presence of impurities in the agent appears to be the cause of resistance

to gas absorption. Cullen and Davidson mention possible effects on the surface viscosity and diffusivity but some experiments on the motion of small particles showed that there was little relation between increased surface viscosity and reduced mass transfer.

In their work on absorption of carbon dioxide into a liquid jet, Scriven and Pigford (46) conclude that "phase equilibrium prevails at freshly formed, relatively clean interfaces between water and slightly soluble gases". Their work goes a long way towards answering the question of whether the interface can be assumed saturated, a matter first doubted by Higbie (32). The measurements of other workers agree with the conclusions of Scriven and Pigford.

On the other hand Scriven and Pigford (46) in an analysis of the effect of surface active agents mention the considerable end effect which can be produced. The influence of the agents apart from the end effect they sum up as follows "The action probably depends upon the rate at which they diffuse from the bulk liquid to freshly formed surfaces, the properties of the absorbed film they form on the surface and possibly interaction between them and the solute molecules". The effect of the rate at which the agents diffuse to the surface will be discussed more fully later in the light of experimental work.

In all the cases mentioned above in which the resistance to absorption introduced by surface active agents has been measured, the liquid and gas have moved relative to one another. The effect of the agents on absorption of CO_2 into a quiescent liquid has been studied by Harvey and Smith (31) who find that, at concentrations of Lissapol and Teepol of the same order as those used by Cullen and Davidson, there exists in their system an interfacial resistance of the same order as that in the moving systems. This indicates that the resistance is due to the adsorbed layer rather than to any effect the agents have on the hydrodynamics of the system. However this does not explain why, in several of the cases mentioned earlier, the absorption goes through a minimum and even returns to the theoretical at higher concentrations of the agent.

Up to the present time there has been no satisfactory explanation of the effects produced by surface active agents and the present work was undertaken with the hope that some of the phenomena discussed above might be explained.

CHAPTER II

THE DEVELOPMENT of the EXPERIMENTAL PROGRAMME

It was felt that any study of the surface effects produced by surface active agents must be concerned with investigations of both the absorption characteristics and the fluid mechanics of the system involved. Consequently the experimental set-up was chosen with these considerations in mind.

The Choice of the Method of Gas-Liquid Contacting.

As has already been mentioned much of the fundamental work on gas-liquid mass transfer has been carried out using wetted-wall columns of various lengths and diameters. More recently Lynn et al (37) and Davidson and Cullen (15) have used wetted spheres both singly and in columns partly in an attempt to simulate more exactly the conditions in a packed column but also because of certain advantages which the single wetted sphere has over other systems, viz.

(1) The system is compact giving a large area of film in a small volume of space.

(2) The entry and end effects involved in gas absorption are reduced to a very small proportion of the total absorption partly because of the smallness of the radii at inlet and outlet.

To illustrate these points a 3" diameter sphere supported on a $\frac{3}{8}$" diameter rod (as used in the present work) is equivalent for gas absorption purposes, to a wetted wall column $41\frac{1}{2}$" long x $\frac{3}{8}$" diameter (Appendix IIa).

The main disadvantage encountered with the spherical system concerns the mathematical treatment of the hydrodynamics and diffusion which proves to be a little more involved than for a vertical falling film. However it was felt that the advantages to be gained from the spherical set-up were sufficient to outweigh this especially in the light of the good agreement obtained between theory and experiment by other workers and this was the system of gas-liquid contacting eventually chosen.

The Gas-Liquid System.

The choice of a gas-liquid system for examination of the mechanism of gas absorption depends to a large extent upon the possibility of finding in the literature accurate values of Diffusivity and Solubility. This consideration makes the carbon dioxide/water system an attractive choice since it has been very frequently used in the past. It is a liquid-film controlled absorption, carbon dioxide is easily obtainable in a high degree of purity and water is possibly the easiest of liquids to employ. For thisreason it was decided to design the experimental set-up to suit the carbon dioxide/water system but to make it sufficiently adaptable to accommodate other gas liquid systems which could be used.

The Experimental Programme.

The experimental programme divides itself conveniently into two parts viz.

Measurement of Gas Absorption

Examination of Fluid Mechanics.

It is possible to measure the rate of absorption of carbon dioxide into water flowing over the whole sphere and over only part of the sphere so that the absorption for differing amounts of exposure could be examined. This part of the work resolved itself into an analysis of the end effects encountered at the point where the moving film is terminated. The effect of surface active agent concentration on the gas absorption is also examined in detail.

The examination of the fluid mechanics of the system is concerned mainly with the measurement of liquid film thickness which proved to be of great importance in analysing the effect of surface active agents. It was also possible to make crude measurements of the surface velocity of the film.

The Theoretical Treatment.

The theoretical analysis of the diffusion of gas into a spherical liquid film has been tackled by Davidson and Cullen (15) who make certain assumptions about the liquid flow which allow the problem to be solved in a manner similar to the solution for a vertical falling film. The basic assumption is that at all points in the film the streamlines are parallel to the solid surface when in fact on the upper half they converge radially and diverge circumferentially while on the lower half the procedure is exactly reversed.

However the analysis, given in outline in Appendix I, leads to the following results.

(1) For small depths of penetration

$$G = 4.49 \left(\frac{2\pi\rho g}{3\mu}\right)^{1/6} D^{\frac{1}{2}} R^{7/6} L^{\frac{1}{3}} (C_i - C_o)$$

(2) For large depths of penetration

$$G = LC_i \sqrt{1 - 0.7857 \exp(-3.414p) - 0.1001 \exp(-26.21p) - 0.03599 \exp(-70.43p) - 0.01811 \exp(-136.5p) \ldots}$$

$$\text{where } p = 3.36 \left(\frac{2\pi\rho g}{\mu}\right)^{\frac{1}{3}} \frac{DR^{7/3}}{L^{4/3}}$$

By direct comparison of the differential equations for the absorption to a vertical and a spherical falling film it can be shown that a spherical film is equivalent to a wetted wall column of the same radius and of a length 1.68 times the radius.

To calculate the absorption for the complete experimental system, which consists of a sphere plus a short supporting length of wetted-wall column, the degree of mixing at the junction of the sphere and the off-take must be known. The two extremes of no-mixing and complete mixing of the film can normally be considered. The complete mathematical analysis of the absorption for the sphere and the off-take with and without mixing (Appendix II) and for various amounts of exposure (Appendix VI) are to be found in the Appendices. A few typical values are quoted here since an approximate knowledge of the absorption rate was required in the design of the experimental set-up which is considered in the next chapter.

Flow Rate (cc/sec)	1.00	2.00	3.00	6.00
Absorption (mg/sec)	1.116	1.436	1.652	2.094

The values of the constants used in the evaluation of the theoretical rates were as follows.

Diffusivity of CO_2 in water ($15^{\circ}C$) = 1.38×10^{-5} cm^2/sec
Solubility of CO_2 in water ($15^{\circ}C$) = 1.888 mg/sec.

The diffusivity is taken from the work of Davidson and Cullen (15) while the solubility was chosen after considering a number of values (28, 42, 43, 46). The exact value of these constants is not of great importance to this work since the results and conclusions derived therefrom depend upon relative rather than absolute values.

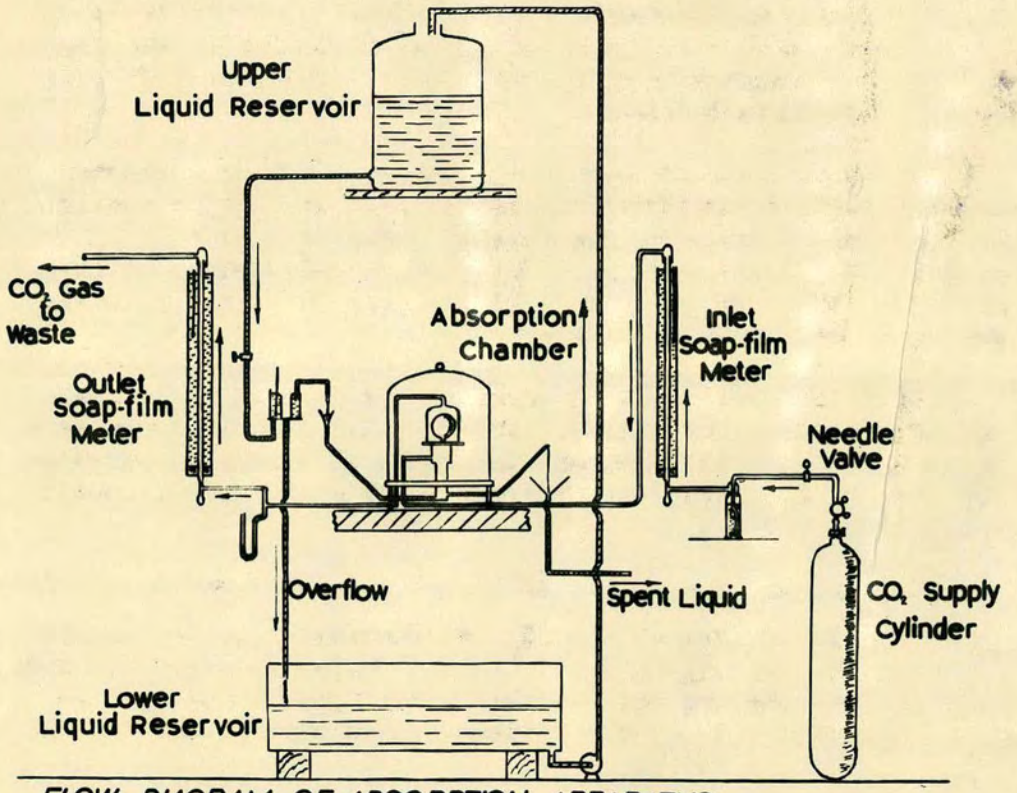

FIG. 1 FLOW DIAGRAM OF ABSORPTION APPARATUS.

CHAPTER III

EXPERIMENTAL METHODS

The Design and Construction of the Apparatus.

In their experimental work Lynn et al (37) and Davidson and Cullen (15) used table tennis balls of 1.49" diameter which are of the order of size of packing pieces and are very convenient for the construction of columns of spheres. However in this case, in which the single wetted sphere is used because of the advantages it affords, it was felt that a somewhat larger sphere would be desirable expecially since film thickness measurements were intended. A 3" diameter brass sphere was made by Ferranti Ltd. of Edinburgh and the design of the apparatus was based on the absorption rates to be anticipated with this.

Since analysis of carbon dioxide in water is a rather complicated and laborious business it was decided to measure the absorption rates by the change in volume of gas as it passed through the system. The rates of absorption being small (of the order of 1 cc/sec) the best type of flow meter proved to be a soap film meter.

Some time was spent in trying to perfect an analytical method for carbon dioxide content in water both to serve as a check on the volume measurements and to allow absorption over any amount of exposure to be measured by sampling the liquid film.

Two methods were attempted, viz.

(1) Absorption of the CO_2 (regenerated from the sample by boiling in dilute H_2SO_4) in Barium Hydroxide and estimating the CO_2 absorbed by the change in conductivity of the hydroxide (reference Noll and Polsky (39)).

(2) Absorption of the CO_2 (regenerated as before) in sofnolite, a commercial CO_2 absorbent, and estimation by weight increase.

Neither method proved satisfactory when tested on standard samples of Sodium Carbonate and the analytical method was abandoned.

The Flow Sheet of the experimental apparatus is shown in fig. 1. The carbon dioxide was supplied in 14 lb. cylinders by D.C.L. and was guaranteed to contain less than 50 p.p.m. of impurities and on average less than 100 p.p.m. of water vapour. From the cylinder the gas passes through a pressure reducing valve and a needle valve before passing into a liquid contactor in which the gas is saturated with the liquid being used in the absorption chamber. This prevents evaporation of the absorption liquid in the chamber and the consequent upset of the volume measurements. Check measurements using calcium chloride absorption tubes showed that the gas emerging from the saturator was in fact saturated with water vapour at the gas rates involved in the present work (up to 3 cc/sec).

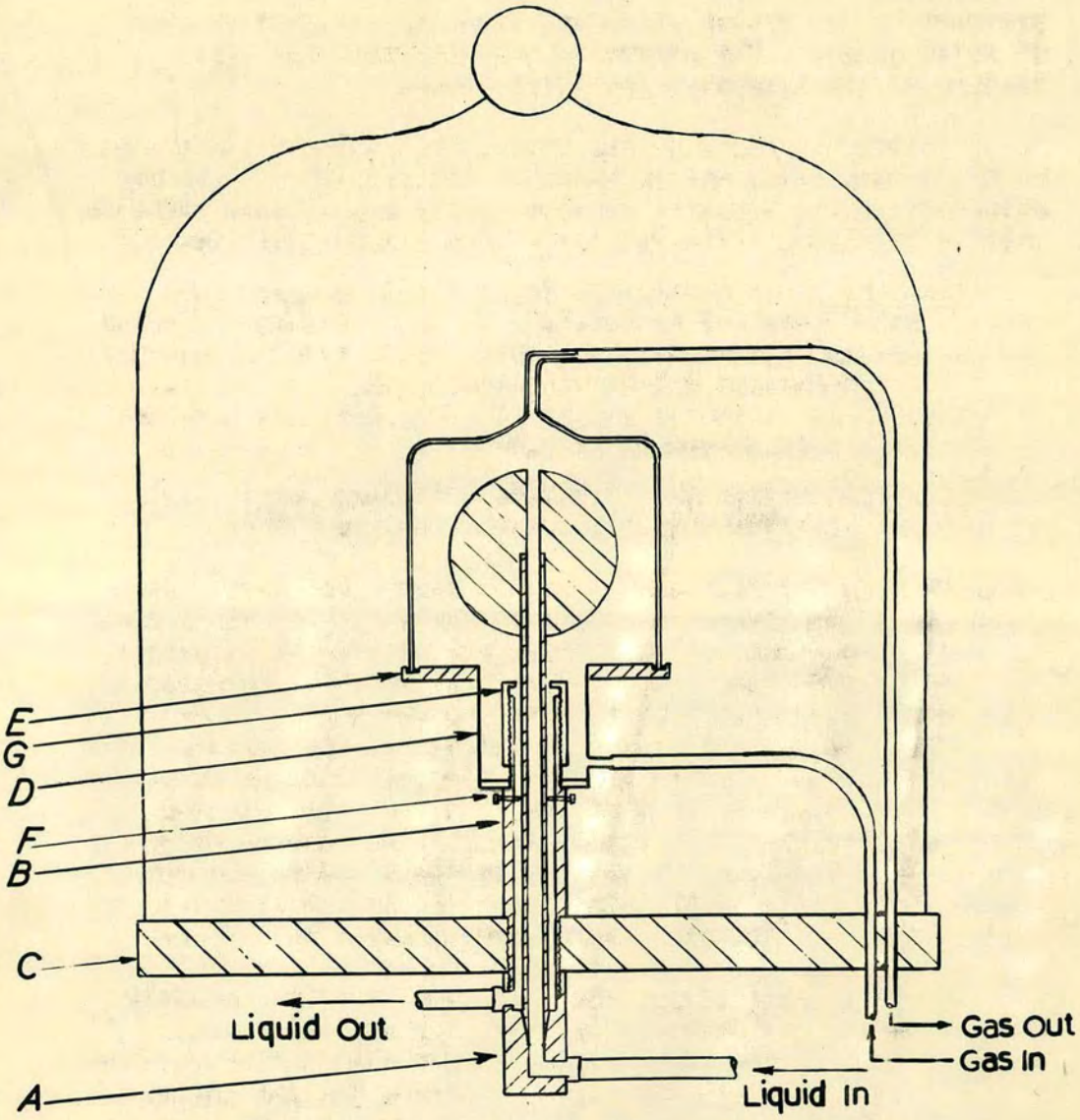

FIG.2 ABSORPTION CHAMBER.

From the saturator the gas passes through the inlet soap film meter, into the foot of the absorption chamber and out at the top, through the outlet soap film meter and off to waste. A manometer is included in the line between the chamber and the outlet meter to serve as a check on the pressure in the system which was normally not greater than $\frac{1}{4}$" water gauge. The manometer was also used for pressure testing of the apparatus to detect leaks.

The only liquid used for absorption measurements in this work has been water and no special care with its purity has been taken since normally surface active agents were added to prevent rippling. The surface active agents used were

Lissapol N - A commercial surface active agent (non-ionic) supplied by I.C.I. It is an aqueous solution of nonyl phenol ethylene oxide condensate represented by the formula $R\text{-}O\text{-}C_2H_4(\text{-}O\text{-}C_2H_4)_n\text{-}OH$. The mean molecular weight is about 638 (n = 8-9) and the specific gravity is 1.024.

n-Hexanol - Supplied by B.D.H. Boiling range - not less than 95% distills between 155 and 158°C.

The absorbing liquid, made up in the lower liquid reservoir of capacity 70 litres, is pumped to the upper reservoir from which it flows under gravity through a control valve into a constant head device, the overflow from which is returned to the lower reservoir. The flow to the absorption chamber is by syphon and gravity feed onto the top of the sphere. The liquid leaves the chamber through an overflow which is adjustable in height to control the level of liquid in the chamber. The liquid flow rate range is restricted at the lower end of the range by wetting problems and at the upper end by instability in the small crest of liquid at the entry to the sphere. The practical range is 0.5 - 7.0 cc/sec.

The Soap Film Meters each consist of a 50 ml. burette tube fitted at the foot with a glass T-piece where soap solution is injected into the gas stream when a flow measurement is required. At the top of the tube the gas leaves through a side arm while the soap solution collects in a circular trough. Both meters are jacketted with water the temperature of which is not controlled but is measured during a reading. Using a stop watch beating 1/5ths of a second flows of up to 2 cc/sec can be measured to an accuracy of 1%.

The Absorption Chamber. This is shown in fig. 2. The sphere, which Talyrond measurements show to have a diameter of 3" ± 0.002", is push fitted onto a 9" long x $\frac{3}{8}$" O.D. brass tube. Two pieces of hexagon brass tube (A and B on the figure) screw together through a central hole in the 14" diameter base plate, C. On top of this hexagonal tube is fitted a 2" length of 2" diameter copper tube (D) with a $4\frac{3}{4}$" diameter brass flange (E) braised to its upper end. The sphere, on its support, is fitted by means of a cone and socket joint into the hexagonal tube piece (A) and is steadied by the three supporting screws F. The gas atmosphere around the sphere is contained beneath a $4\frac{1}{2}$" diameter glass bell jar which fits into a trough of mercury in the brass flange.

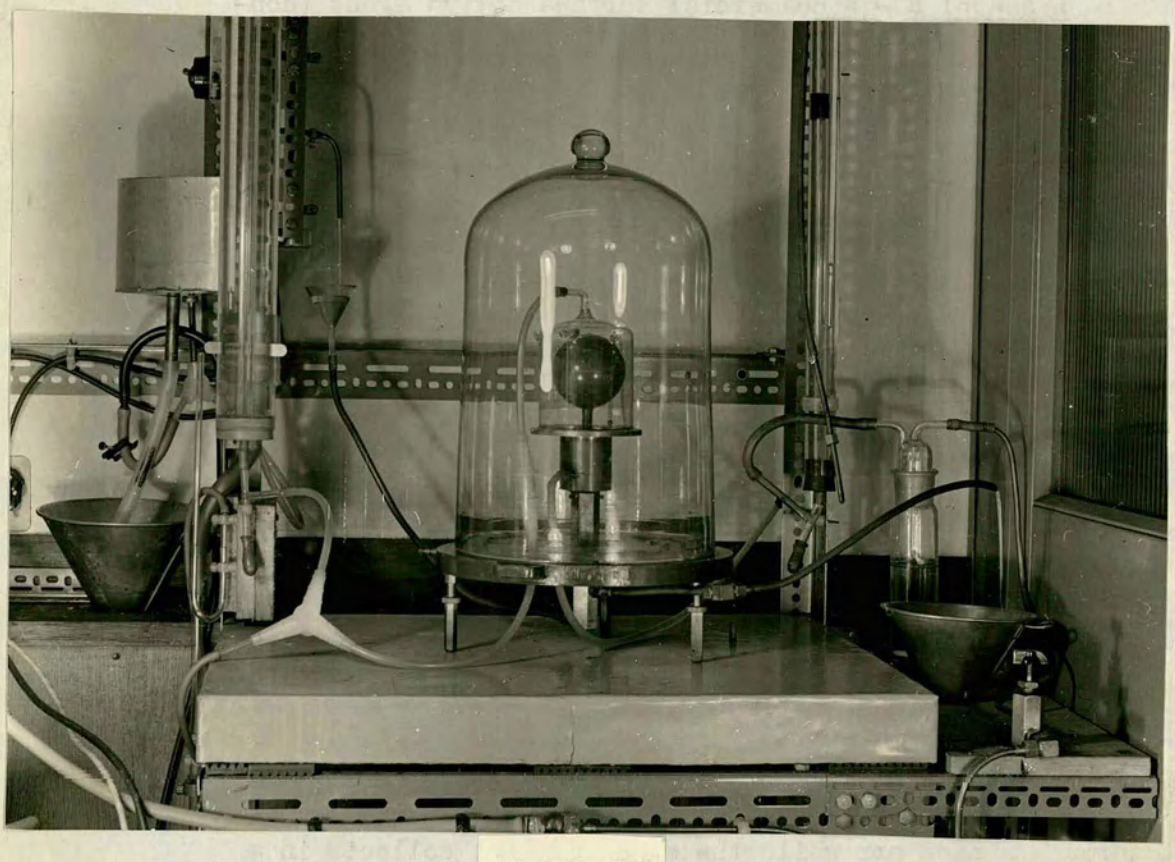

PLATE I

The length of the take-off tube beneath the sphere is made adjustable by a short length of brass tube, G, screwed onto the top of the tube B. The base plate is supported on three adjustable legs for levelling (not shown) and the chamber is shielded from draughts by a 13" diameter bell jar. In order to reduce vibrations the apparatus is sited on a concrete slab which is supported on shock absorbing rubber pads. General views of the apparatus are shown in plates I and II.

Liquid Flow through the Chamber - Liquid enters the system through copper tubing at the base of the central hexagon tube, flows upwards through the sphere support tube, over the outside of the sphere and support tube and leaves the system through the annulus between the hexagon brass and the support tube.

Some difficulty was encountered at first in achieving complete wetting of the sphere, especially with water containing no wetting agent, but gentle heating of the brass with a bunsen burner was found to improve the surface wettability perhaps by producing an oxide film or merely by burning off traces of oil and grease. Once wet the sphere was kept wet continuously, it being possible to remove it from the rest of the apparatus.

Gas Flow through the Chamber - Gas enters the system at the foot of the absorption chamber, flows upwards past the sphere and leaves through a tube at the top of the bell jar. In this way good purging of the gas space is obtained since carbon dioxide is denser than air or water vapour. Since all gas flows are small the pressure drop through the outlet tubes is small and the chamber can be taken to be at atmospheric pressure.

Methods of Measurement of Absorption.

Gas absorption measurements can be made in two ways.

(1) Inlet and outlet gas flow rates can be measured simultaneously and the temperatures of the meter jackets noted. The difference between the rates is converted to a mass flow and, assuming Henry's Law to hold over small intervals this is converted to the absorption rate at 760 m.m.

(2) When an absorption measurement is required a soap film is allowed to rise to the top of the outlet meter at which point the needle valve controlling the gas flow is closed. The soap film immediately begins to drop and its movement is timed over 50 mls. This gives an absorption rate directly and this is again converted from atmospheric pressure to 760 m.m. In order to prevent the possible penetration of air into the meter, the waste pipe for the gas is long; the rate of rise of the soap film before the measurement is kept small in order to reduce to negligible proportions the pressure change resulting from stopping the inlet flow.

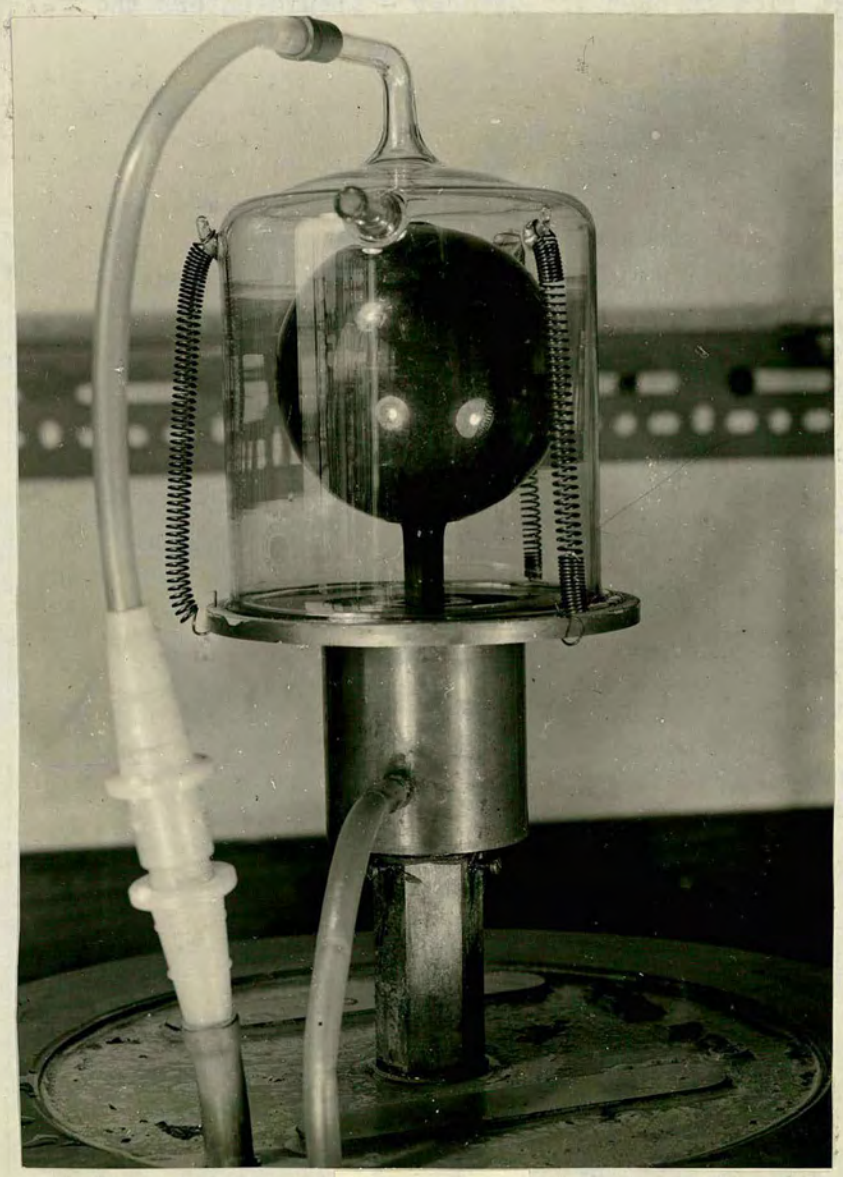

PLATE II

In the first case the pressure in the chamber is very slightly above atmospheric while in the second it is slightly below. Agreement between the results obtained by the two methods verifies that the pressure drop through the system is unimportant. Daily checks for leaks were carried out by submitting the system to a pressure of 2-3" H_2O. The gas flow rate is controlled by the needle valve close the entry to the system and the flow rate in each case is adjusted to give inlet and outlet rates which are convenient for measurement.

The liquid flow rate is measured by weighing a quantity of the chamber overflow collected over a known time interval. The flow rate is controlled by the depth of immersion of the syphon in the constant head device; the flow to the constant head device is controlled by the valve in the feed line and is adjusted to give a steady overflow. The temperature of the feed liquid is measured by a thermometer in the constant head device.

Calculation of the Results.

The volumetric absorption rate at the prevailing partial pressure of CO_2 is converted to an absorption rate in mgs/sec at a CO_2 partial pressure of 760 m.m. Hg. by the following formula.

$$G = 536.6 \left(\frac{V_i}{T_i} - \frac{V_o}{T_o}\right) \qquad \text{(Appendix III)}$$

where V_i = Inlet Volume Rate of Gas (cc/sec) T_i = Temp of Inlet Meter Jacket (^oK).
V_o = Outlet Volume Rate of Gas (cc/sec) T_o = Temp of Outlet Meter Jacket (^oK).

Two Corrections are applied to this value.

(1) The rate is converted to a standard temperature of 15°C using the factors calculated in Appendix IV which are based on the variation with temperature of the various constants involved.

(2) The rate is multiplied by a factor of 1.018 to allow for the desorption of air from the water as it enters the atmosphere of CO_2 (Appendix V).

The applicability of these corrections is in a little doubt but, since most of the conclusions to be drawn from the present work depend upon the relative values of absorption rate rate than upon absolute rates, the corrections are not of great importance.

/Note:- Using Method 2 to measure absorption the inlet flow rate is zero and the outlet flow rate is negative in the above formula./

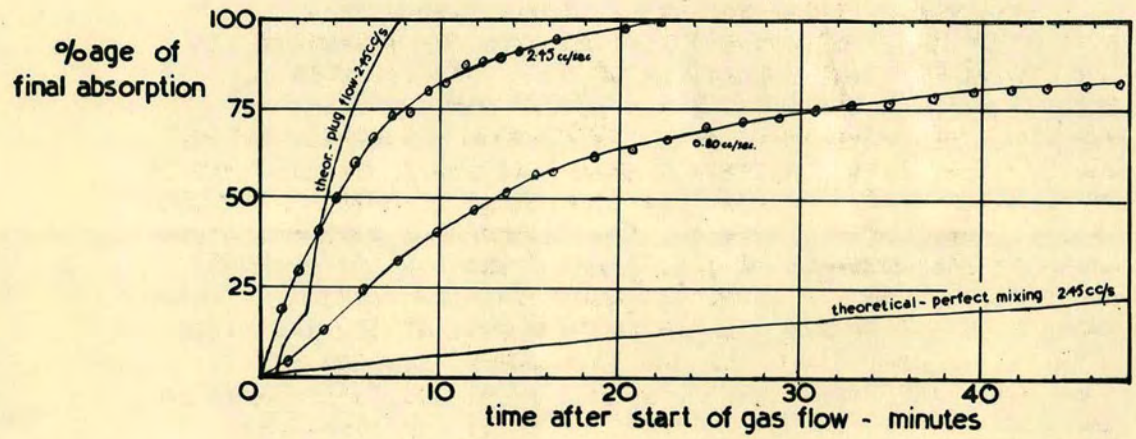

FIG. 3 START-UP MEASUREMENTS FOR TWO GAS RATES

(plot of results in table I)

Accuracy of the Measurements.

The gas absorption rates can be measured to an accuracy of 1% and before accepting any measurement timings were taken until successive values were concordant withing 1%. The liquid rate is measureable to well within 1% accuracy. The greatest source of inaccuracy in the measurements was probably the influence of stray vibrations on the liquid film despite precautions taken to prevent this. However since vibrations generally occurred in a random manner the taking of two or more readings in every case helps to reduce their effect on the general accuracy of the measurements.

Check on the Start-Up.

Some measurements were made of absorption rate versus time after starting the gas flow in order to determine the time taken to purge the system of air. With a fixed gas inflow rate measurements of the outlet rate were made at intervals of 1-2 minutes until it reached a constant value. The results for two different gas inlet rates are reported in table I and shown in fig. 3 as percentage of final absorption versus time. For comparison the theoretical start-up curves assuming the extremes of plug flow of the gas and perfect mixing of the CO_2 on entry are shown for one of the gas rates used. It can be seen that at a flow rate of 2-3 cc/sec an interval of some 25-30 minutes is required for purging. Also the experimental curve for a gas rate of 2.45 cc/sec is reasonably close to the theoretical curve for plug flow indicating that purging of the gas space is good.

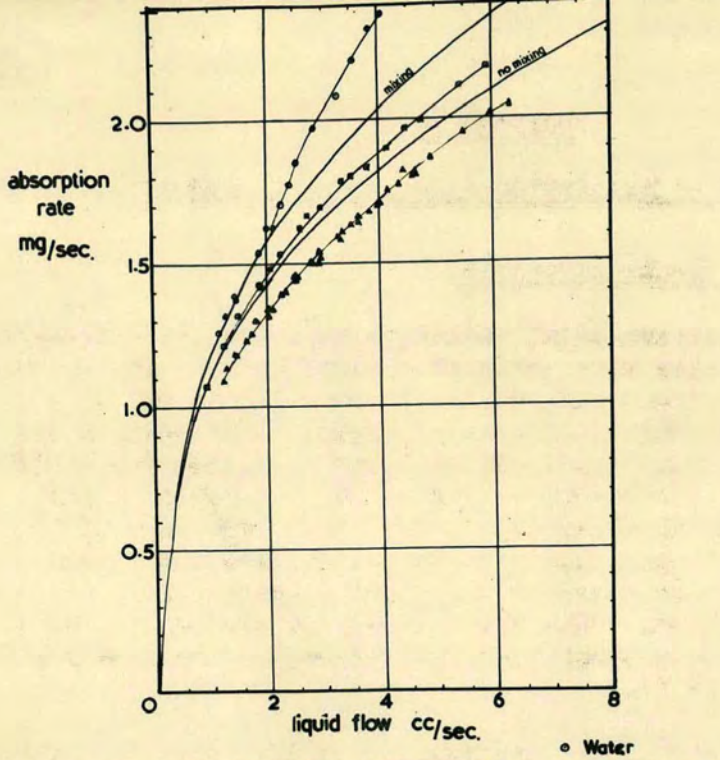

FIG. 4 WHOLE SPHERE ABSORPTION
(plot of results in table IIA,B&C)

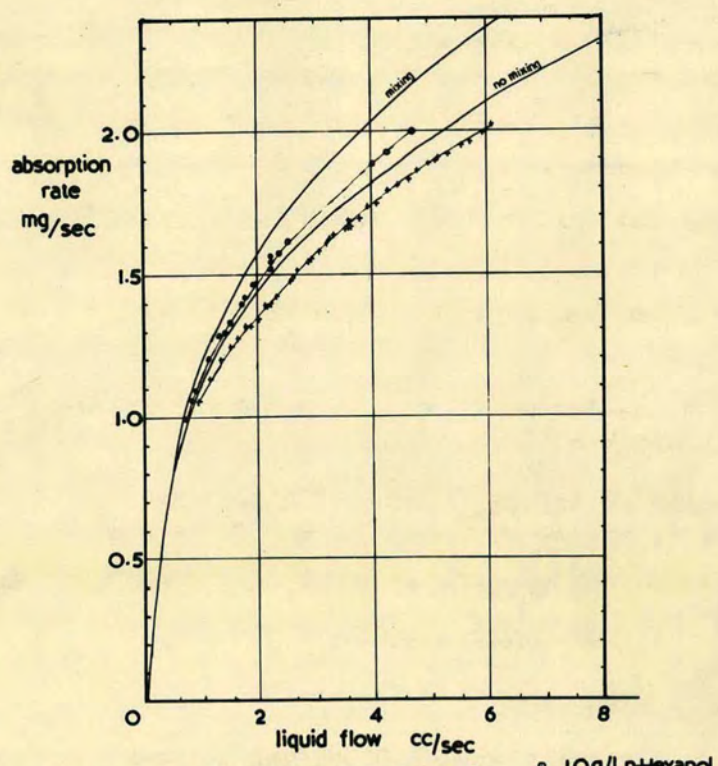

FIG. 5 WHOLE SPHERE ABSORPTION
(plot of results in table II D&E)

CHAPTER IV

RESULTS of ABSORPTION over the WHOLE SPHERE.

Explanation of the Measurements.

Using the experimental technique described in Chapter III a number of results were taken of absorption over the whole sphere plus the short take-off. In general, method 2, that of stopping the inlet flow, was employed. The results are shown in figs. 4 and 5 and are reported in tables IIA - IIE. The absorbing liquids are, as indicated, tap water, a few dilute solutions of Lissapol and one dilute solution of n-Hexanol; in each case the results have been subjected to the corrections indicated in the description of the experimental method. The two theoretical curves are for complete mixing and no-mixing; the theoretical values may be found in Appendix II.

A typical set of results from table IIC is as follows.

Flow Rate L cc/sec	Time to Absorb 50 ml t sec	Temperature °C		Measured Abspn. Rate G mgs/sec	Temp. Corrected G	Fully Corrected G	G^3
		Meter	Abspn. Liquid				
1.22	87.5	16.4	16.0	1.059	1.071	1.080	1.292

Using method (2) the time for the soap film to move 50 mls. is 87.5 sec.

The calculation proceeds $V_o = -50/87.5$ ml/sec.
$T_o = 289.6\ ^oK$

Substitution in the equation quoted above give the measured absorption G = 1.059.

From Appendix IV the factor for 16°C is 1.011
∴ Temp. corrected G = 1.059 x 1.011 = 1.071

Correcting for the desopption of air give the final value

G = 1.018 x 1.071 = 1.090.

Discussion of the Results.

At flow rates greater than 2.00 cc/sec the results for water are considerably greater than either of the theoretical predictions (fig. 4). This can be accounted for by the presence of excessive rippling at flow rates greater than 2.00 cc/sec which has frequently been associated with high rates of transfer. At flow rates below 2.00 cc/sec the results for water are close to the theoretical solution calculated on the basis of mixing at the junction.

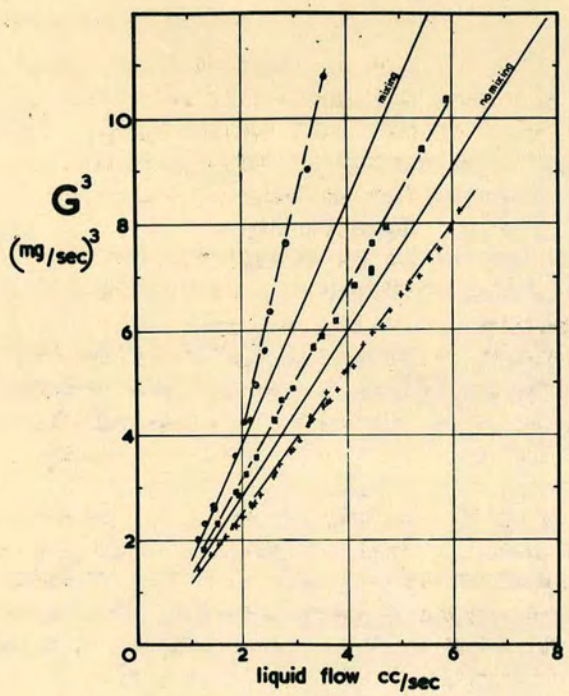

FIG. 6 ABSORPTION CUBED VERSUS FLOW RATE.
(plot of results in table II A,B&D) ○ Water □ 0.1 g/l Lissapol + 1.0 g/l Lissapol

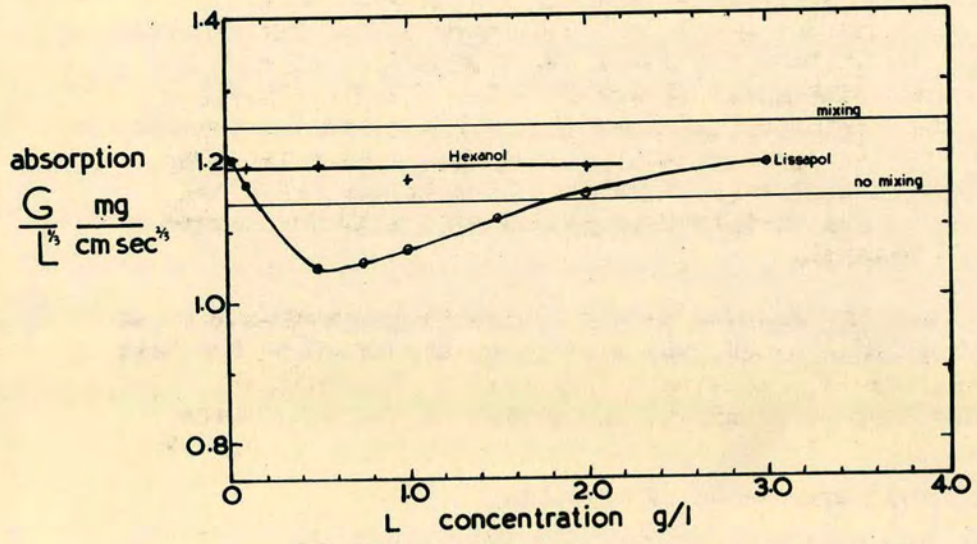

FIG. 7 WHOLE SPHERE ABSORPTION VERSUS SURFACE ACTIVE AGENT CONC. L~2.00 CC SEC
(plot of results in tables III A & B)

The Lissapol results (figs. 4 and 5) show that the mass transfer is a function of Lissapol concentration and this effect is examined more closely below. It would appear that the presence of Lissapol inhibits mixing at the junction which is in agreement with results for columns of spheres reported by Davidson et al (16). Results for one Hexanol concentration only are reported as it is shown below that the absorption is not a function of Hexanol concentration once rippling has been suppressed. The results for n-Hexanol are in reasonably close agreement with the curve for no mixing but it is not certain whether the small difference is due to some degree of mixing, to erroneous values of the constants or to the use of inapplicable correction factors.

In order to test the proportionality of G to $L^{\frac{1}{3}}$ (predicted by the solution for small depths of penetration) plots of G^3 versus L have been constructed and are shown in figure 6. These show that in general the proportionality is obeyed in the flow rate range examined and it is interesting to note that this applies even to water in the rippling regime.

The effect of Surface Active Agent Concentration on the whole sphere absorption was examined more closely by measuring the absorption rates for several different concentrations of Lissapol and of n-Hexanol. The results are reported in tables IIIA and B and shown in figure 7 where they are plotted as $G/L^{\frac{1}{3}}$ versus the s.a.a. concentration although all the values were taken at around 2.00 cc/sec.

The results show that while Hexanol appears to have no effect on the absorption Lissapol has a pronounced effect between zero and 3.0 gms/l. The minimum in the curve occurs at 0.7 g/l at which point the absorption is 13% below the value at zero concentration and 8% below the theoretical value. Extrapolating the results for low concentrations of Lissapol back to zero concentration gives a value for $G/L^{\frac{1}{3}}$ of 1.21 mgs/cm $sec^{\frac{1}{3}}$ and, while this is a little above the theoretical value of 1.127, it agrees well with the values of $G/L^{\frac{1}{3}}$ for n-Hexanol.

The results reported by previous workers, reviewed in an earlier section show effects similar to the above in the case of jets wetted-wall columns and spheres. Explanations which have been advanced for the effect of the agent have included

(1) The suppression of rippling.

(2) The suppression of mixing at a junction.

In order to account for the increase beyond the minimum these explanations require that there be an optimum concentration in one case for the elimination of rippling and in the other for the suppression of mixing. In the present case, considering the points enumerated below, neither explanation seems satisfactory.

(1) Rippling is apparently absent beyond 0.1 g/l and shows no sign of reappearing up to 4.0 g/l. The only way of observing rippling was by microscopic examination of the surface and this is capable of detecting ripples with an amplitude greater than about a thousandth of an inch.

(2) The difference between the values of absorption at 0.7 g/l and 3.0 g/l Lissapol is about 14%. An estimate of the amount of rippling required to produce this difference can be made by comparing the results for water with the theoretical curve for mixing. The difference between these curves is about 14% at a flow rate of 4.0 cc/sec and an amount of rippling similar to that for water at this flow rate was never observed at any Lissapol concentration.

(3) Hexanol appears to be as effective in suppressing ripples as the Lissapol yet it does not depress the mass transfer.

(4) The curves for both Lissapol and Hexanol extrapolate back to a similar point which is considerably lower than the point for zero concentration obtained with water. i.e. very samll amounts of agents succeed in reducing to a marked extent (possibly completely) the amount of rippling.

(5) The difference between the minimum and the extrapolated value on the experimental curve is greater than the difference between the values for mixing and for no mixing, i.e. any explanation based only on the effect of the agents on the mixing would not suffice.

These points do not exclude the possibility of a combination of the two explanations but as a result of subsequent measurements a different explanation will be put forward.

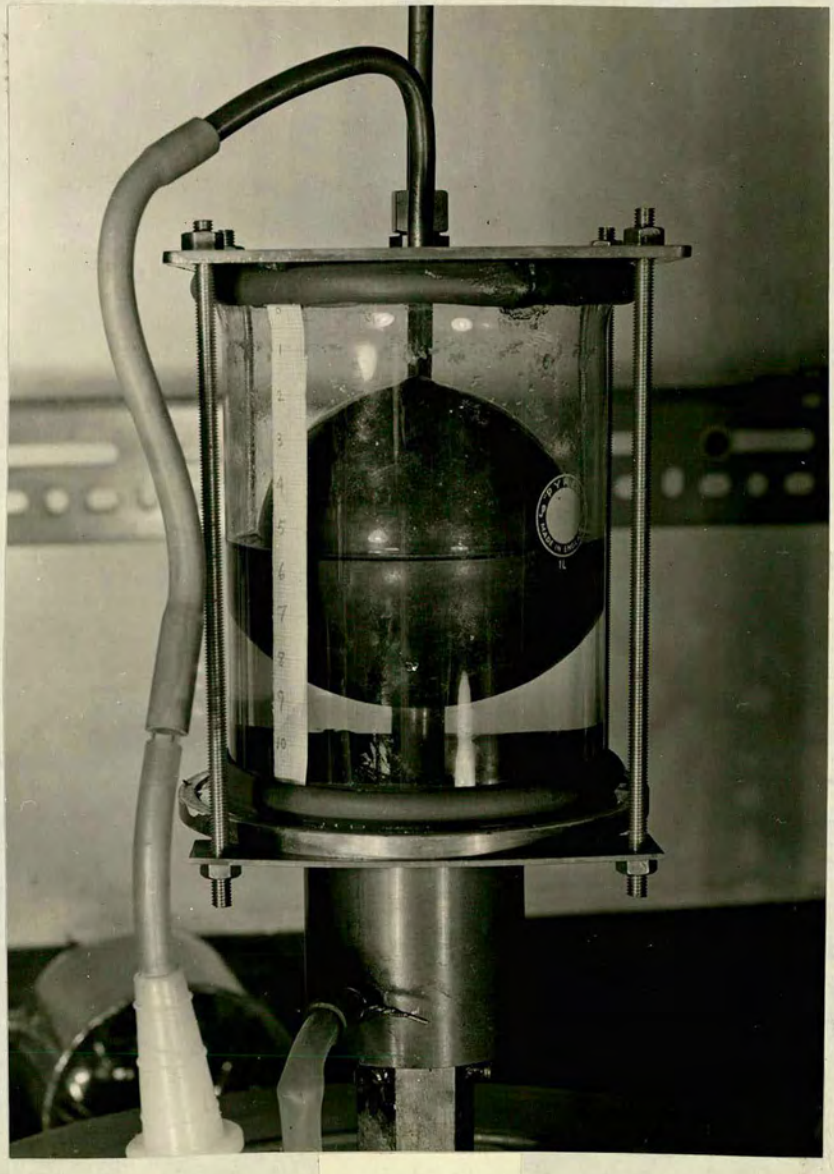

PLATE III

CHAPTER V

ABSORPTION over VARYING AMOUNTS of EXPOSURE

Having confirmed that the apparatus and experimental technique were giving reproducible results which agree with theoretical predictions and results of other workers, alterations were made to the set-up to allow measurement of the absorption rate, G, for different amounts of exposure, θ, on the sphere. It was hoped that such measurements would show whether such a G versus θ curve would follow the theoretical prediction (Appendix VI) or whether in fact the hydrodynamic differences between the top and bottom of the sphere would have an effect on the absorption. In point of fact the G versus θ measurements with water and surface active materials proved to be more interesting from the point of view of end effects produced by the presence of the surface active agents.

Alteration to Apparatus and Technique.

The alteration to the apparatus concerns only the absorption chamber itself and the new arrangement is shown in plate III. The liquid flow is unaltered apart from the fact that the chamber over-flow level is raised to bring the liquid off-take level onto the sphere itself. The gas lines and the methods of sealing had to be considerably modified however. The small glass bell jar is replaced by a glass cylinder $4\frac{1}{2}$" in diameter by $6\frac{1}{2}$" long fitted top and bottom with rubber sealing rings, made from rubber tubing split along its length, to give a good fit over the cylinder ends. This cylinder is clamped between the lower brass flange and an upper brass plate to give a good liquid seal at the foot and a gas tight seal at the top. The gas enters at the top through a copper tube with a nut and O-ring seal so that the position of the tube is easily variable. This allows the gas always to enter at the foot of the gas space thereby giving good purging, the gas exit being at the top of the chamber.

The liquid level, which is controlled by the external overflow, is measured by means of a scale fixed to the outside of the glass cylinder. Liquid flow rates are measured as before but reliable absorption measurements can be made only by the first method described in Chapter III, i.e. by measurement of inlet and outlet gas flows simultaneously. The disadvantage of the second method (i.e. closing the inlet valve) lies in the slight pressure change resulting from stopping the gas flow. This change causes the liquid level in the chamber to rise a little, and because of the larger interface involved, the slight change in the volume of the chamber takes longer to complete, for a particular flow rate, than in the case of the whole sphere absorptions where the interface at the off-take was small. The slight volume change has a pronounced effect on the volumetric gas absorption measurement and besides, the change in liquid level makes the evaluation of θ less accurate.

A further problem resulting from the alteration to the liquid off-take concerns the possibility of absorption into the off-take causing high values of absorption to be obtained. To prevent this it was proposed to cover the off-take with a liquid lighter than and immiscible with water and in which carbon dioxide is insoluble. A suitable liquid could not be found but some measurements were made with a paraffin seal. Although carbon dioxide is soluble in paraffin the thin layer (approx. $\frac{1}{8}$") of the liquid should quickly become saturated with gas, so that absorption into it would be extremely small and the water from the sphere would flow smoothly under the sealing layer. It was found that there was no significant difference between the results with and without the paraffin seal indicating that the off-take absorption was not important. Further confirmation for this was obtained from some absorption measurements made on a system (to be described in Chapter VI) which has a fixed off-take level at 90° and involves only a small off-take area. Results with this system agree well with results taken with the above set-up.

Also some dye-stream observations showed that the liquid flowing off the sphere tended to flow under the off-take liquid leaving the interface comparatively undisturbed. Thus it appears that the surface layers of the off-take liquid quickly become saturated with gas reducing the resulting absorption to negligible proportions.

Explanation of the Measurements.

Using the modified experimental technique described above, a number of results of absorption at various latitudes were taken using aqueous solutions of Lissapol. As has been shown theoretically (Appendix VI) and experimentally for whole sphere absorptions, the absorption is proportional to the cube root of the liquid flow rate. In the plotting the results for absorption over different latitudes therefore, the ratio of G to $L^{\frac{1}{3}}$ has been plotted against θ to bring points for all flow rates onto the same curve. The results are shown in figures 8 and 9 and reported in tables IVA - D and V. The corrections applied to the results are the same as in the case of the whole sphere absorptions and the calculation is carried out in a similar fashion.

Accuracy of the Measurements.

The error in measuring the absorption is slightly greater in this case since, in general, G is found by subtracting two gas rates each of which is subject to an error, but it proved possible to obtain concordancy of about 1% in every case. The measurement of the latitude θ is also subject to an error which can be large at values outside the range 20°-160° where the angular position cannot be determined to better than $\pm 3^{\circ}$. Outside the range 10°-170° the error becomes $\pm 5^{\circ}$. Inside the range 20°-160°, however, the

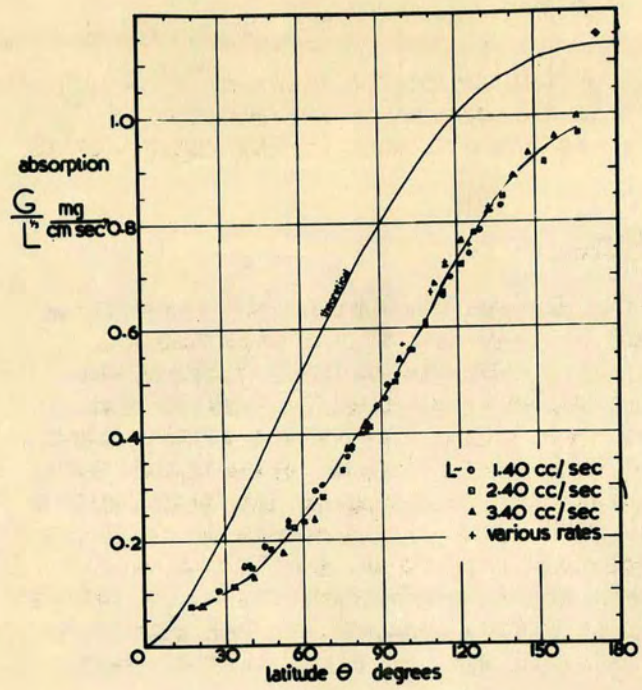

FIG 8 ABSORPTION VERSUS LATITUDE FOR 0.1 G/L LISSAPOL
(plot of results in table IVA,B,C&D)

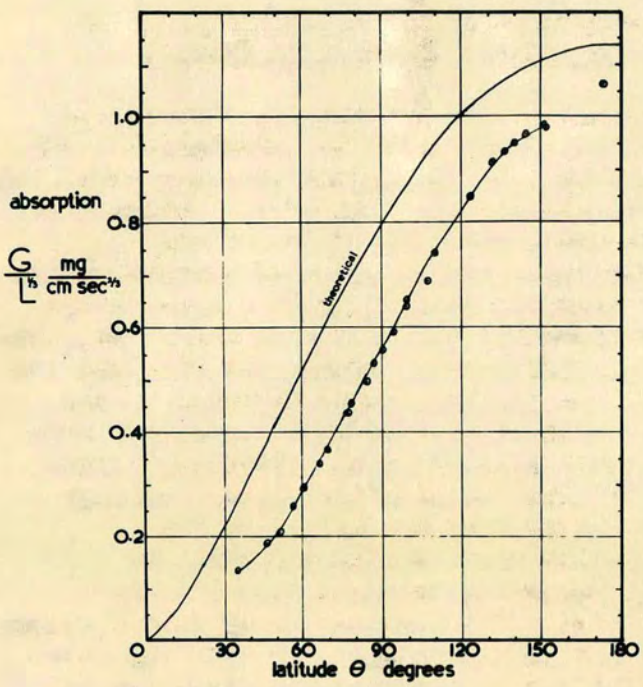

FIG 9 ABSORPTION VERSUS LATITUDE FOR 1.0 G/L LISSAPOL L~2.40 CC/SEC.
(plot of results in table V)

accuracy is better than $\pm 3^{\circ}$ while in the range 40°-140° it is better than $\pm 2^{\circ}$. This inaccuracy is reflected in a greater spread of points at the extremes of the experimental curve.

Discussion of the Results.

The most immediately obvious fact about the results is that, for all angles and in both cases, the experimental values are considerably below the theoretical prediction. However the experimental curve is similar in form to the theoretical curve apart from slight variations at the extreme ends where, as has been mentioned, angular measurement becomes less accurate. Also, at very small angles the tendency for the absorbing liquid to flow under the off-take is considerably reduced and the off-take interface is a little more distrubed. Consequently the distortion at the lower end of the curve may be due to interface absorption, the points in figure 8 indicating a value of $G/L^{\frac{1}{3}}$ of about 0.06 at zero angle.

In the case of the 0.1 g/l Lissapol the variety of flow rates explored gave results which, within reason, fall onto one curve indicating that G is proportional to $L^{\frac{1}{3}}$ as predicted theoretically.

The End Effect - An Explanation of the difference between Experimental and Theoretical Values.

The reason for the difference between experimental and theoretical results is almost certainly the considerable end effect which can exist when a moving liquid enters a relatively stagnant one. This has already been observed by workers on wetted-wall columns and jets, noteably by Cullen and Davidson (13) who showed that, when a trace of surface active agent was present, the last 1-2 cms. of their jet was stagnant. They explain this on the basis of free energy suggesting that surface tension differences between the film and the stagnant off-take cause the surface active material on the off-take to be drawn up onto the jet to form a stagnant surface layer which will reach a height such that shear forces on the underside of this layer balance the surface tension forces. The existence of such an end effect on the spherical film would cause a considerable reduction in absorption since the diffusion takes place into a fully parabolic velocity profile. The mathematics of such a system has been worked out by Ratcliffe and Reid (44) for the case of Liquid-liquid transfer but the equation can be adjusted for gas absorption. The equation and the ratio of the rates into a stagnant and non-stagnant film are quoted in Appendix IX.

In the light of this explanation of the difference between the results and the theory a further inspection of the experimental curves in figures 8 and 9 reveals some interesting information. Remembering that the stagnant layer end effect depends on the shear beneath the surface

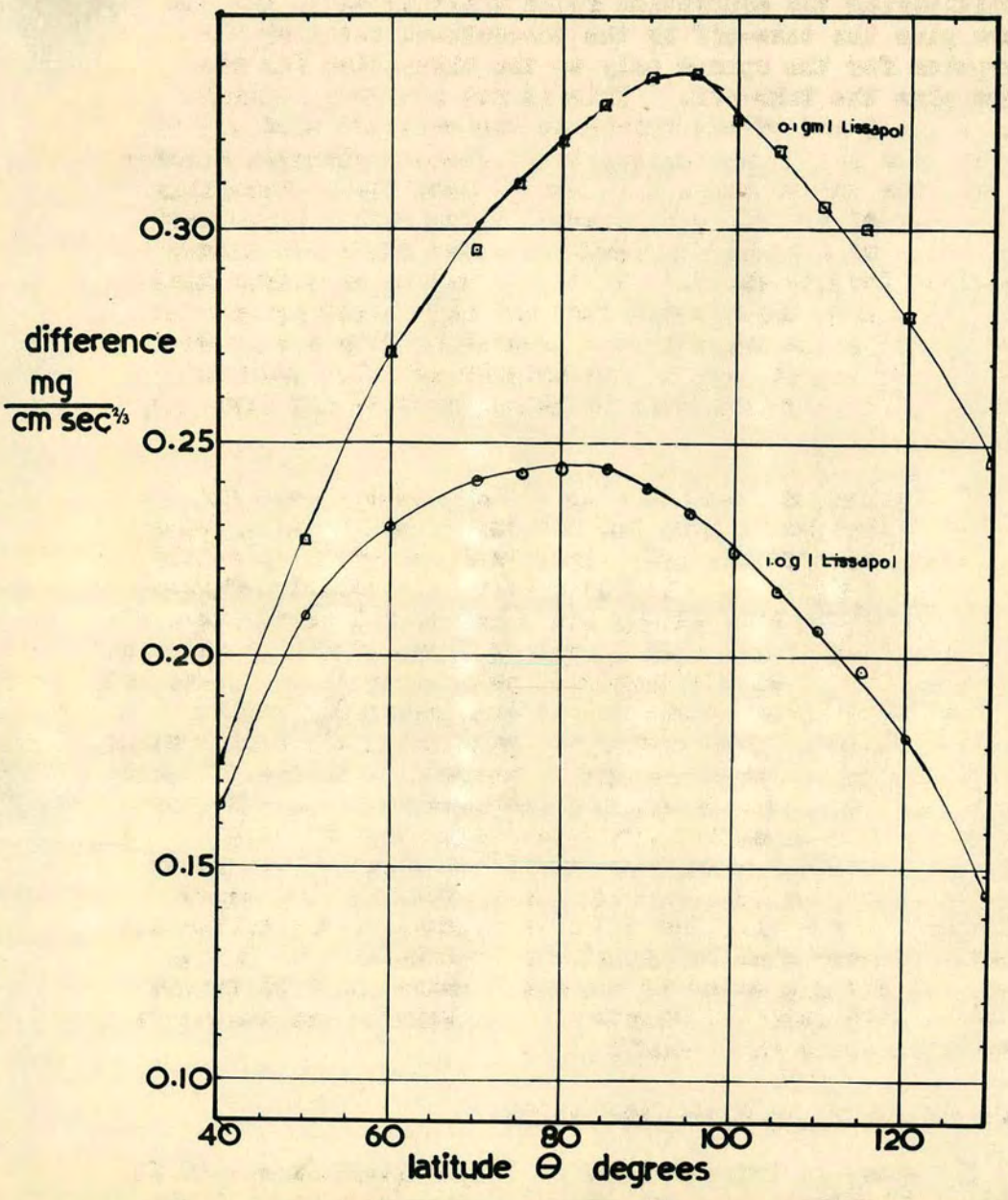

FIG. 10 DIFFERENCE BETWEEN THEORETICAL AND EXPERIMENTAL CURVES IN FIGS. 8 & 9

(plot of results in table VI)

layer, it is significant that at the junction of the sphere and the take-off tube, where there is a sudden jump in the shearing rate, there is a corresponding jump in the absorption rate. In both figures a point has been included for 173°, the end point of the sphere. This has been obtained by multiplying the absorption found experimentally for the sphere plus the take-off by the theoretical ratio of the absorption for the sphere only to the absorption for the sphere plus the take-off. This is not strictly accurate since a small end effect exists on the take-off tube but it results in a slight underestimate of the experimental absorption for the sphere only. It can be seen that, especially in the case of the 0.1 g/l Lissapol solution the experimental curve tends to a point considerably below the whole sphere absorption despite the fact that this may be an underestimate. This agrees with the concept that the high shearing rate on the take-off pulls the stagnant layer down from the sphere which is, of course, one of the properties which makes a sphere with a short take-off length attractive for absorption studies.

If the surface tension - shear balance applies, the stagnant layer should have its maximum effect at the equator (i.e. when the off-take level is just beyond 90°) where the shear is at a minimum. To put this to the test the differences between the theoretical and experimental curves were plotted against the angular position. The result is shown in figure 10. The general trend of both curves is in accord with the prediction although the maxima occur slightly earlier than anticipated. The curves are not a rigorous test however, since the off-take area and the circumference of the off-take-sphere interception also vary in the same fashion. It may be argued that the maxima are produced by the off-take absorption being at a minimum but it has already been noted that the likely maximum off-take absorption is 0.06 mg/cm sec$^{\frac{1}{3}}$ which is too small to cause the maxima in the difference curves. It may also be argued that the maxima are due to absorption being greater at the point where the film enters the off-take liquid but this seems unlikely as the amount of disturbance seems to be negligible.

Absorption over the Upper Hemisphere.

The shear on the underside of the stagnant layer, if it is indeed stagnant, is proportional to the cube root of the liquid flow rate which suggests that the height of the layer and hence the gas absorption, should depend, for any particular angle of exposure, on the liquid flow rate. However, since the results for 0.1 g/l Lissapol (fig. 8) suggest that flow rate has little effect on the $G/L^{\frac{1}{3}}$ versus θ curve, it was decided to examine more closely the effect of flow rate on $G/L^{\frac{1}{3}}$ for a fixed amount of exposure, chosen for convenience to be 90°.

Using the experimental set-up described above, measurements were made of absorption for each flow rate at two or three levels between 88° and 92° and the value for 90° found

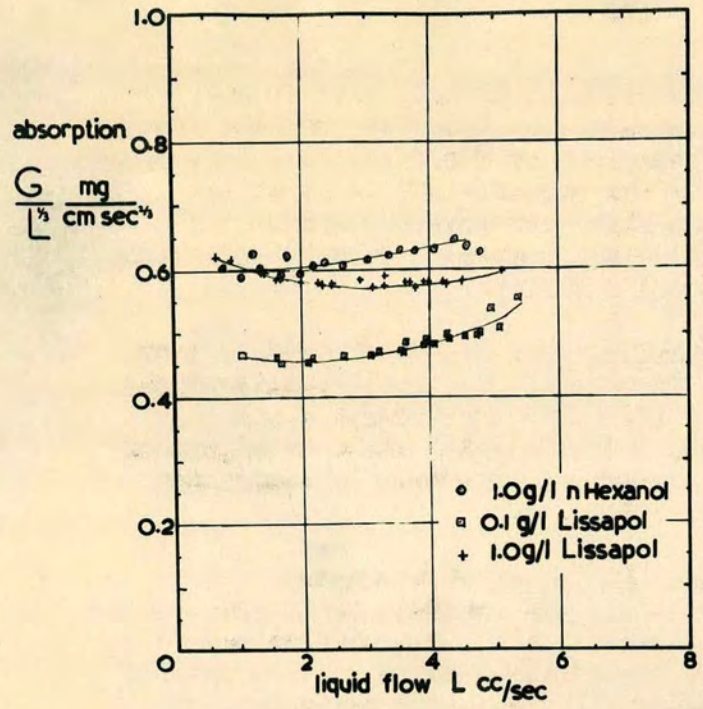

FIG. 11 EFFECT OF LIQUID FLOW RATE ON THE ABSORPTION OVER THE UPPER 90°
(plot of results in table VII A, B & C)

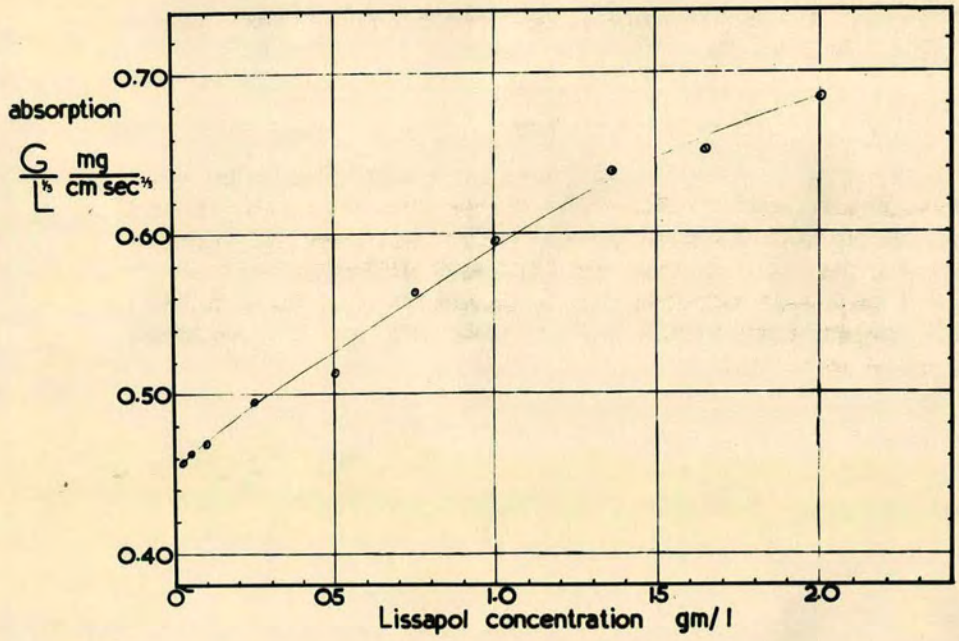

FIG. 12 EFFECT OF LISSAPOL CONCENTRATION ON ABSORPTION OVER THE UPPER 90° L ~ 2.00 CC/SEC
(plot of results in table VIII)

by interpolation. The results, shown in figure 11 and tables VII A, B and C, indicate that the flow rate has little effect on the absorbing behaviour of the film, i.e. G remains proportional to $L^{\frac{1}{3}}$ despite the presence of the layer and apparently increase in the flow rate does not affect the stagnant layer end effect to any degree. This is especially true of the 1.0 g/l Lissapol solution.

The Effect of Lissapol Concentration on the absorption over the upper hemisphere was examined for several concentrations between 0.025 g/l and 2.0 g/l using the interpolation technique described above. The results, shown in figure 12 and in table VIII, show a continual increase in absorption with rise in Lissapol concentration.

Measurements with n-Hexanol Solutions of absorption over varying amounts of exposure was not possible using the experimental arrangement for Lissapol solution because of poor purging of the gas space. n-Hexanol vapour is considerably denser than carbon dioxide and it tended to accumulate at the opposite side of the gas space to the CO_2 entry tube resulting in a steady falling off of absorption rate with time. However, using an apparatus to be described in the following section, it was possible to measure the absorption over 90° exposure purging the gas space from below as in the case of the whole sphere absorptions. The results of these measurements are shown in figure 11 and table VIIC. Although the absorption is greater than that with Lissapol solutions it still fails to reach the theoretical value ($G/L^{\frac{1}{3}} = 0.797$ at $\theta = 90^\circ$).

The evidence so far advanced for the presence of the end effect is based entirely on absorption measurements and it was felt that a closer examination of the film flow was required to elucidate further the nature of this end effect. Consequently a separate experimental investigation into film flow over the upper hemisphere was carried out and is reported in the following section.

PLATE IV

CHAPTER VI

THE STAGNANT LAYER END EFFECT

Alteration to Apparatus.

In order to examine the nature of the flow over the upper hemisphere only, minor alterations were made to the apparatus. The new arrangement isshown in plate IV. The lower half of the sphere is shielded by a 3¼" I.D. x 2" long P.V.C. tube which is supported by a short length of P.V.C. tube screwed onto the central brass tube. The liquid level is held at the top of the P.V.C. tube which is just at the equator of the sphere. With this arrangement it is possible not only to examine the liquid flow but also to measure the absorption rate over the upper hemisphere using the small glass bell jar with the mercury seal to contain the CO_2 atmosphere. These measurements of absorption to Lissapol solutions were found to agree very well with those reported in the previous section showing that off-take absorption was not a problem in the absorption/latitude measurements.

Examination of the Surface Flow.

The nature of the flow on the surface of the film can be conveniently examined using aluminium particles sprinkled onto the film close to the inlet. Using water as the feed liquid it was observed that the particles came to a sudden stop about 1-1½" from the equatorial off-take, indicating that the lower part of the film had a totally stagnant surface. This is clearly indicated in plate IV which shows the particles held on the surface of the film at a water flow rate of 2.00 cc/sec. The particles are retained for a considerable time and show no tendency to be swept towards the outlet.

Using Lissapol solutions as the feed liquid the behaviour of the particles was slightly different. They were not brought to a sudden stop above the equator but they were obviously moving with a considerably reduced velocity over the last 1-1½" of the film. It would seem therefore that, with Lissapol solutions, although the surface is not entirely stagnant, a considerable end effect exists.

The Effect of the Stagnant Zone on the Film Thickness.

At the point where the surface of the film becomes stagnant there is established the condition of total liquid shear at the surface and a fully parabolic velocity profile will develop. Under this condition the film must thicken in order to accommodate the same flow rate as exists above the stagnant zone where the profile is half-parabolic. The mathematical treatment, shown in Appendix VII, predicts that the film in the stagnant zone should be 1.587 times as thick as it is in the normal condition of no surface shear.

PLATE V

Observation of the Film Thickness Change - It is possible to detect this sudden change in film thickness by observing the reflection in the liquid surface of the overhead strip lighting. This reflection was found to show a distinct distortion at a point some 1-1½" above the equator and it was confirmed that this point corresponded with the point at which the aluminium particles came to a stop. The distortion of the image is shown in plate V; no such distortion was observed with Lissapol solution as the feed liquid.

Measurement of the Film Thickness Change - Using an experimental technique to be described in the next chapter it is possible to measure film thickness with reasonable accuracy and a number of measurements in the presence of the end effect were made. At a fixed position (close to the equator) on the sphere, values of film thickness were obtained firstly with the off-take level at 90° (i.e. in presence of the end effect) and secondly with the off-take below 180° (i.e. in the absence of the end effect). With water as the feed liquid the following results were obtained.

Flow Rate cc/sec	1.85	1.89	2.12	2.44
Thickness, F^1 cm x 10^2	2.28	2.31	2.41	2.54
Thickness, F cm x 10^2	1.45	1.47	1.52	1.60
Ratio F^1/F	1.57	1.57	1.59	1.59

F^1 = Thickness in presence of the end effect.

F = Thickness in same position but in the absence of the end effect.

These values of the ratio agree very well with the predicted value of 1.587 (Appendix VII) and would seem to confirm that, with water as the feed liquid, the surface above the off-take has zero velocity.

Using Lissapol as the feed liquid the following results were obtained.

0.1 g/l Lissapol at 2.00 cc/sec $F^1 = 1.98 \times 10^{-2}$ cm

$F_1 = 1.42 \times 10^{-2}$ cm

$\therefore F^1/F = 1.39.$

1.0 g/l Lissapol

Flow Rate cc/sec	1.70	2.05	2.43
Thickness, F^1 cm x 10^2	1.78	1.86	2.01
Thickness, F cm x 10^2	1.58	1.66	1.75
Ratio F^1/F	1.13	1.12	1.15

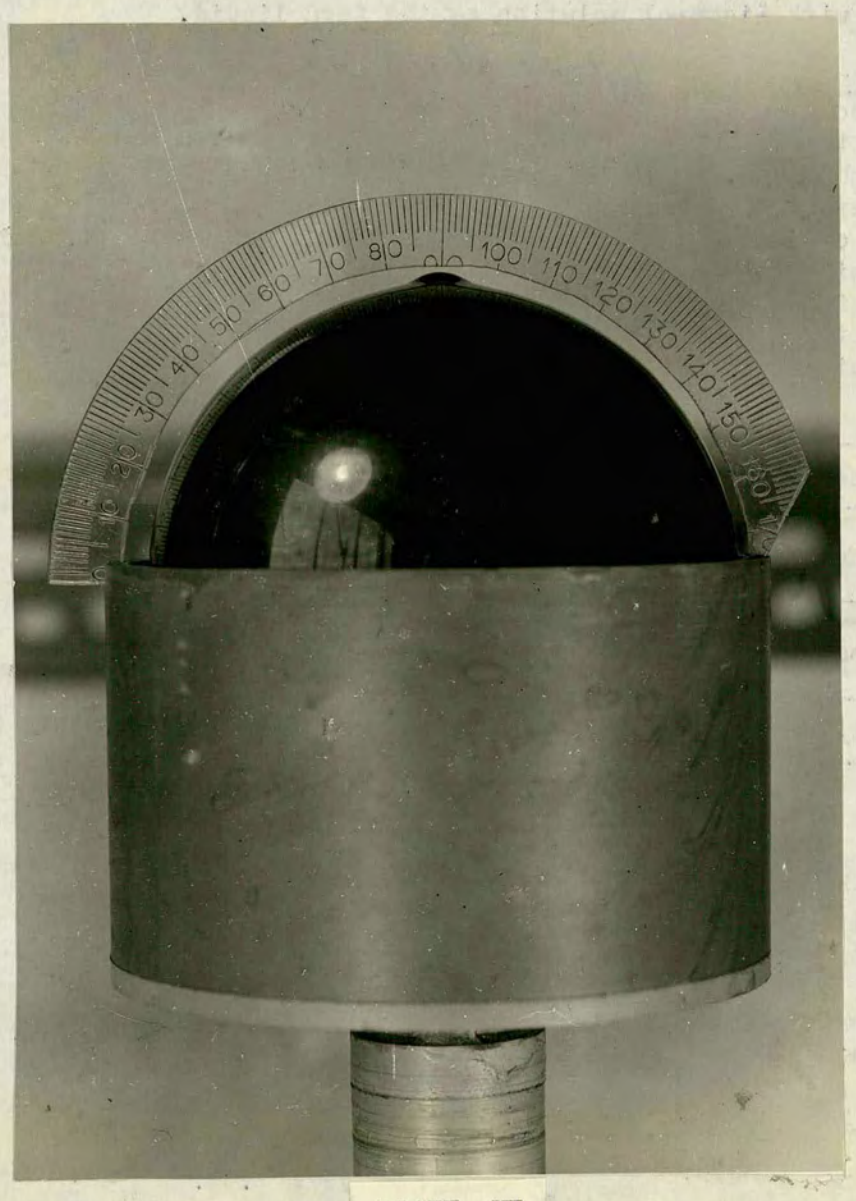

PLATE VI

These results for Lissapol suggest that the surface above the off-take is not stagnant but is retarded to some degree to give this increase in film thickness. This agrees with the observations of the flow of aluminium particles on the Lissapol surface and with the fact that no distortion of an image in the surface is observed.

Also, from the above results for two concentrations, it appears that the extent of the surface retardation decreases as the concentration of Lissapol increases. This would help to explain the results of absorption for 90° exposure at different Lissapol concentrations (fig. 12) which increase towards the theoretical value as concentration increases.

Measurement of Stagnant Film Height on a Water Film.

The height of the stagnant layer can be found theoretically assuming that there is, as mentioned earlier (page 20) a balance between shear forces and surface tension. The analysis, to be found in Appendix VIII, gives the following result

$$\frac{\sin^2\theta_s}{\int_{\theta_s}^{\pi/2} \sin^{7/3}\theta.d\theta} = \left[\frac{3\mu L R^2 \rho^2 g^2}{4\pi(s_1-s_2)^3}\right]^{1/3}$$

where

θ_s = Latitude at which the stagnant surface begins.

$s_1 - s_2$ = Surface tension difference between the liquid surface above the layer and the surface of the stagnant layer.

The value of s_2 is uncertain since the stray surface active agent causing the end effect is not known. However s_2 can be taken to be 30 dynes/cm which is the order of magnitude of most surface active materials including Lissapol which is likely to be present in trace quantities. By choosing values of θ_s the above equation can be solved graphically for L and in this way a table of values of L and θ_s can be constructed. However it is more convenient to plot values of η, the angle subtended by the stagnant layer ($\eta = 90 - \theta_s$). The result of the calculation is shown as the theoretical curve on fig. 13.

Using the distortion of an overhead image to locate the top of the stagnant zone values of η were measured using a protractor incorporated in the set-up as shown in plate VI. The accuracy in the values of η was of the order of $\pm 2^{\circ}$. The results of these measurements, shown in figure 13 and table IX, show considerable scatter although there is a general trend towards a rise in layer height as flow rate decreases. The results lie above the theoretical curve indicating that in general the stagnant layer is higher than

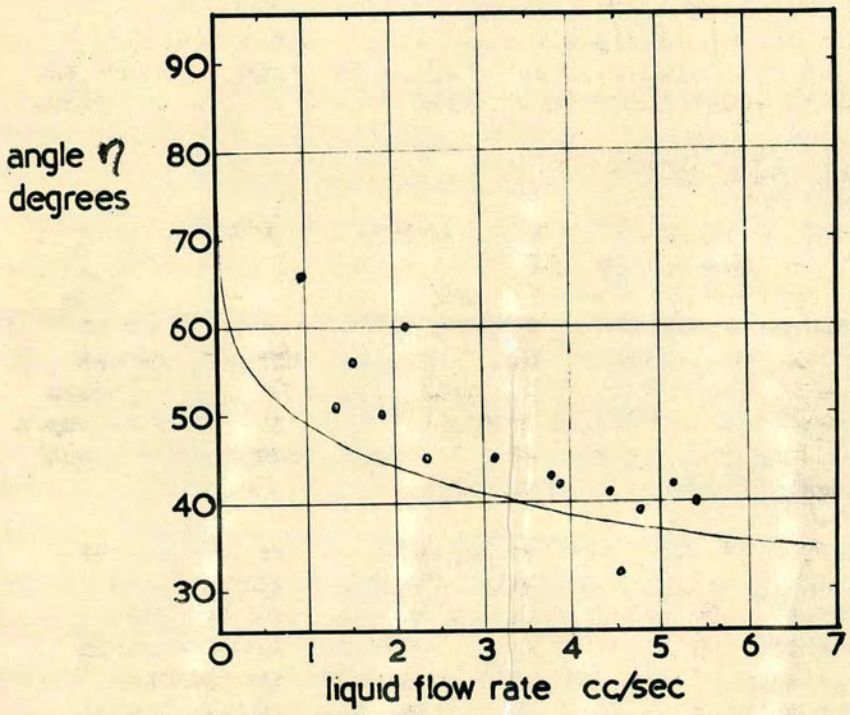

FIG. 13 HEIGHT OF THE STAGNANT LAYER

(plot of results in table IX)

it should be according to the theory. This indicates either that the value of $S_1 - S_2$ is incorrect or that an additional force is acting in the system. In order that the theoretical curve should pass through the scatter of points the value of $S_1 - S_2$ would have to be of the order of 55 dynes/cm which means that, if S_1 is taken to be 72 dynes/cm (water value) S_2 would have to be in the range 15-20 dynes/cm. This latter value is rather lower than that given by most surface active materials and in any case the value of S_1 may not be as high as 72 dynes/cm since the water is contaminated with surface active agent. Consequently the possibility that the theoretical analysis does not apply to the situation must be considered. The large scatter in the experimental results, which cannot be attributed entirely to experimental error, indicates that the height of the layer does not follow as rigid a theory as that suggested and a possible alternative is suggested below.

The Behaviour of a Hexanol Film.

Examination of the flow of an n-Hexanol solution over the top half of the sphere showed it to exhibit an end effect very similar to that obtained with tap water. Aluminium particles are brought to a sudden stop, the distortion of an image is observed and film thickness ratios are of the correct order for total stagnation. Thus it appears that n-Hexanol does not alter the end-effect in the same way as Lissapol does and the difference in action of Hexanol and Lissapol requires further examination.

The height of the stagnant layer on a film of aqueous Hexanol (1 g/l) was found to be of the same order as the values obtained with water although the surface tension above the layer should be somewhat lower in the case of n-Hexanol solution. This fact indicates that the surface tension - shear balance is probably not the controlling factor in determining the height of the layer.

Suggested Mechanism for the Build-Up of a Stagnant Surface Film.

Experimental measurements have shown that the stagnant layer height is much more a function of time than of liquid flow rate and it appears that the controlling factor may be the amount of agent present at a given time. Surface active molecules present in the film diffuse to the surface of the liquid and are swept downwards to the off-take where they "stack" against the P.V.C. off-take tube and climb upwards over the film until the shear on the underside causes the layer to collapse and some of the material to be carried away in the off-take. This is similar to the behaviour suggested by Frumkin and Levich (23) for the action of surface active agent in mass transfer between bubbles and liquids.

They suggests that in this case the active molecules are swept to the rear of the bubble where they stack against themselves thus building up into a layer which cuts down the mass transfer rate. The controlling factors in this case are the amount of surface active agent present and the amount of lateral compression which the layer is capable of withstanding.

The Influence of the End Effect on Mass Transfer.

It has already been noted that absorption into a film with zero surface velocity is considerably less than that into a normal film. Although the equations for the absorption in the two cases are available, it is rather difficult to associate them to give the absorption for a hemisphere with a known stagnant layer height since the flow pattern at the jump in the film is uncertain. However, as a rough check, some calculations (Appendix IX) were made for the Hexanol film assuming the layer to begin at 50° and the concentration profile to become flat at 50°. The results of this calculation are close to the values obtained experimentally and also forecast the slight negative gradient in the $G/L^{\frac{1}{3}}$ versus L curve (fig. 11) at low flow rates.

It was felt that a more rigorous calculation was not warrented since it is not certain if this type of end effect is of practical significance. It appears to arise in bubble mass transfer where the surface active molecules stack against themselves at the rear of the bubble. The spherical and hemispherical systems used here are similar in geometry to bubbles encountered in practice but in general the shearing rates in bubbles are considerably larger so that end effects may be less significant there.

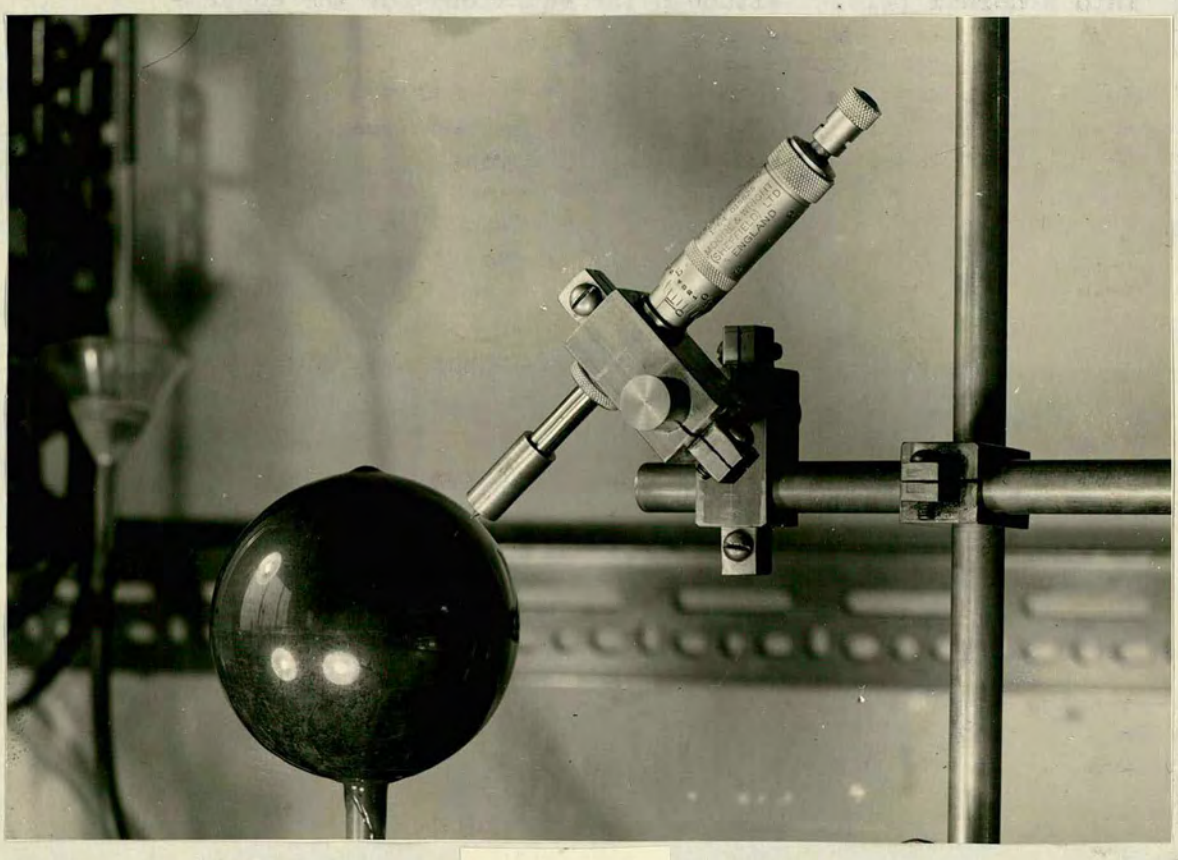

PLATE VII

CHAPTER VII

THE MEASUREMENT of LIQUID FILM THICKNESS

Introduction.

Measurements of liquid-film thickness on wetted-wall columns and flat plates have been made by a number of workers using a variety of techniques ever since Nusselt (40) published his analysis of liquid film flow. A good review of the earlier work is given by Cooper et al (11) while details of more recent work can be found in references 21, 24, 33 However, no mention of any attempt to measure the thickness of a liquid film on a sphere has been found in the literature. The nearest approach to this is the work of Davidson et al (16) on the liquid hold-up on a column of spheres the results of which gave good agreement with the theory.

Many of the methods used to measure liquid film thickness are applicable to the sphere but the ones considered were

(1) Using a capacitometer which determines the gap between a small flat plate and the water surface.

(2) Using a micrometer.

Both methods give local measurements which is essential in the case of a sphere since the thickness changes rapidly with angular position. Method (1) was used by Dukler and Bergelin (21) with great success. Not only does it give the mean thickness when ripples are present but, in conjunction with an oscilloscope, it forms a powerful tool for investigation of the rippling. Method (2) was used by Kirkbride (34) in the course of some work on heat transfer but the method suffers from the disadvantage of giving the maximum thickness when rippling is present.

However, since, in the presence of surface active agents rippling is not a problem, it was decided to use the second method because it is more direct, requiring no calibration. The experimental arrangement was designed to allow measurement of the thickness at any angle of latitude to investigate the variation of thickness with θ, and at any angle of longitude to check that the distribution of liquid was uniform.

The Experimental Method.

The apparatus used in the measurement of film thickness is shown in plate VII. An arrangement of clamps was constructed in such a way that a micrometer could be positioned at any angle θ between zero and 160°, at any longitudinal position. The micrometer used was graduated in thousandths of an inch and was fitted with a pointed brass cap to allow accurate determination of angular position which was determined using a protractor cut to the curvature of the sphere.

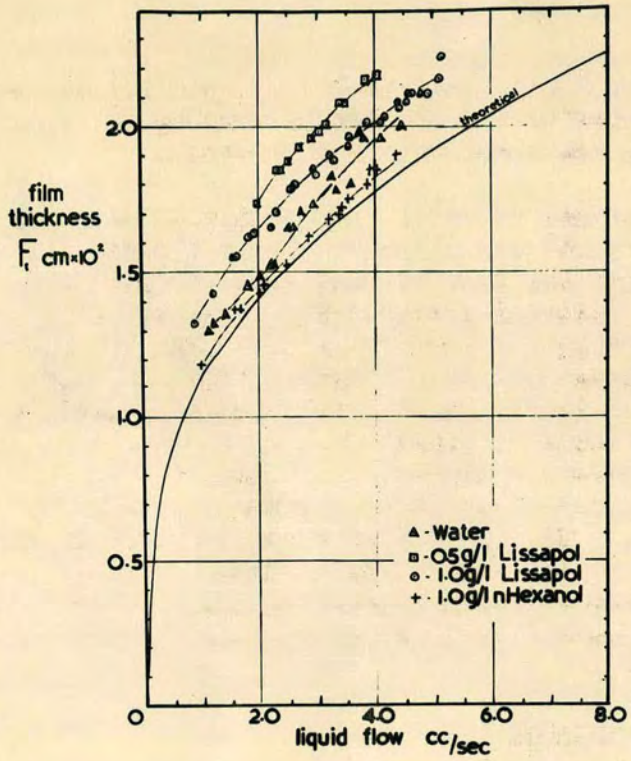

FIG. 14 EQUATORIAL FILM THICKNESS VERSUS LIQUID FLOW RATE
(plot of results in table X A,B,C & D)

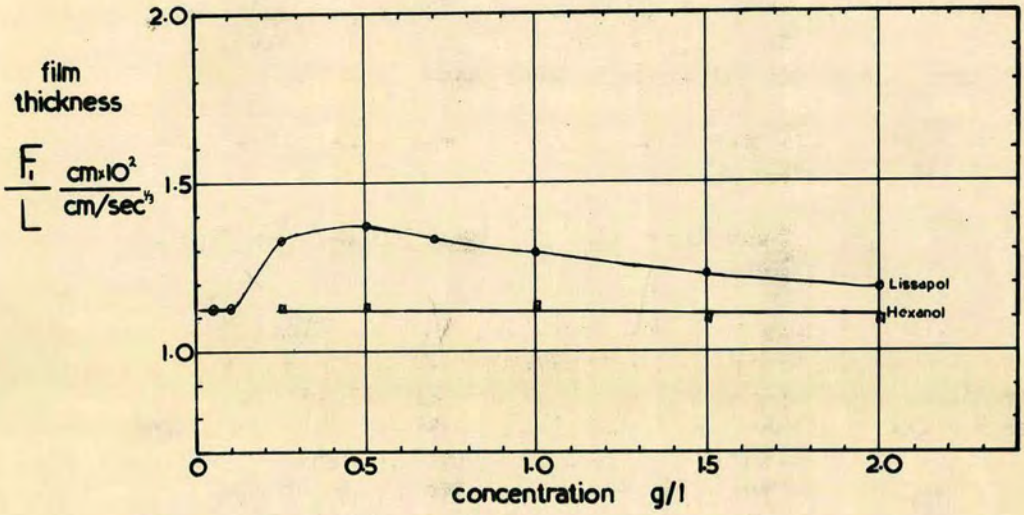

FIG. 15 EQUATORIAL FILM THICKNESS VERSUS SURFACE ACTIVE AGENT CONCENTRATION L ~ 2.00 CC/SEC
(plot of results in table XI A & B)

At each new position care was taken to insure that the micrometer was at right angles to the surface by viewing the point of the instrument and its image with a microscope.

The liquid surface was detected very simply by watching the microscope as the point was advanced slowly towards the surface until the liquid was seen to jump onto the point. The solid surface was detected electrically after stopping the liquid flow and drying the surface in the vicinity of the measurement. The sphere and the micrometer were mutually insulated and connected to a potential difference so that, as soon as contact was obtained between the two, a current flowed in the circuit. This was amplified and caused a post-office connector to close in an external mains circuit, lighting a small lamp. The film thickness is simply the difference between the two readings. Two or three readings were taken in every case to check concordancy and the point of the micrometer was carefully dried after each determination.

Accuracy of the Measurements.

With the 1 thou. micrometer it was possible to interpolate, for each reading, to 0.0002" and it is probably safe to say that the thicknesses were measured to an accuracy of better than 0.0004" which, for the thinnest measurement, represents an accuracy of 6 to 7%. The angular position could be determined to the nearest degree using the protractor. Some comparison results taken by measuring the circumferential distance between the position of the micrometer point and zero degrees showed that the protractor measurements were sufficiently accurate for angles greater than 20°. For angles smaller than this the position was determined by careful circumferential measurement.

The theoretical equations and values of film thickness are given in Appendix Ia.

Results (1) - Film Thickness at the Equator versus Liquid Flow Rate.

A number of measurements of thickness were taken for different flow rates with the micrometer fixed at 90° and the results, for four different liquids, are shown in figure 14 and reported in tables X A, B, C and D. In every case the points lie above the theoretical prediction although the values for n-Hexanol are very close to the theoretical curve. The proportionality of the thickness to the cube root of the flow rate is followed fairly well apart from the results for water which show a definate break at about 2.00 cc/sec which corresponds with the point at which rippling begins to affect the absorption rate (fig. 4).

However rippling did not affect the results for Lissapol solutions which have film thicknesses considerably greater (up to 22%) than the theoretical values. To examine this difference more thoroughly a number of results of equatorial thickness for various surface active agent concentrations

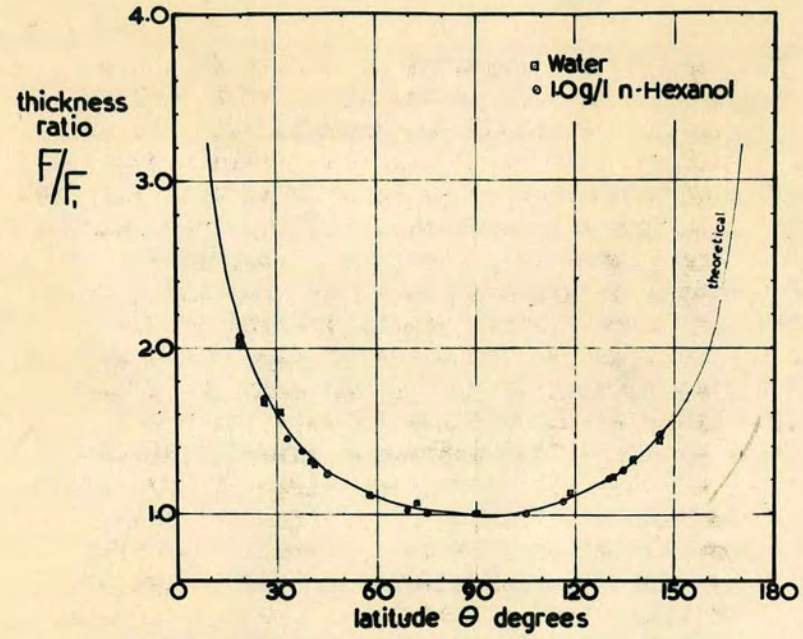

FIG. 16 FILM THICKNESS RATIO VERSUS LATITUDE
(plot of results in table XIIA B & C)

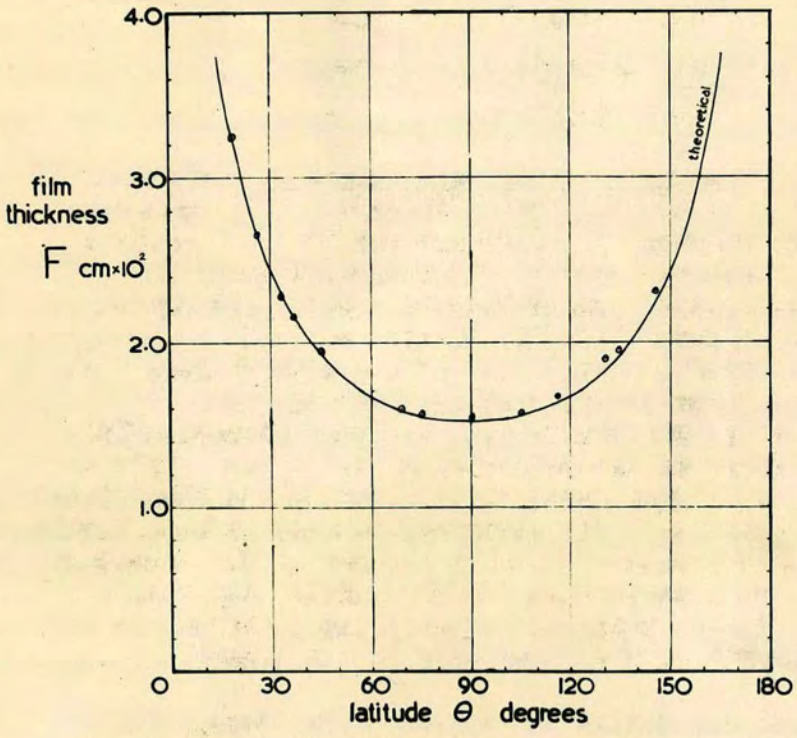

FIG. 17 FILM THICKNESS VERSUS LATITUDE FOR
1.0 G/L n HEXANOL L = 2.50 CC/SEC
(plot of results in table XIIC)

were taken. The results are reported in tables XI A and B and shown in figure 15 as a plot of the ratio of F to $L^{\frac{1}{3}}$ against the concentration although the results were all taken at close to 2.00 cc/sec. It was found that while n-Hexanol had no appreciable effect on the film thickness, Lissapol, in small concentrations, had a considerable effect. The thickness is seen from the figure to go through a maximum at around 0.5 g/l Lissapol at which point it is some 22% greater than the theoretical value. The general pattern of the curve is strikingly similar to the curve of mass transfer versus Lissapol concentration (fig. 7), the maximum in film thickness corresponding to the minimum in mass transfer. This, coupled with the fact that n-Hexanol affects neither the film thickness nor the mass transfer, suggests that there is some relation between the film thickness and the mass transfer. The development of this relationship must wait until the results of the film thickness at various angular positions have been considered. Suffice it to say for the moment that the increase in film thickness suggests some interfacial shear giving a lower interfacial velocity and an altered velocity profile which in turn causes a reduction in mass transfer.

Results (2) - Film Thickness at Various Angular Positions.

A large number of measurements of thickness at different angular positions were made and in order to simplify their presentation they have been split into groups.

(1) Using Hexanol Solutions and Water.

(2) Using Lissapol Solutions.

The results for n-Hexanol (1 g/l) and for water are shown in figure 16 as a plot of the ratio - thickness at θ/thickness at 90° - versus θ bringing points for any flow rate onto a single curve. The values for n-Hexanol were taken at a flow rate of 2.50 cc/sec while those for water were taken at 2.00 cc/sec for angles above the equator and 1.20 cc/sec for those below in order to reduce the effect of rippling. The figure shows that the values obey very closely the $\sin^{\frac{2}{3}}\theta$ law as predicted by the theoretical analysis (Appendix Ia). The absolute values of the thickness of the Hexanol film are plotted on figure 17 and agree very well with the theoretical curve for 2.50 cc/sec. The water values tend to be a little higher than the prediction probably because of the effect of stray vibrations, which affect the water film more than a Hexanol or a Lissapol film, and of rippling which cannot be entirely eliminated on the lower half of the sphere.

The general conclusion to be drawn from these results is that, as far as can be ascertained by film thickness measurements, the Hexanol film behaves as theory predicts while the water film appears to behave in a similar fashion although the instability of the flow does not allow a thorough investigation of the film thickness using this technique.

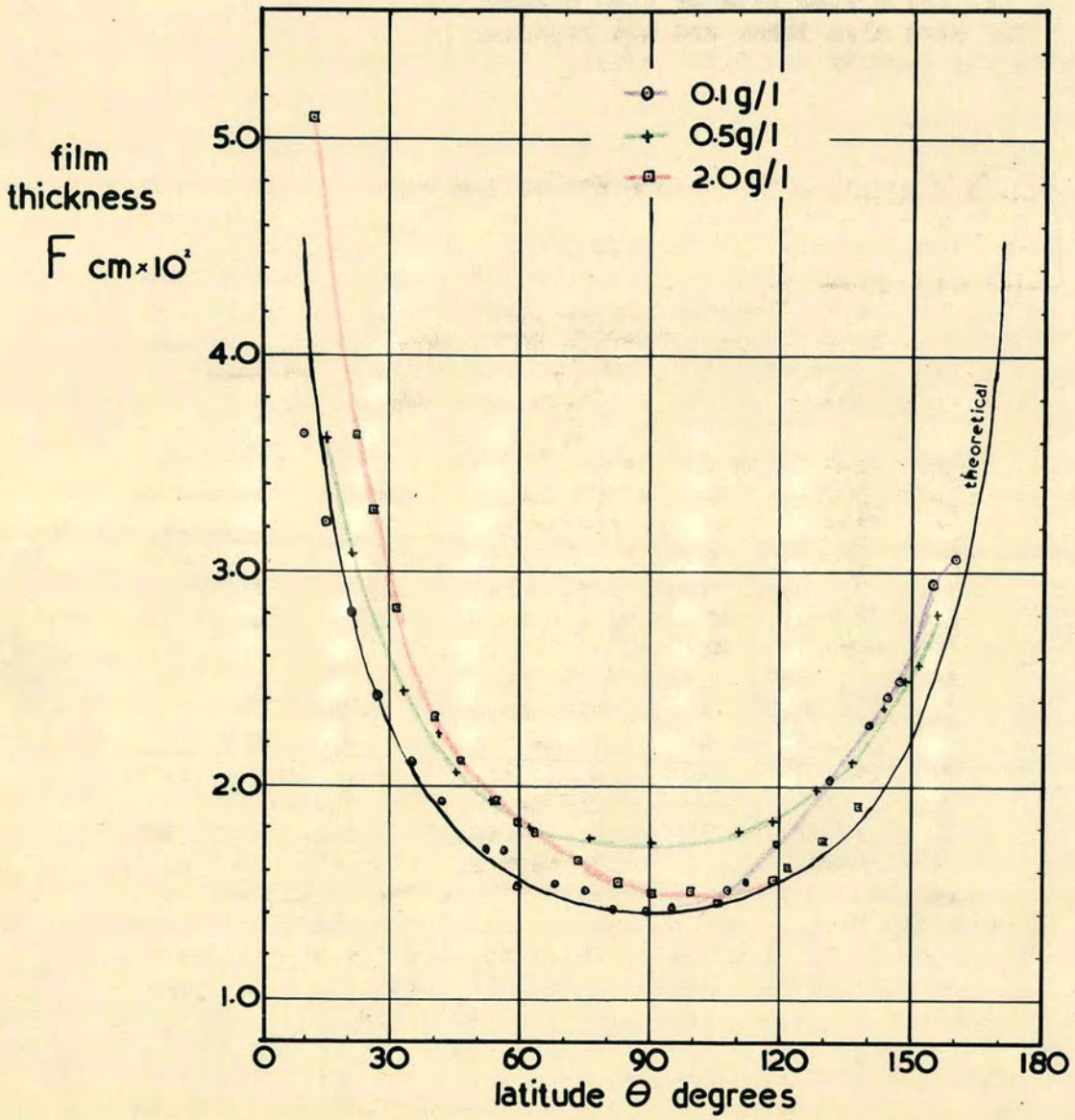

FIG.18 FILM THICKNESS VERSUS LATITUDE FOR LISSAPOL SOLUTIONS L = 2·00 CC/SEC
(plot of results in table XIII)

The results for Lissapol Solutions are a little more difficult to interpret as it was found that the shape of the curve depended to a large extent on the concentration of Lissapol in the feed solution. The results for three different Lissapol concentrations are shown in figure 18. The values are all for a flow rate of 2.00 cc/sec; values for 3.00 cc/sec were also taken and are reported in table XIII along with the results for 2.00 cc/sec.

Figure 18 needs some explanation.

0.1 g/l Lissapol - The points follow the theoretical curve fairly closely down to 95° at which point the film begins to thicken until at around 140° it is some 20% thicker than the theoretical prediction. Beyond 150° the points show a tendency to return to the theoretical curve and by extrapolation it is found that the experimental curve should return to the theoretical at about 165°. (It was not possible to take values below about 160° with the set-up used.)

0.5 g/l Lissapol - The points all lie above the theoretical curve although the points at 15° and 155° are fairly close to the curve. The maximum divergence between theoretical and experimental occurs at around 90° where the film is some 22% thicker than the theoretical prediction. Again by extrapolation it is found that the film is thicker than the theoretical over the range 15°-165°.

2.0 g/l Lissapol - The points are considerably above the theoretical curve over the upper half of the sphere but beyond 120° the experimental values are close to the theoretical curve. The maximum divergence from the theoretical occurs about 20° where the film is some 32% thicker than the theoretical prediction. Points very close to the inlet to the sphere are likely to be affected by the entry conditions and consequently it is difficult to interpret how the film behaves over the first 10° and the point of maximum divergence may be nearer the inlet. However, in this case, the film appears to be thicker over the region 3° (inlet) to 120°.

Measurements of thickness versus latitude for other concentrations of Lissapol (0-4 g/l) have also been made and the results are reported in tables. The region of thickened film has been noted for each particular concentration and the results are shown graphically in figure 19. For each concentration the region of increased film thickness is defined by two points viz. the point at which the experimental and theoretical values begin to diverge - the point of divergence and the point at which the curves converge again - the point of convergence. In the figure, which is for a flow rate of 2.00 cc/sec the former is shown by the lower curve and the latter by the upper curve. It can be seen that, as the concentration increases both points move up the sphere but the point of divergence moves up much more quickly. In fact for concentrations greater than 1.0 g/l the film appears to be thicker than the prediction as soon as it is formed. The

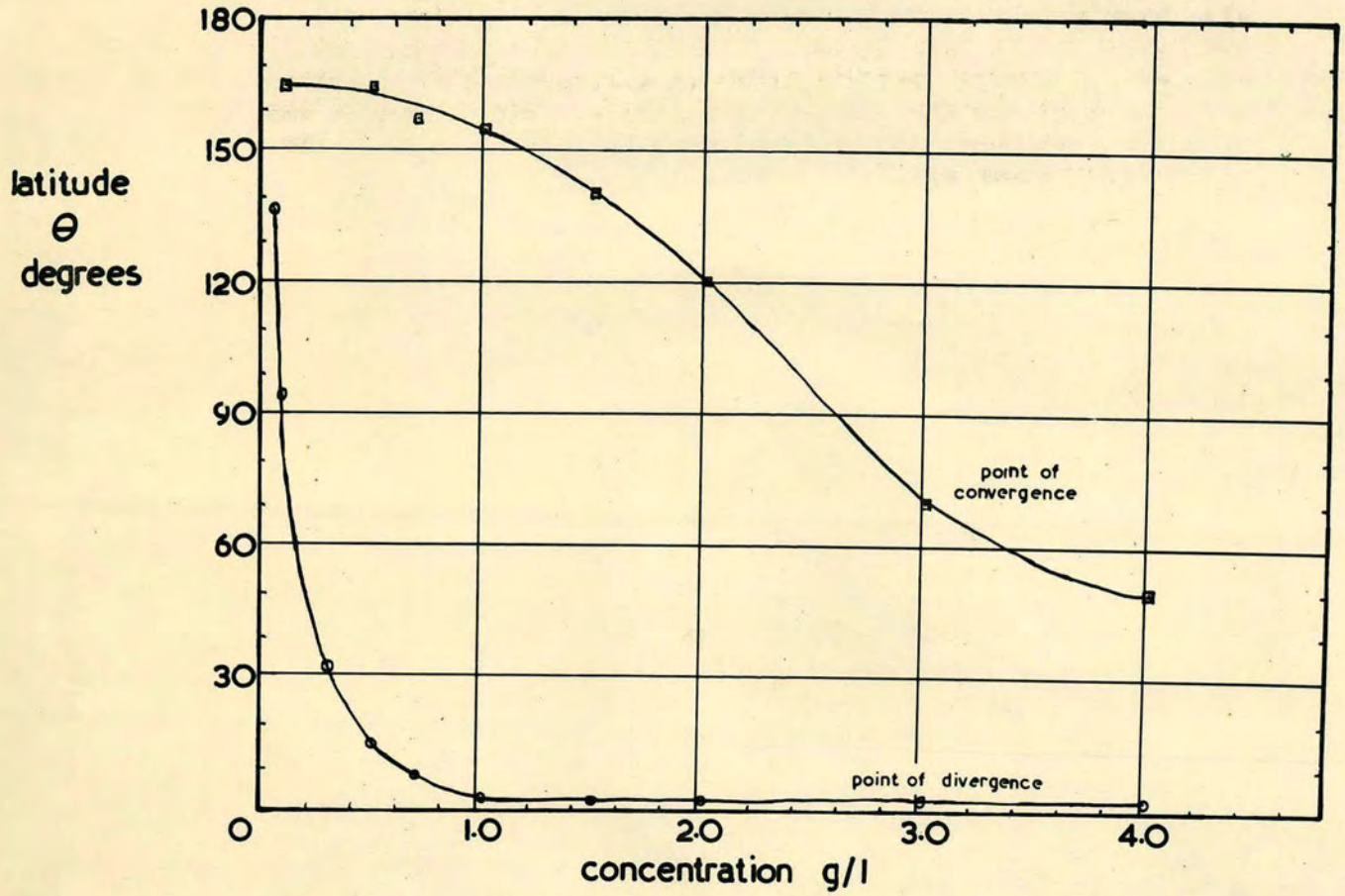

FIG. 19 POINTS OF DIVERGENCE AND CONVERGENCE VERSUS LISSAPOL CONCENTRATION AT L = 2.00 CC/SEC
(plot of results in table XIV)

region of thicker film is represented by the distance between the curves in the figure and it can be seen that this passes through a maximum at around 0.5 g/l.

Although the measurements of thickness at different latitudes have been carried out mainly for a fixed flow rate of 2.00 cc/sec, a number of measurements at 3.00 cc/sec have also been made and can be found in table XIV. In general the behaviour at 3.00 cc/sec is exactly similar to that at 2.00 cc/sec except that the point of divergence occurs somewhat later in all the cases investigated. The values of the point of divergence can be found in table XIV along with the equivalent values for 2.00 cc/sec.

CHAPTER VIII

THE FLUID MECHANICS of the FLOW of LISSAPOL SOLUTIONS

Observations.

The film thickness measurements reported in the previous chapter show that, when Lissapol solutions are used as feed liquids, the fluid mechanics of the spherical film flow are somewhat different to the theoretical predictions. The observations made so far may be summarised as follows.

(1) A moving spherical film of an aqueous solution of Lissapol has a distinct region of increased film thickness (i.e. increased above the theoretical predictions of Appendix Ia).

(2) The region of increased film thickness is closer to the inlet the higher the concentration of Lissapol.

(3) For a fixed Lissapol concentration, the region occurs further from the inlet for a flow rate of 3 cc/sec than for one of 2 cc/sec.

(4) No region of increased thickness is encountered with n-Hexanol solutions.

(5) Visual observation suggests that Aluminium particles flow more slowly on a Lissapol film than on a water film.

The presence of the region of increased thickness suggests that the velocity profile for the Lissapol film is different from that deduced in Appendix Ia. The basis of the prediction is the Gravity - Shear balance

$$\mu \frac{\partial^2 u}{\partial z^2} = -\rho g \sin\theta$$

with the boundary conditions (1) Zero velocity at the solid surface

i.e. $u = 0$ at $z = 0$.

(2) Zero shear at the liquid surface

i.e. $\frac{\partial u}{\partial z} = 0$ at $z = F$.

It is unlikely that the presence of Lissapol in small quantities could alter the gravity-shear balance, the constants involved or the assumption of zero velocity at the solid surface. The second boundary condition however may not be obeyed. The presence of some upwards shear at the liquid surface would lead to an altered velocity profile with a reduced surface velocity and an increased film thickness. A theoretical reason for the existence of such a shear is discussed below on the basis of dynamic surface tension and the Marangoni Effect.

The Dynamic Surface Tension of Lissapol.

The surface tension of an aqueous solution of a surface active agent is dependent not only on the bulk concentration of the agent but also on the age of the surface of the solution, since the agent takes time to diffuse to the surface Consider a solution of Lissapol being fed onto the sphere used in the present work. If the solution is dilute the surface tension at the instant of creation will be that of water since the number of molecules of Lissapol in the surface will be small. Immediately, however, Lissapol begins to diffuse to the surface, reducing the surface tension until it reaches its static value i.e. the value for an old (theoretically infinitely old) surface on a solution of the same bulk concentration. The varying surface tension at any instant is the dynamic surface tension as opposed to the static or equilibrium value.

If the diffusion takes a considerable fraction of the time of exposure of the film on the sphere (about 1-2 secs) a surface tension gradient exists on the film and the conditions for surface shear are set up. At any point on the surface of the sphere where the surface tension is changing there will be a force in the direction of increasing surface tension (i.e. upwards in this case) and the boundary condition of zero shear at the liquid surface is upset. This will cause a change in the film thickness so that according to this hypothesis the region of increased film thickness detected in the measurements of chapter VII is caused by and so coincides with the changing surface tension.

The behaviour of the films of Lissapol and Hexanol solutions must now be re-examined in the light of this hypothesis.

(1) The measurements indicate that the greater the concentration of Lissapol the earlier the surface tension changes begin. This agrees with the work done on dynamic surface tension e.g. by Addison (1).

(2) For a higher flow rate the region of surface tension change begins later. This is reasonable since the smaller the flow rate the older the film is at any fixed position. The ages of the film at the point where the surface tension begins to change can be calculated using the figure in Appendix Ia.

For 0.05 g/l at 2.00 cc/sec Point of Divergence is 137°
Age 0.90 sec.
at 3.00 " " " " is 145°
Age 0.72 sec.

For 0.10 g/l at 2.00 cc/sec Point of Divergence is 95°
Age 0.59 sec.
at 3.00 " " " " is 113°
Age 0.55 sec.

For 0.25 g/l at 2.00 cc/sec Point of Divergence is 33° Age 0.15 sec.
at 3.00 " " " " is 40° Age 0.15 sec.

For 0.5 g/l at 2.00 cc/sec Point of Divergence is 15° Age 0.048 sec.
at 3.00 " " " " is 25° Age 0.077 sec.

In all the cases the points of divergence occur later in space for 3.00 cc/sec but only in the cases of 0.1 g/l and 0.25 g/l do the ages of the surface agree. It is significant that in these cases the point of divergence was easier to determine since it occurred away from the regions where the accuracy of the film thickness measurements is poorer. In general the agreement between the ages can be said to be reasonable.

(3) Since Hexanol does not affect the film thickness at any of the points investigated on the sphere, it must be concluded that the surfacetension changes occur much more rapidly for n-Hexanol than for Lissapol. (It is assumed the Hexanol has diffused to the surface of the spherical film since it succeeds in eleminating ripples.) A literature search for dynamic surface tension data yielded the following values for n-Hexanol (Defay and Hommeln (18))

1.29 g/l n-Hexanol - Reaches its static value after 9×10^{-3} sec.
0.35 g/l n-Hexanol - Reaches its static value after about 1.5×10^{-2} sec.

At 2.00 cc/sec these ages represent positions on the sphere of less than 7° latitude. No information on the dynamic surface tension of Lissapol has been traced but work e.g. by Addison (1,2) and by Defay and Hommeln (18) indicates that increasing molecular weight reduced the rate of attainment of surface equilibrium.

These three points add weight to the hypothesis and a more mathematical approach is merited.

<u>The Mathematical Analysis of the Altered Velocity Profile</u>.

The most logical way to attack the problem mathematically would be to obtain data on the dynamic surface tension of Lissapol from which values for the surface shear could be obtained and used as a boundary condition in the gravity-shear balance. However no information is available on the dynamic surface tension and in any case the theoretical treatment of the diffusion of surface active agents is far from complete. It is not yet certain in what way convection affects dynamic surface tension so that measurements made on one system may not be applicable to another. (A short sur-

vey of the literature of dynamic surface tension is contained in Chapter IX.) This lack of information has led to a different approach being adopted. An arbitrary value of interfacial velocity in the so-called retarded region of the film has been chosen and related to the film thickness. Using the experimental film thickness measurements, values of dynamic surface tension have been deduced and compared with the expected order of values.

The mathematical treatment is as follows -

Assume the interfacial velocity in the region of changing surface tension (called for short the retarded region) to have the value V

The gravity-shear balance is $\mu \frac{\partial^2 u}{\partial z^2} = -\rho g \sin\theta$

Boundary Conditions (1) $u = 0$ at $z = 0$
(2) $u = v$ at $z = f$

where f is the film thickness in the retarded region.

Integrating and inserting the boundary conditions leads to the equation

$$u = -\frac{\rho g \sin\theta}{2\mu} z^2 + \frac{\rho g f \sin\theta}{2\mu} z + \frac{v}{f} z$$

now

$$L = 2\pi R \sin\theta \int_0^f u.dz$$

whence

$$L = 2\pi R \sin\theta \left[\frac{\rho g f^3 \sin\theta}{12\mu} + \frac{vf}{2}\right]$$

i.e. $$v = \frac{L}{\pi R f \sin\theta} - \frac{\rho g f^2 \sin\theta}{6\mu}$$

To simplify the equation the values of v and f are related to the values of film thickness and interfacial velocity for a normal film

i.e. $v = \beta u_i$ and $f = \alpha F$

Substituting theserelationships along with the equations

$$u_i = \frac{3L}{4\pi R \sin^{1/3}\theta}\left(\frac{2\pi R \rho g}{3\mu L}\right)^{1/3}, \quad F = \left(\frac{3\mu L}{2\pi R \rho g \sin^2\theta}\right)^{1/3}$$

in equation (2) leads to the result

$$\beta = \frac{4}{3\alpha} - \frac{\alpha^2}{3}$$

which relates the ratio of the interfacial velocities of the retarded film and the normal film (β) to the ratio of the film thicknesses for the retarded and normal film (α). Using this expression the value of the interfacial velocity can be found at any point for which the value of α has been found experimentally. Values of α have been deduced from the thickness measurements and are reported in table XV.

Also when $\beta = 0$ i.e. for a film with zero surface velocity equation (3) gives $\alpha = 4^{\frac{1}{3}}$ which agrees with the

ratio already deduced in Appendix VIII which is merely a special case of the analysis carried out above. For $\beta = 1$ equation (3) gives $\alpha = 1$, i.e. when the surface velocity returns to normal the film thickness does also, as it must.

An Estimation of the Dynamic Surface Tension.

From the velocity profile deduced above and the experimental values of α it is possible to calculate the surface shear and the surface tension at any point on the spherical film.

Consider a point on the surface of the film at θ where the surface tension is s. At a point $\frac{1}{2}d\theta$ before this the surface tension will be

$$s - \frac{ds}{d\theta}\,\frac{d\theta}{2}$$

and at a point $\frac{1}{2}d\theta$ after θ the surface tension will be

$$s + \frac{ds}{d\theta}\,\frac{d\theta}{2}$$

A force balance on the element $d\theta$ for unit latitudinal are

$$\text{Net upwards force at surface} = s - \frac{ds}{d\theta}\frac{d\theta}{2} - \left(s + \frac{ds}{d\theta}\frac{d\theta}{2}\right)$$

$$= -\frac{ds}{d\theta}\,d\theta \quad \text{[Note: } \frac{ds}{d\theta} \text{ is negative]}$$

The surface area for unit latitudinal arc $= Rd\theta$ [neglecting the film thickness]

$$\therefore \text{Surface Shear} = -\frac{1}{R}\frac{ds}{d\theta}$$

The velocity profile from equation (1) is

$$\mu u = -\tfrac{1}{2}\rho g \sin\theta . z^2 + \tfrac{1}{2}\rho g F \sin\theta . z + \mu \frac{v}{f} z$$

whence $\mu \frac{\partial u}{\partial z} = -\rho g \sin\theta . z + \frac{1}{2}\rho g f \sin\theta + \mu \frac{v}{f}$

$$\therefore \text{Shear at the liquid surface} = \mu \left(\frac{\partial u}{\partial z}\right)_{z=f}$$

$$= \mu \frac{v}{f} - \tfrac{1}{2}\rho g f \sin\theta .$$

This must be equal and opposite to the shear produced by the surface tension gradient given in equation (4).

i.e. $\frac{ds}{d\theta} = \frac{\mu R v}{f} - \frac{1}{2} R \rho g f \sin\theta .$

Now $f = \alpha F = \alpha F_1 \sin\theta .$

$$v = \beta u_1 = \beta \frac{3L}{4\pi R F_1} \sin^{-\frac{1}{3}}\theta .$$

whence

$$\frac{ds}{d\theta} = R \rho g F_1 \sin^{\frac{1}{3}}\theta \left(\frac{3\mu L \beta}{4\pi \alpha R \rho g F_1^3} - \frac{\alpha}{2}\right)$$

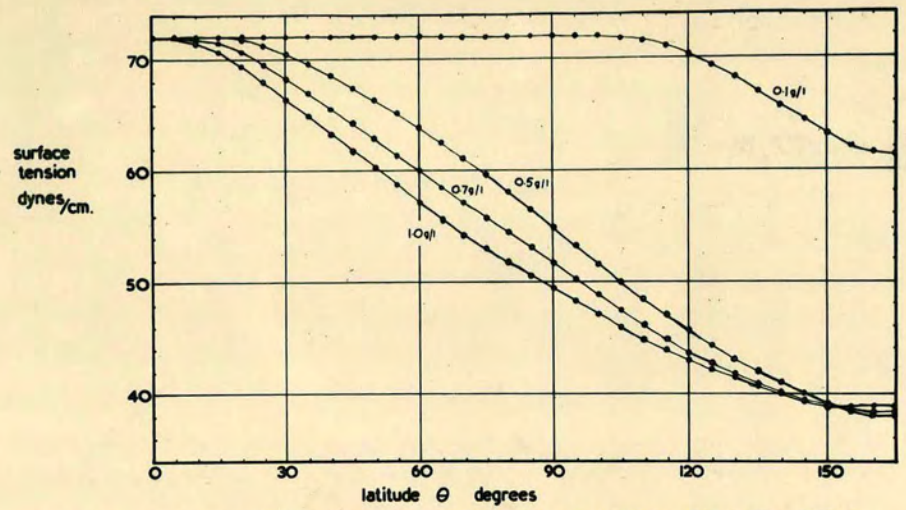

FIG. 20 DYNAMIC SURFACE TENSION OF LISSAPOL SOLUTIONS ESTIMATED FROM FILM THICKNESS OF THE SPHERICAL FILM

(plot of results in table XVI)

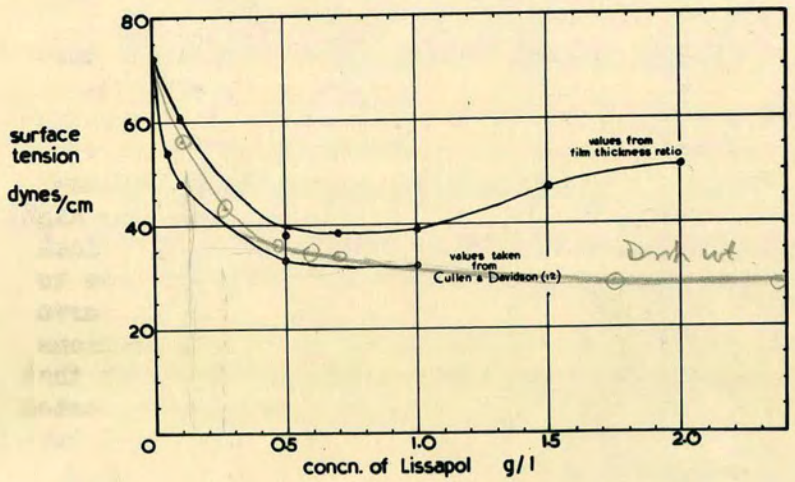

FIG. 21 COMPARISON OF STATIC SURFACE TENSION VALUES

$$F_1^3 = \frac{3\mu_L}{2\pi R \rho g}$$

whence

$$\frac{ds}{d\theta} = \rho g R F_1 \sin^{\frac{1}{3}}\theta \left(\frac{\beta}{2\alpha} - \frac{\alpha}{2}\right)$$

$$\beta = \frac{4-\alpha^3}{3\alpha}$$

whence

$$\frac{ds}{d\theta} = 2\rho g R F_1 \sin^{\frac{1}{3}}\theta \left(\frac{1-\alpha^3}{3\alpha^2}\right)$$

The surface tension at any point is given by integrating this equation with the boundary condition s = 72 dynes/cm at $\theta = 0$.

i.e. $$\int_{72}^{s} ds = 2\rho g R F_1 \int_0^{\theta} \sin^{\frac{1}{3}}\theta \left(\frac{1-\alpha^3}{3\alpha^2}\right) d\theta$$

i.e. $$s = 72 + 2\rho g R F_1 \int_0^{\theta} \frac{1-\alpha^3}{3\alpha^2} \sin^{\frac{1}{3}}\theta . d\theta$$

[The integral is negative since $\alpha \geq 1$]

This equation was programmed for a Ferranti Sirius computer using the values of α from table XV and evaluating the integral by the trapezium rule using intervals of 5°. Some values of dynamic surface tension so obtained are shown in figure 20 and all are given in table XVI. They are of the expected order although the curves for 1.5 and 2.0 g/l Lissapol, not shown in the figure, give final values which are larger than the final values for 0.5, 0.7 and 1.0 g/l. In figure 21 the final values obtained (i.e. the static surface tension) on the spherical film are compared with the curve of static surface tension versus Lissapol concentration taken from Cullen and Davidson (12), who made the measurements by the drop weight method. The agreement is reasonable although in every case the values obtained here are high. It is interesting to note that the values from the spherical film for concentrations of 0.5, 0.7 and 1.0 g/l are close to being equal as predicted by the static surface tension curve and this is the value to which the curves for concentrations of 1.5 and 2.0 g/l would be expected to fall. The fact that these curves level off some 15-20 dynes/cm above the expected value may be because it was not possible to obtain accurate film thickness measurements close to the inlet (below 10°) which is the important region in the case of these higher concentrations. Also there is a suspicion of an entry effect giving low values of film thickness in the range 0-15° The only values reported to substantiate this are those for 0.1 g/l Lissapol which has values of α of 0.785 and 0.905 at 10° and 15° respectively (although for calculation these were taken as unity). If there is an entry effect present (which could account for the slightly high values of mass transfer obtained with Hexanol and from extrapolation of the Lissapol curve) the values of α for the higher concentrations of Lissapol should be inflated giving lower values of surface tension.

In general then the values of dynamic surface tension obtained by assuming the presence of surface shear due to the diffusion of surface active agent add weight to the hypothesis. In order further to test the theory, measurements of the time of exposure were made using cine film as explained below.

Measurements of the Time of Exposure.

The presence of surface shear reduces the interfacial velocity and consequently increases the time of exposure of the surface of the spherical film. It has been assumed that $v = \beta u_i$

Now $$u_i = \frac{3L}{4\pi RF_1 \sin^{\frac{1}{3}}\theta}$$

so that $$v = \frac{3L\beta}{4\pi RF_1 \sin^{\frac{1}{3}}\theta}.$$

and the time of exposure becomes $$\frac{4\pi R^2 F_1}{3L} \int_0^{\theta} \frac{\sin^{\frac{1}{3}}\theta}{\beta} d\theta$$

This was programmed for the Ferranti Sirius computer using the values of α already reported and using the trapezium rule. The results, given in table XVII, show the age of the surface for increasing θ, for the six Lissapol concentrations at a flow rate of 2.00 cc/sec. These ages can be used along with the dynamic surface tension values to give the curves of surface tension versus surface age. To discover whether these predictions of the exposure time agree with the true values on the sphere some measurements were made of the time of travel of aluminium particles down the surface.

Using a Magazine Cine-Kodak camera at a nominal camera speed of 64 frames/sec a number of film sequences were taken of aluminium particles flowing from top to bottom of the sphere. In the cases of 0.5 g/l Lissapol solution and of water the timing was made by counting frames between the start and the finish of the path of travel of a particular particle or group of particles. However, this depends on the camera running at a constant speed of 64 f.p.s. and, in the cases of 0.1 g/l, 3.0 g/l Lissapol and of 1.0 g/l Hexanol, a graduated wheel driven at a constant speed of 200 r.p.m. was included in the film sequence to give more accurate timing. The camera speed was checked with this wheel and was found to be fairly constant (within 2%) at 62 f.p.s. This camera speed was used to calculate the exposure times for the water and 0.5 g/l Lissapol.

The measurements were made at flow rates close to 2.00 cc/sec and corrected to exactly 2.00 cc/sec. It proved to be very difficult to make measurements of the time of exposure from 0° to 180° since firstly the particles were difficult to follow over the first 20° when they are travelling almost towards the camera, and secondly since the particles could not be placed on the surface exactly at the inlet. Consequently it was found to be much more accurate to make timings between 30° and 150° to give the following results for the time of exposure in seconds.

	30°-90°	90°-150°	30°-150°
1 g/l n-Hexanol	0.38	0.37	0.75
water	0.33	0.33	0.66
0.1 g/l Lissapol	0.36	0.44	0.80
0.5 g/l Lissapol	0.56	0.51	1.07
3.0 g/l Lissapol	0.40	0.33	0.73

The theoretical values, based on the experimental α's are as follows (taken from table XVII).

	30°-90°	90°-150°	30°-150°
1 g/l n-Hexanol	0.42	0.42	0.85
Water	0.42	0.42	0.85
0.1 g/l Lissapol	0.42	0.53	0.95
0.5 g/l Lissapol	0.62	0.63	1.25

(No measurements of α are available for 3.0 g/l.)

The experimental values are in all cases below the theoretical prediction but the difference between the upper and lower parts of the sphere are in the right direction and of the correct order. Even in the case of 3.0 g/l Lissapol, for which no values of α are available, it can be seen from figure 19 that the upper half is retarded while the lower is not. The difference between the measurements and the predictions of exposure time was thought to be due to the slipping of aluminium particles down the surface since a particle at the surface is bound to introduce some shearing action in the liquid. Assuming the slippage of the particles to be approximately proportional to the time of exposure the results can be compared to n-Hexanol as a standard giving the following experimental and predicted values for the ratio of time of exposure to time of exposure for n-Hexanol.

	30°-90°		90°-150°		30°-150°	
	Measured Values	Predicted Values	Measured Values	Predicted Values	Measured Values	Predicted Values
1 g/l n-Hexanol	1.00	1.00	1.00	1.00	1.00	1.00
Water	0.88	1.00	0.88	1.00	0.88	1.00
0.1 g/l Lissapol	0.95	1.00	1.19	1.26	1.07	1. 12
0.5 g/l Lissapol	1.47	1.47	1.38	1.50	1.43	1.47

Considering the methods of measurement employed the values are not greatly different except that in the case of water the time of exposure is below that expected. This is possibly due to the rippling which has been shown by Friedman and Miller (24) to increase the surface velocity, while Grimley (27) gives values of surface velocity greater than the theoretical for water on a wetted wall column.

These estimates of dynamic surface tension and of time of exposure have added weight to the assumption of an altered velocity profile in the region of Lissapol diffusion. Some independent measurements of the dynamic surface tension of Lissapol would be of value as an unrelated check on the assumptions made here but in the absence of such measurements the velocity profile put forward has been taken as representing the situation and the analysis of the way in which Lissapol affects gas absorption is carried out in the next chapter on the basis of the proposed alteration to the velocity profile.

CHAPTER IX

THE EFFECT of the DIFFUSION of SURFACE ACTIVE AGENTS on GAS ABSORPTION

In the last chapter it has been shown to be reasonable to assume an altered velocity profile of the form

$$u = \frac{\rho g \sin\theta}{2\mu}(fz - z^2) + \frac{z}{f}v \qquad (1)$$

in the region in which the diffusion of surface active material is causing interfacial shear. The surface velocity for such a profile is less than that obtained in the case of zero shear at the interface and it is intuitively obvious that the diffusion into such a profile will be less than that into a half parabolic profile. Before examining the effect of this velocity profile mathematically it is perhaps advisable to consider qualitatively the influence of Lissapol diffusion on the gas absorption to the spherical film.

In figure 19 the region in which the above profile applies is represented by the distance between the two curves and it can be seen that this starts at a low value and increases rapidly to maximum at a Lissapol concentration of 0.5 - 0.7 g/l where after it drops steadily as the concentration of the agent increases. This suggests that the curve of gas absorption versus Lissapol concentration should pass through a minimum in the range 0.5 - 0.7 g/l as indeed experimental measurement has shown. The film thickness measurements with n-Hexanol solutions, along with literature data on their dynamic surface tensions, suggest that the region of reduced mass transfer is extremely small and that there should be no effect of Hexanol concentration on gas absorption. This is also in agreement with experimental observation.

Mathematical Analysis of the Effect of the Altered Profile.

To examine the effect of the new profile quantitatively, the fundamental differential equation for diffusion into the profile must be deduced. If it is assumed, as it was in the case of the normal spherical film, that the stream lines are everywhere parallel to the solid surface, the stream function is independent of θ and the basic mass transfer equation is as before (Appendix Ib, equn. 7).

$$u\left(\frac{\partial c}{\partial \theta}\right)_y = \frac{DR}{f^2}\left(\frac{\partial^2 c}{\partial y^2}\right)_\theta$$

Substituting $z = f - x$ and $y = \frac{x}{f}$ in equation (1) above gives

$$u = \frac{\rho g f^2 \sin\theta}{2\mu}(y - y^2) + v(1 - y) \qquad (3)$$

and from equation (2), chapter VIII

$$v = \frac{L}{\pi R f \sin\theta} - \frac{\rho g f^2 \sin\theta}{6\mu} \qquad (4)$$

Substitution of equations (3) and (4) in equation (2) leads to

$$\left[\left(\frac{L}{\pi Rf\sin\theta} - \frac{\rho g f^2 \sin\theta}{6\mu}\right) + \left(\frac{4\rho g f^2 \sin\theta}{6\mu} - \frac{L}{\pi Rf\sin\theta}\right) y - \frac{\rho g f^2 \sin\theta}{2\mu} y^2\right]\left(\frac{\partial c}{\partial \theta}\right)_y = \frac{DR}{f^2}\left(\frac{\partial^2 c}{\partial y^2}\right)_\theta \quad \text{---} \quad (5)$$

This equation can be solved if the term in y^2 is neglected, which restricts the resulting solution to small depths of penetration.

The relationship for the film thickness of the retarded film is

$$f = \alpha F = \alpha F_1 \sin^{-\frac{2}{3}}\theta = \alpha\left(\frac{3\mu L}{2\pi R\rho g}\right)^{\frac{1}{3}} \sin^{-\frac{2}{3}}\theta.$$

Substituting this in equation (5) and neglecting the y^2 term gives

$$\frac{LF_1}{\pi R^2 \sin^{5/3}\theta}\left[(\alpha^4 - \alpha)y + \left(\alpha - \frac{\alpha}{4}\right)\right]\left(\frac{\partial c}{\partial \theta}\right)_y = D\left(\frac{\partial^2 c}{\partial y^2}\right)_\theta \qquad (6)$$

Put

$$\frac{d\phi}{d\theta} = \frac{\pi R^2}{LF_1} \sin^{5/3}\theta \qquad (7)$$

i.e. ϕ is a function of θ only so that

$$\left(\frac{\partial^2 c}{\partial y^2}\right)_\theta = \left(\frac{\partial^2 c}{\partial y^2}\right)_\phi$$

and substituting (7) in (6) gives

$$\left[(\alpha^4 - \alpha)y + \left(\alpha - \frac{\alpha}{4}\right)\right]\left(\frac{\partial c}{\partial \phi}\right)_y = D\left(\frac{\partial^2 c}{\partial y^2}\right)_\phi \qquad (8)$$

or $(ay + U)\left(\frac{\partial c}{\partial \phi}\right)_y = D\left(\frac{\partial^2 c}{\partial y^2}\right)_\phi \qquad (9)$

where $a = \alpha^4 - \alpha$ and $U = \alpha - \frac{\alpha^4}{4}$

This equation has been solved by Beek and Bakker (3) in the case where a and U are constant and although in this case a and U are weak functions of θ (and so of), the solution has had to be used.

The solution, which applies to the case of small D, is

$$-\frac{1}{ci}\left(\frac{\partial c}{\partial y}\right)_{y=0} = \left(\frac{U}{\pi D\phi}\right)^{\frac{1}{2}} + \frac{a}{4U} - \frac{15}{48}\left(\frac{Da^4\phi}{\pi U^5}\right)^{\frac{1}{2}} \qquad (10)$$

which consists essentially of two correction terms to the normal Higbie type solution.

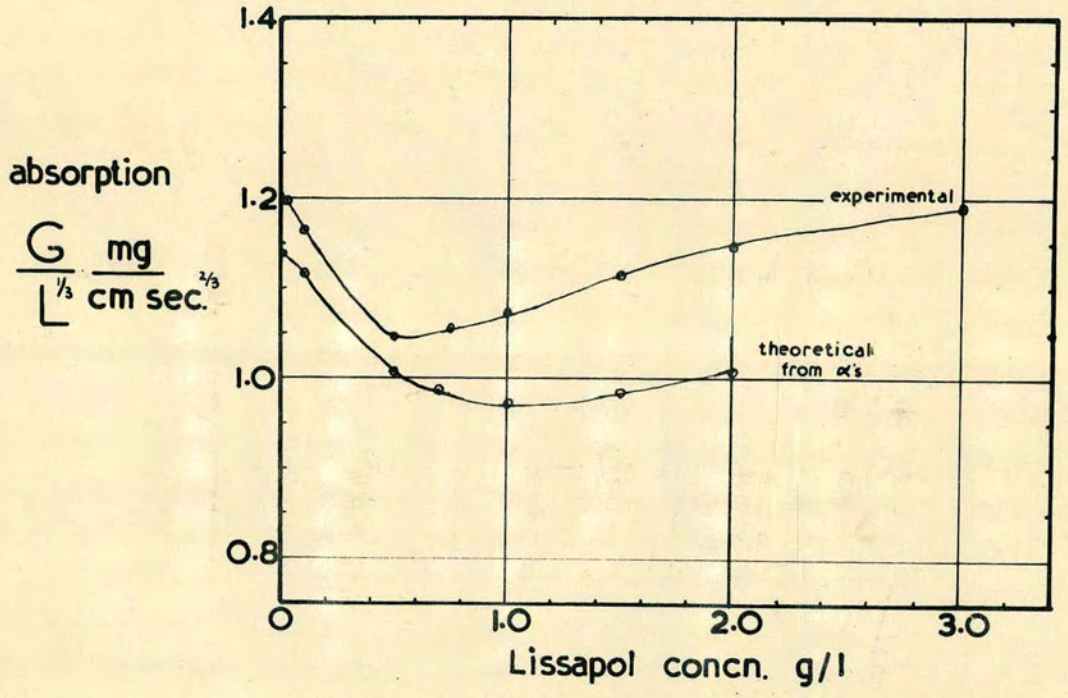

FIG. 22 COMPARISON OF THEORY AND EXPERIMENTAL CURVE FOR EFFECT OF LISSAPOL

The gas absorption for the retarded film, Gr, is given by

$$Gr = -D \int_{\theta_1}^{\theta_2} 2\pi R^2 \sin\theta \left(\frac{\partial c}{\partial x}\right)_i \, d\theta \qquad (11)$$

$$\left(\frac{\partial c}{\partial y}\right)_{y=0} = f \left(\frac{\partial c}{\partial x}\right)_i = \alpha F_1 \sin^{-2/3}\theta \left(\frac{\partial c}{\partial x}\right)_i \qquad (12)$$

and from equation (10)

$$-\frac{1}{c_i} \alpha F_1 \sin^{-2/3}\theta \left(\frac{\partial c}{\partial x}\right)_i = \left(\frac{U}{\pi D \phi}\right)^{\frac{1}{2}} + \frac{a}{4U} - \frac{15}{48} \left(\frac{Da^4 \phi}{\pi U^5}\right)^{\frac{1}{2}} \qquad (13)$$

whence, substituting (13) in (11)

$$Gr = Dc_i \int_{\theta_1}^{\theta_2} \frac{2\pi R^2}{\alpha F_1} \sin^{5/3}\theta \left[\left(\frac{U}{\pi D \phi}\right)^{\frac{1}{2}} + \frac{a}{4U} - \frac{15}{48} \left(\frac{Da^4 \phi}{\pi U^5}\right)^{\frac{1}{2}}\right] d\theta \qquad (14)$$

From equation (7) $\phi = \frac{\pi R^2}{LF_1} \int_{\theta_1}^{\theta_2} \sin\theta^{5/3} d\theta$ (15)

so that finally

$$Gr = 2\pi R^2 \frac{Dc_i}{F_1} \int_{\theta_1}^{\theta_2} \frac{\sin^{5/3}\theta}{\alpha} \left[\left(\frac{U}{\pi D}\right)^{\frac{1}{2}} \left(\frac{LF_1}{\pi R^2}\right)^{\frac{1}{2}} I^{-\frac{1}{2}} + \frac{a}{4U} - \frac{15}{48} \left(\frac{Da^4 R^2}{U^5 LF_1}\right)^{\frac{1}{2}} I^{\frac{1}{2}}\right] d\theta \qquad (16)$$

where $I = \int_{\theta_1}^{\theta_2} \sin^{5/3}\theta . d\theta$

This was programmed for the Sirius computer, for a flow rate of 2.00 cc/sec at which F = 0.0141 cm. The limits of θ were taken as θ° and 175° and the integration was carried out using the trapezium rule in steps of 5° with the α values from table XV.

[Note - The end point of the sphere was taken as 175° instead of 173° for ease of computation.]

The values resulting from this calculation are as follows -

Lissapol Concⁿ. (g/l)	g (sphere only) (mg/sec)	$G/L^{\frac{1}{3}}$	$G/L^{\frac{1}{3}}$ (with take-off)
0.1	1.391	1.104	1.124
0.5	1.248	0.991	1.011
0.7	1.225	0.972	0.992
1.0	1.206	0.957	0.997
1.5	1.222	0.970	0.990
2.0	1.250	0.992	1.012

The correction for the take-off is made merely by adding the same amount of absorption as is obtained in the case of a normal film. Since the concentration profile is slightly different in the case of the retarded film this is not strictly correct but the difference is small.

In figure 22 the result of this computation of the gas absorption from the experimental film thickness is compared with the experimental curve of gas absorption versus Lissapol concentration (from fig. 7). The difference between the

curves at concentrations up to 0.5 g/l is not significant since the theoretical values of the constants used and the corrections applied to the results may not be correct. The agreement up to 0.5 g/l, therefore, is fairly good the gradients of the two curves being very nearly equal. Beyond this value however the curves diverge considerably and the minimum predicted by the theoretical analysis is shallower and at a higher concentration than on the experimental curve.

Reasons for the disagreement between the curves may be

(1) Inadequacy of the mathemetical analysis. At the higher values of concentration the values of α are large and α becomes a stronger function of θ making the assumptions of constant a and u less valid.

(2) At higher concentrations the important region is close to the inlet where measurements are more difficult to make accurately. There is somewhat of a paradox here since the calculation of dynamic surface tension requires α to be larger at the higher concentrations while the mass transfer correlation requires α to be lower. It may be, however, that, at the higher concentrations the diffusion of surface active material in the small crest of liquid at the inlet is important and here the effect of such diffusion on gas absorption is not known.

(3) The dynamic surface tension may be different when CO_2 is dissolving in the film to that obtained when film thickness measurements are made in air. This point is substantiated by some work on the effect of ionic materials on the surface ageing which is reviewed below.

On the whole the agreement between the curves is fairly good and merits deeper experimental investigation the possible lines of which will be discussed in the next chapter. A further look at the literature in the light of the present theory is informative.

A Comparison of the Present Work with the Literature.

Some work on the flow of films of surface active agent solutions has been done by Jackson (33) who used a radioactive tracer method to measure film thicknesses for water and 0.1% (weight) solutions of Ethomeen c/15 on a wetted-wall column. He reports no difference between the thicknesses with and without the agent. However, his point of measurement was 12" from the inlet and from his flow rate values the surface ages in his work were in the range 1.5 - 70 seconds. Thus in his case it is possible that the surface tension had reached its equilibrium value before the point of measurement.

Grimley (27) gives a graph of velocity distribution on a wetted-wall column fed with water containing traces of surface active agent. This shows a peak velocity some tenth of the depth of the film beneath the surface, i.e., the surface velocity, as in the present case, is not the maximum velocity. He also finds the thickness to be greater with surface active agent present but no details of surface age are given. Brotz (6) also reports the thickness of films containing agents to be greater than for water.

Much of the work reviewed in chapter I on the effect of surface active agents on gas absorption can also be explained on the basis of diffusion of the agents. Ternovskaya and Belopolskii (49), who found agents could have a similar effect to that detected in the present case, used a column 16" long by 1.4" diameter with a flow rate of 80 cc/sec. This gives an exposure time of just under a second which is of the same order as that obtained on the sphere. The agents they used were Mersolat (c 15-20), Sulfonol and Mekol (Sodium - 2 Butyl naphthalen sulphonate). The latter gave a curve very similar to that obtained here with Lissapol.

Raimondi and Toor (43) examined the effect of Petrowet on absorption in a liquid jet and found that for a fixed contact time of 0.002 sec. the absorption passed through a minimum at a particular surface active agent concentration. They mention the possible effect of the diffusion of the agent but do not consider the influence of surface shear. Also using Petrowet, Emmert and Pigford (22) found an 11% decrease in absorption in a small column giving a contact time of about 0.1 seconds while in the larger column in which they detected a mimimum mass transfer rate at a particular concentration of Petrowet the exposure time was about 2 seconds. In all of these cases the exposure time is such that the agents could be affecting the absorption by altering the hydrodynamics.

Cullen and Davidson (12) have examined the effect of Lissapol on the absorption in a system geometrically similar to the present one and obtain a similar shape of curve on which they find

At 2.00 cc/sec Minimum at 0.72 g/l Lissapol
At 5.00 cc/sec Minimum at 0.82 g/l Lissapol.

These figures are exactly in accordance with the theory since for the shorter contact time the Lissapol concentration needs to be higher to produce the maximum effect. They also find that they have to go up to a concentration of 10 g/l before the absorption rate returns to the theoretical. This is also in accordance with the theory since, forthe smaller system, giving about a third of the contact time, the concentration needs to be about three times greater before the agent diffuses quickly enough to have a negligible effect on the absorption.

Cullen and Davidson also found that pure sodium dodecyl sulphate had no effect on absorption unless it was contamin-

ated with dodecanol. To explain this on the present theory requires that the ageing of the surface be slower with dodecanol present. This is confirmed by some work of Burcik and Newman (8) whose measurements of dynamic surface tension by the vibrating jet technique show that dodecanol decreases the rate of fall of the surface tension of sodium dodecyl sulphate as well as reducing the equilibrium value. As an example a 0.015 M solution of sodium dodecyl sulphate takes 0.01 secs. to fall to an equilibrium value of 37.7 dynes/cm. while the same solution with 7% (weight) of dodecanol (i.e. % of the sulphate weight) took 0.03 secs to reach an equilibrium value of 22.1 dynes/cm. They claim that this reduction in the ageing rate is due to the formation of organic complexes and this could be the cause of the effect noted by Cullen and Davidson.

The literature so far reviewed is capable of explanation on the basis of the theory developed from this work but the work of Harvey and Smith (31) appears not to fit into the pattern. In an entirely static system they find an interfacial resistance when CO_2 is absorbing in Lissapol solutions. At 0.83 g/l Lissapol they find k_s = 0.023 cm/sec while the smallest k_s in the present case is about 0.03 cm/sec (i.e. of the same order). The present theory has no explanation for an effect in a static system where surface tension gradients should not exist. The work of Garner and Skelland (25) on droplet mass transfer mentioned in chapter I, showed that in the presence of surface active agents the transfer rate could fall below the rate for solid spheres and again it is difficult to see how the present theory could explain this fact. However in liquid-liquid transfer the influence of shearing rates is more important and the situation is somewhat different from the gas absorption case.

In the case of bubble mass transfer however it has been noted that surface active agents reduce the rate of rise or fall of bubbles or droplets. The work has been reviewed in a paper by Gibbons et al (26) who examined the rate of rise of benzene drops in water. The reduction in the rates of rise could be explained by the presence of shear due to the surface active agent diffusing to the surface which is being continually renewed.

A Review of the Theory of Surface Active Agent Diffusion.

At present it is not possible to analyse the diffusion mechanism of surface active agents and no mathematical anaylsis of the diffusion of Lissapol has been attempted here. The first reliable measurements of dynamic surface tension were made by Addison (2) who developed the vibrating jet technique, mathematical analysis of the measurements was attempted by Ward and Tordai (51) who suggested that material in the sub-surface layers moved immediately to the interface and this was followed by normal diffusion from the bulk liquid to the sub-surface. The diffusion coefficients obtained by this

method are, in many cases, very small and the problem is to explain why the attainment of surface equilibrium is so slow. Burcik and his co-workers (7, 8, 9) have done a considerable amount of work on surface ageing in the presence of other organic materials and foreign ionic substances. They claim (8) that "the rate of fall (of surface tension) is a function of the structure and concentration of the surface active agent the temperature, the pH of the solution when the agent hydrolyses and the concentration of added electrolyte when the surfactant is ionic". In the case of ionic agents it is claimed that the presence of the surface active ion at the surface sets up a repulsion to other active ions diffusing to the surface. This could explain the low rates of ageing in some cases. In the light of this work of Burcik, future investigation of the effect of surface activity on the mass transfer may have to include examination of the effect of pH and electrolyte concentration. In the present case the ageing of the Lissapol solutions may be different when CO_2 is present in the solution and in fact this may be part of the explanation of the difference between the experimental and theoretical curves in figure 23. To test this it would be necessary to measure the film thicknesses when absorption is taking place.

Rideal and Sutherland (45) claim that convection plays a part in the diffusion of surface active agents and they also mention that, in the oscillating jet, the surface age may be increased because of the hindering effect of the surface tension gradients. This is the only mention of surface shear arising from surface ageing that has been found in the literature.

Recent work on the theory of surface active agent diffusion and dynamic surface tension measurements may be found in references 7-9, 18-20, 29, 30, 35, 38, 41 some of which are not reviewed here since they contain nothing with a direct bearing on the present work.

CHAPTER X

GENERAL CONCLUSIONS

(1) Absorption rates obtained with the entire spherical film are in general agreement with theoretical predictions (Chapter IV).

(2) n-Hexanol in small concentrations in water has no effect on the gas absorption rate apart from eliminating the rippling encountered with a water film (Chapter IV, page 16).

(3) Lissapol, in the concentration range 0 - 3.0 g/l, in water causes a reduction in gas absorption to the spherical film which cannot be explained on the basis of elimination of the rippling alone (Chapter IV, pages 16 and 17).

(4) A stagnant layer end effect has been detected on a hemispherical falling film. Measurements made of this end effect can be explained by assuming that a fully parabolic velocity profile develops beneath the stagnant surface layer (Chapter VI).

(4) The height of the stagnant layer is not dependent only upon surface tension and shear forces but probably also depends on the ability of surface active molecules to "stack" upon one another (Chapter VI).

(6) Aqueous solutions of n-Hexanol have an end-effect similar to that obtained with water but Lissapol solutions exhibit a somewhat different behaviour. The surface of the Lissapol film close to its termination is not entirely stagnant but is greatly retarded and the amount of retardation depends on the bulk concentration of Lissapol, (Chapter VI).

(7) Absorption rates to films of Liquid flowing over less than the entire sphere are considerably below experimental predictions. This can be explained by the reduced absorption into the fully parabolic profile of the end effect (Chapter V).

(8) The film thickness of water and of dilute aqueous solutions of n-Hexanol flowing over a sphere are close to theoretical predictions (Chapter VII, pages 29 and 30).

(9) Dilute aqueous Lissapol solutions have a region on the sphere in which the film thickness is greater than the prediction. The extent and position of this region depends on the bulk concentration of Lissapol (Chapter VIII, pages 29-32).

(10) The measured time of exposure of dilute aqueous Lissapol films on the sphere is greater than that of aqueous n-Hexanol solutions or of water and the retarded region has been shown roughly to correspond with the thickened region (Chapter VIII, pages 39 and 40).

(11) A velocity profile, based on interfacial shear arising from surface tension gradients on the film before surface equilibrium with respect to Lissapol has been established, explains the region of thickened and retarded film (Chapter VIII, pages 35-37).

(12) Estimates of the dynamic surface tension of Lissapol, made using this altered velocity profile and the film thickness measurements, are in general agreement with expected values (Chapter VIII, pages 37-39).

(13) The altered profile and film thickness measurements give times of exposure of the same order of magnitude as the measured times, (Chapter VIII, page 40).

(14) Estimates of the gas absorption to the film of aqueous Lissapol with the altered velocity profile are in reasonable agreement with experimental measurements of the effect of Lissapol on the absorption (Chapter IX).

(15) The effect of surface active materials on gas absorption to a falling liquid film can be split into three parts -

viz. The suppression of rippling.
The effect of their diffusion to the surface.
The end effect they produce.

At least part of the interfacial resistance frequently postulated in gas absorption systems using surface active materials can be explained by hydrodynamic alterations produced by the diffusion of the materials to the surface. It cannot be said with certainty, however, that the effect of the agent is purely hydrodynamic.

SUGGESTIONS for FURTHER WORK

One of the drawbacks of the present work is the fact that the film thickness measurements were made independently of the absorption measurements. Consequently it would be extremely interesting to make some measurements of film thickness in the present system while absorption was taking place. This would show whether the presence of carbon dioxide has any effect on the surface ageing. Such measurements could perhaps best be made using a capacitometer (21) and, if the results were promising, work could be extended to other agents.

It might be possible to develop a method of estimating dynamic surface tensions by film thickness measurement using a cylinder rather than a sphere which is useful only when absorption measurements are also being made. Careful design could produce a column in which entry effects were unimportant and exposure times and perhaps even velocity profiles could be measured more easily than on the sphere. It would also be interesting to make dynamic surface tension measurements using an apparatus described by Defay and Hommeln (19) to compare with the results obtained here.

APPENDIX I

ANALYSIS of the FLUID MECHANICS and MASS TRANSFER for a SPHERICAL LIQUID FILM

The system has already been studied by Lynn et al (37) and by Davidson and Cullen (15) and the relationships derived by these workers for the theoretical evaluation of the film thicknesses and the mass transfer rates have been used in the present work. The assumptions made and the important steps in the development of the theory are shown below along with some of the theoretical values; complete details may be found in the references to the literature.

(a) The fluid mechanics of the System.

The basic assumptions made are as follows -

(1) The streamlines of flow in the liquid film are everywhere parallel to the solid surface.

(2) The velocity profile in the film is half parabolic.

This leads to the following equations

$$u = u_i (1 - y^2) \qquad (1)$$

$$u_i = \frac{3L}{4\pi R F_1} \operatorname{Sin}^{-\frac{1}{3}}\theta \qquad (2)$$

$$F = F_1 \operatorname{Sin}^{-\frac{2}{3}}\theta \qquad (3)$$

$$F_1 = \left(\frac{3\mu L}{2\pi R \rho g}\right)^{\frac{1}{3}} \qquad (4)$$

At a point θ from the inlet to the sphere the interfacial velocity is given by equation (2). Considering an element subtending an angle $d\theta$ at θ the elemental time of exposure is given by.

$$de = \frac{4\pi R^2 F_1}{3L} \operatorname{Sin}^{\frac{1}{3}} \theta \, d\theta$$

Thus the time of exposure to angle θ is given by

$$e = \frac{4\pi R^2 F_1}{3L} \int_0^{\theta} \operatorname{Sin}^{\frac{1}{3}} \theta \, d\theta \qquad (5)$$

Values of F, F_1 and the product $eL^{\frac{2}{3}}$ are given below.

Values of Equatorial Thickness F_1 for Various Flow Rates.

Flow Rate, L cc/sec	0.2	0.5	0.7	1.0	2.0
Thickness, F_1 cm x 10^2	0.655	0.889	0.995	1.120	1.410

3.0	4.0	5.0	6.0
1.618	1.773	1.912	2.035

Values of the Ratio F/F_1 for Various Values of θ. (symmetrical about 90°).

Angle, θ°	5	7	10	15	20	30	40	50
Ratio, F/F_1	5.12	4.10	3.22	2.46	2.05	1.59	1.35	1.20
Angle, θ°	175	173	170	165	160	150	140	130

60	70	80	90
1.10	1.04	1.01	1.00
120	110	100	90

Substituting equation (4) in equation (5)

$$e = \left(\frac{32\pi^2 R^5 \mu}{9 \rho g L^2}\right)^{\frac{1}{3}} \int_0^{\theta} \mathrm{Sin}^{\frac{1}{3}} \theta \, d\theta \qquad (6)$$

i.e. e is a function of L_2 and of θ and to simplify evaluation of exposure times $eL^{\frac{1}{3}}$ is evaluated for various values of θ.

Angle, θ	10	20	30	40	50	60
Integral, Rads.	0.059	0.168	0.299	0.444	0.598	0.760
$eL^{\frac{1}{3}}$ cm^2 $sec^{\frac{1}{3}}$	0.040	0.116	0.206	0.306	0.412	0.524

70	80	90	100	110	120
0.930	1.100	1.274	1.448	1.619	1.782
0.641	0.758	0.878	0.998	1.116	1.228

130	140	150	160	170	180
1.950	2.111	2.256	2.387	2.497	2.555
1.344	1.455	1.555	1.645	1.721	1.761

(b) <u>The Mass Transfer to the Spherical Film</u>.

The differential equation for diffusion in the liquid film is constructed by carrying out a mass balance on an element in the film to give ultimately the equation

$$\frac{F^2 u}{R}\left(\frac{\partial c}{\partial \theta}\right)_y = D\left(\frac{\partial^2 c}{\partial y^2}\right)_\theta \qquad (7)$$

substituting equation (1) i.e. $u = u_i (1 - y^2)$

and putting $\frac{d\phi}{d\theta} = \frac{R}{u_i F^2}$ (8)

gives $(1 - y^2)\left(\frac{\partial c}{\partial \phi}\right)_y = D\left(\frac{\partial^2 c}{\partial y^2}\right)_\phi$ (9)

with boundary conditions.

(1) The surface of the liquid is in equilibrium with the gas

$c = c_i$ at $y = o$ all θ.

(2) No solute crosses the solid boundary

$\frac{\partial c}{\partial y} = 0$ at $y = 1$ all θ.

(3) $c = c_o$ at $\theta = \theta_1$ (entry to system) all y.

The rate of gas absorption is given by

$$G = 2\pi R^2 D \int_{\theta_1}^{\theta_2} - \sin\theta \left(\frac{\partial c}{\partial x}\right)_i d\theta \qquad (10)$$

which simplifies to

$$G = \frac{3}{2} LD \int_0^\phi - \left(\frac{\partial c}{\partial y}\right)_{y=o} d\phi \qquad (11)$$

$\left(\frac{\partial c}{\partial y}\right)_{y=o}$ is found by solving equation 9 with the given boundary conditions.

The solutions for small depths and larger depths of penetration are given by Davidson and Cullen (15) and are quoted on page 8. For small depths of penetration the y^2 term is ignored and the solution is of the Higbie type. Including the y^2 term gives a series solution which gives a better value at large depths of penetration. For purposes of comparison the values of G for the 3" diameter sphere excluding the take-off are given in the table below.

Flow Rate L cc/sec	G by Simple Solution mg/sec	G by Series Solution mg/sec
0.20	0.659	0.376
0.50	0.894	0.795
0.70	0.001	0.949
1.00	1.127	1.102
1.25	1.214	1.198
1.50	1.290	1.280
1.75	1.358	1.352
2.00	1.420	1.417
2.50	1.530	1.531
3.00	1.625	1.630
3.50	1.711	1.718
4.00	1.789	1.798
4.50	1.861	1.872
5.00	1.927	1.940

5.50	1.989	2.005
6.00	2.048	2.067
7.00	2.156	2.182
8.00	2.254	2.291

The figures show that the two solutions agree very closely in the range 2.00 - 3.00 cc/sec.

APPENDIX II

Evaluation of the Absorption for the Experimental System

The experimental system used consists of a 3" diameter sphere supported on a $\frac{3}{8}$" tube $1\frac{1}{4}$" long. The absorption is evaluated for the two extremes of no-mixing and complete mixing at the junction.

(a) No Mixing.

According to the theoretical treatment employed by Davidson and Cullen (15) a spherical film is equivalent to a wetted wall column of the same radius R and of length 1.676R.

Thus, in this case the sphere is equivalent to column of length 6.39 cms. and radius 3.81 cms. In order to allow for the short supporting tube this column must be converted into the equivalent length column of radius 0.476 cms., the same as that of the supporting tube.

Pigfords solution for the wetted wall column is (22)

$$\frac{c_i - c_1}{c_i - c_o} = 0.7857 \exp(-5.121p) + 0.1001 \exp(-39.31p) + 0.0360 \exp(-105.6p) + 0.01811 \exp(-204.7p) \text{ etc.}$$

where c_i = interfacial concentration
c_o = concentration at entry to system and $p = \frac{De}{F^2}$
c_1 = concentration at outlet of system.

$$e = \frac{4\pi rhF}{3L} \qquad F = \left(\frac{3\mu L}{2\pi r \rho g}\right)^{\frac{1}{3}}$$

$$\therefore p = \frac{4\pi rhD}{3L}\left(\frac{2\pi r\rho g}{3\mu L}\right)^{\frac{1}{3}}$$

Column (1) $h = 6.39$, $r = 3.81$ $\therefore p_1 = \frac{4\pi D}{3L}\, 6.39 \times 3.81 \left(\frac{2\pi\rho g}{3\mu L}\right)^{\frac{1}{3}} (3.81)^{\frac{1}{3}}$

Column (2) $h = h_2$, $r = 0.476$ $\therefore p_2 = \frac{4\pi D}{3L}\, 0.476 h_2 \left(\frac{2\pi\rho g}{3\mu L}\right)^{\frac{1}{3}} (0.476)^{\frac{1}{3}}$

For the columns to be equivalent $p_1 = p_2$

$$\therefore h_2 = 6.39 \left(\frac{3.81}{0.476}\right) = 102.1 \text{ cms.}$$

$\therefore$ Sphere is equivalent to a wetted-wall column of 0.476 cms. radius and 102.1 cms. long.

The take-off length is 3.18 cms.

$\therefore$ Complete system is equivalent to a column of h = 105.3 cms
r = 0.476 cms

Using these values along with $D = 1.38 \times 10^{-5}$ cm^2/sec
$\mu/\rho = 0.0114$ cm^2/sec
$g = 981$ cm/sec^2
) at 15°C

We have $p = \frac{0.1279}{L^{4/3}}$

From the series solution above with $C_o = 0$

$$G = Lc_i \left[1 - 0.7857 \exp(-5.121p) - 0.1001 \exp(-39.31p) - 0.0360 \exp(-105.6p) - 0.01811 \exp(-204.7p)\right]$$

At 15°C $c_i = 1.888$ mgs/cm^3

Using this solution values of G for flow rates in the range 0-8.0 cc/sec were calculated on a Ferranti Pegasus Computer. The values are quoted in the table below.

(b) Mixing.

The absorption for the sphere only (using the series solution) has been given in Appendix I. Using these figures the mean concentration at the outlet can be calculated and used as the entry concentration to the short wetted-wall column take-off for which the absorption can be evaluated by

$$G_{t.o.} = 4r \left(\frac{\pi D}{2}\right)^{\frac{1}{2}} \left(\frac{9\rho g}{\mu}\right) \left(\frac{1}{2\pi r}\right)^{\frac{1}{3}} l^{\frac{1}{2}} L^{\frac{1}{3}} (c_i - c_o).$$

Flow Rate, L cc/sec	0.20	0.50	0.70	1.00	1.25
Concn. C_o mg/cc	1.882	1.590	1.356	1.102	0.959
Take-off Absorption G mg/sec	0.000	0.025	0.050	0.083	0.105

1.50	1.75	2.00	2.50	3.00
0.853	0.773	0.708	0.612	0.543
0.119	0.141	0.156	0.182	0.204

3.50	4.00	4.50	5.00	5.50
0.491	0.450	0.416	0.388	0.365
0.223	0.239	0.255	0.270	0.283

6.00	7.00	8.00
0.344	0.312	0.286
0.295	0.317	0.331

(c) The complete set of results of the calculations for the two cases (a) and (b) for the whole system (sphere and take-off) are shown below.

Flow Rate, L cc/sec	0.20	0.50	0.70	1.00	1.25
Absorption with Mixing G mg/sec	0.376	0.820	0.999	1.185	1.303
Absorption no Mixing G mg/sec	0.376	0.801	0.959	1.116	1.214

1.50	1.75	2.00	2.50	3.00
1.399	1.493	1.573	1.713	1.834
1.297	1.370	1.436	1.551	1.652

3.50	4.00	4.50	5.00	5.50
1.941	2.037	2.127	2.210	2.288
1.741	1.822	1.897	1.966	2.032

6.00	7.00	8.00
2.362	2.499	2.628
2.094	2.211	2.321

APPENDIX III

CALCULATION of the ABSORPTION RATE from the EXPERIMENTAL DATA

Let - Inlet Gas Rate = V_i cc/sec Outlet Gas Rate = V_o cc/sec

Then if Q_i and Q_o are the total pressures at inlet and outlet respectively and q_i and q_o are the respective saturated water vapour pressures

$$\text{Inlet } CO_2 \text{ rate} = \frac{Q_i - q_i}{Q_i} V_i$$

$$\text{Outlet } CO_2 \text{ rate} = \frac{Q_o - q_o}{Q_o} V_o$$

The pressure drop through the system is very small so that $Q_i = Q_o = Q$, the prevailing atmospheric pressure.

The change in temperature of the gas is also small so that q_i can be taken as equal to q_o or simply q.

Thus Inlet CO_2 rate $= \frac{Q - q}{Q} V_i$ Outlet CO_2 rate $= \frac{Q - q}{Q} V_o$.

The gm. molecular volumes at inlet and outlet are given by

$$\frac{22.4 \times T_i \times 760}{273.2 \times Q} \text{ and } \frac{22.4 \times T_o \times 760}{273.2 \times Q} \text{ litres/gm Mole resp.}$$

Hence the absorption rate as measured, G_m, is given by

$$G_m = \frac{273.2 \times Q \times 44}{22.4 \times 760} \times \frac{Q - q}{Q} \left(\frac{V_i}{T_i} - \frac{V_o}{T_o}\right).$$

This is the absorption at a partial pressure of CO_2 of $Q - q$, correcting to 760 mm. we have

$$G = \frac{Q - q}{Q} \left(\frac{V_i}{T_i} - \frac{V_o}{T_o}\right) \times \frac{273.2 \times Q \times 44}{22.4 \times 760} \times \frac{760}{Q - q}$$

i.e. $G = 536.6 \left(\frac{V_i}{T_i} - \frac{V_o}{T_o}\right)$.

APPENDIX IV

THE EFFECT of TEMPERATURE on the ABSORPTION RATE

The theoretical solution for the Absorption rate at small depths of penetration is

$$G = 4.49 \left(\frac{2\pi}{3}\right)^{\frac{1}{6}} \left(\frac{\rho g}{\mu}\right)^{\frac{1}{6}} D^{\frac{1}{2}} R^{\frac{7}{6}} L^{\frac{1}{3}} (C_i - C_o)$$

for the whole sphere.

The quantities which are temperature dependent are D, ρ, μ and C_i. i.e. $G = KL^{\frac{1}{3}}$ where K is a temperature dependent constant. The variation of D with temperature was taken from Davidson and Cullen (15): the variations of μ and ρ with temperature were taken from Perry (42). The concentration/temperature gradient for CO_2 in water was taken from the Handbook of Chemistry and Physics (28) and was used along with the value C_i = 1.606 mgs/cc at 20°C to find the values of C_i at the required temperatures. Using these values the constant K can be calculated at temperatures between 12 and 20°C as shown below.

Temperature °C	Diffn. Coefft. D $\frac{cm^2}{sec}$ x 10^5	Solubility C_i mgs/sec	Viscosity $\frac{gms}{cm.sec}$	Density $\frac{gms}{cm^3}$	Constant K $\frac{mgs}{cm.sec^{\frac{2}{3}}}$
12	1.23	2.083	0.0124	1.000	1.157
13	1.28	2.016	0.0120	0.999	1.148
14	1.33	1.950	0.0117	0.999	1.136
15	1.38	1.888	0.0114	0.999	1.125
16	1.43	1.821	0.0111	0.999	1.110
17	1.49	1.763	0.0108	0.999	1.102
18	1.54	1.707	0.0106	0.999	1.088
19	1.59	1.655	0.0103	0.998	1.027
20	1.65	1.606	0.0101	0.998	1.068
21	1.69	1.558	0.0098	0.998	1.054
22	1.74	1.508	0.0096	0.998	1.039
23	1.80	1.458	0.0094	0.998	1.026
24	1.87	1.411	0.0091	0.997	1.016
25	1.93	1.366	0.0089	0.997	1.003

A graph of K against T shows that K is proportional to T and is given by the equation

$$K = 1.304 - 0.012T$$

where the units are

$$K - \text{mgs sec}^{-\frac{2}{3}} \text{cm}^{-1} \quad T \ ^{o}C$$

For two different temperatures, T and T^1, we have

$$G^1 = K^1 L^{\frac{1}{3}} \quad \text{and} \quad G = KL^{\frac{1}{3}}$$

$$\therefore \quad \frac{G^1}{G} = \frac{K^1}{K} = \frac{1.304 - 0.012T^1}{1.304 - 0.012T}$$

The results of absorption at T can be corrected, using this ratio, to a standard temperature T^1 taken as 15°C for which the theoretical absorption has been calculated.

Thus

$$\frac{G^1}{G} = \frac{1.304 - 0.012 \times 15}{1.304 - 0.012T} = \frac{0.862}{1.00 - 0.0092T}$$

This ratio G^1/G, denoted by P, is the correction factor by which experimental absorption rates at T°C must be multiplied. Values of P at temperatures between 12 and 20°C are shown below.

T	P
12.0	0.969
12.5	0.975
13.0	0.980
13.5	0.985
14.0	0.990
14.5	0.995

T	P
15.0	1.000
15.5	1.006
16.0	1.011
16.5	1.017
17.0	1.022
17.5	1.028

T	P
18.0	1.034
18.5	1.040
19.0	1.045
19.5	1.052
20.0	1.057
20.5	1.063

Since the theoretical absorption for latitudes less than 180° involves the temperature dependent variables to the same powers as the absorption for the whole sphere, the above factors apply to absorption over any latitude θ.

APPENDIX V

CORRECTION to ALLOW for the DESORPTION of AIR

Since the liquid used is saturated with air while the atmosphere surrounding the absorbing film contains only CO_2 and H_2O vapour, oxygen and nitrogen will desorb from the film. This will be a liquid film controlled desorption for which the differential equation will be the same as that for absorption.

viz. $(1 - y^2)\left(\frac{\partial c}{\partial \theta}\right)_y = D\left(\frac{\partial^2 c}{\partial y^2}\right)$

but the boundary conditions will be different.

For absorption	For desorption
$c = ci$ at $y = 0$	$C = 0$ at $y = 0$
$\frac{\partial c}{\partial y} = 0$ at $y = 1$	$\frac{\partial c}{\partial y} = 0$ at $y = 1$
$C = C_0$ at $\theta = \theta_0$	$C = C$ at $\theta = \theta_0$

The solutions are exactly similar apart from the direction of the concentration gradient and hence, if G^1 = the desorption rate of oxygen or nitrogen, it can be shown that

$$\frac{G}{G^1} = \frac{D_{CO2}^{\frac{1}{2}}\, C_{CO2}}{D^{\frac{1}{2}}\, C}$$

Diffusivity data can be found in a paper by Wilkie (52) and although the value for CO_2 does not agree with Davidson's value the value according to Wilkie is used since the values of D for oxygen and nitrogen are taken from the same source.

Thus $D_{CO_2} = 1.48 \times 10^{-5}$ $D_{O_2} = 0.97 \times 10^{-5}$ $D_{N_2} = 1.24 \times 10^{-5}$ cm/sec all at 15°C.

Solubility data is taken from the Handbook of Chemistry and Physics (28) and is as follows

$C^*_{CO_2} = 2.0$ mgs/cc $C^*_{O_2} = 1.01 \times 10^{-2}$ mgs/cc $C^*_{N_2} = 1.69 \times 10^{-2}$ mgs/cc } at the partial pressures as they occur in air.

Hence

$$\frac{G_{CO_2}}{G^1_{O_2}} = \left(\frac{1.48}{0.97}\right)^{\frac{1}{2}} \left(\frac{2}{1.01} \times 10^2\right) = 244$$

$$\frac{G_{CO_2}}{G^1_{N_2}} = \left(\frac{1.48}{1.24}\right)^{\frac{1}{2}} \left(\frac{2}{1.69} \times 10^2\right) = 129$$

Thus letting

G_a = Actual CO_2 absorption rate mgs/sec
G_m = Measured CO_2 absorption rate mgs/sec.

Vol. of O_2 (at 15°C and 760 mm) desorbed $= \frac{G_a}{244} \times \frac{23.6}{32}$

$= \frac{G_a}{330}$ cc/sec

Vol. of N_2 (at 15°C and 760 mm) desorbed $= \frac{G_a}{129} \times \frac{23.6}{28}$

$= \frac{G_a}{153}$ cc/sec.

i.e. Total volume of gas desorbed $= \frac{G_a}{105}$ cc/sec.

Now Measured Volume change = Volume Rate of Absorption
- Volume Rate of Desorption.

and Measured Vol. change $= \frac{23.6}{44} G_m$

Vol. Rate of Desorption $= \frac{23.6}{44} G_a$

$\therefore \frac{23.6}{44} G_m = \frac{23.6}{44} G_a - \frac{G_a}{105}$

i.e. $G_m = G_a - 0.018\ G_a$

$\therefore G_a = 1.018\ G_m$

i.e. All measured absorption rates must be multiplied by 1.018 to correct for desorption of air.

APPENDIX VI

CALCULATION of THEORETICAL ABSORPTION for DIFFERENT LATITUDES on the SPHERE

Following Davidson's solution, quoted in Appendix Ib

$$G = \frac{3LD}{2}\int_0^{\phi} -\left(\frac{\partial c}{\partial y}\right)_{y=0}\, d\phi \qquad (1)$$

For small depths of penetration the Higbie type solution can be used.

$$\frac{C_i - C_o}{C_i - C_o} = \operatorname{erfc}\left(\frac{y}{2\sqrt{\phi D}}\right) \qquad (2)$$

$C_o = 0$

$$\therefore \frac{C}{C_i} = 1 - \operatorname{erf}\frac{y}{2\sqrt{D\phi}}$$

$$\therefore \frac{1}{C_i}\frac{\partial c}{\partial y} = -\frac{\partial}{\partial y}\left(\operatorname{erf}\frac{y}{2\sqrt{D\phi}}\right)$$

Now $\operatorname{erf} x = \frac{2}{\sqrt{\pi}}\int_0^x e^{-t^2}\, dt = \frac{2x}{\sqrt{\pi}}\left[1 - \frac{x^2}{1!\,3} + \frac{x^4}{2!\,5} - \frac{x^6}{3!\,7} - \right] \quad x^2 < \infty$

$$\therefore \frac{1}{C_i}\frac{\partial c}{\partial y} = \frac{\partial}{\partial y}\left[\frac{2}{\sqrt{\pi}}\frac{y}{2\sqrt{D\phi}} + \text{terms in } y^2 \text{ and higher powers}\right]$$

$$\therefore \frac{1}{C_i}\left(\frac{\partial c}{\partial y}\right)_{y=0} = -\frac{1}{\sqrt{D\pi\phi}}$$

$$\therefore -\left(\frac{\partial c}{\partial y}\right) = \frac{C_i}{\sqrt{\pi D}}\phi^{-\frac{1}{2}} \qquad (3)$$

$$\therefore G = \frac{3LD}{2}\int_0^{\phi}\frac{C_i}{\sqrt{\pi D}}\phi^{-\frac{1}{2}}\, d\phi$$

$$= \frac{3LD}{2}\frac{2C_i}{\sqrt{\pi D}}\phi^{\frac{1}{2}} = 3LC_i\sqrt{\frac{D}{\pi}}\phi^{\frac{1}{2}} \qquad (4)$$

ϕ is defined by $\frac{d}{d\theta} = \frac{R}{u_i F^2}$ and $F = F_1 \operatorname{Sin}^{\frac{2}{3}}\theta$, $u_i = u_i \operatorname{Sin}^{-\frac{1}{3}}\theta$

$$\therefore \frac{d\phi}{d\theta} = \frac{R}{u_i F_1^2}\operatorname{Sin}^{5/3}\theta$$

$$\therefore \phi = \frac{R}{u_{i_1} F_1^2}\int_{\theta_1}^{\theta_2}\operatorname{Sin}^{5/3}\theta\, d\theta \qquad F_1 = \left(\frac{3\mu L}{2\pi R\rho g}\right)^{\frac{1}{3}}$$

$$u_i = \frac{3L}{4\pi R F_1}$$

Substituting for ϕ, u_i and F_1 in equation (4).

$$G = 3LC_i\sqrt{\frac{D}{\pi}}\left(\frac{4\pi R^2}{3L}\right)^{\frac{1}{2}}\left(\frac{2\pi R\rho g}{3\mu L}\right)\left[\int_{\theta_1}^{\theta_2}\operatorname{Sin}^{5/3}\theta\, d\theta\right]^{\frac{1}{2}}$$

Values used (15°C)

$D = 1.38 \times 10^{-5}$ cm^2/sec $g = 981$ cm/sec^2

$\mu/\rho = 0.0114$ cm^2/sec $R = 3.81$ cms.

$C_i = 1.888$ mgs/cc

whence

$$G = 0.870 \times L^{\frac{1}{3}}\left[\int_{\theta_1}^{\theta_2}\operatorname{Sin}^{5/3}\theta\, d\theta\right]^{\frac{1}{2}}$$

The integral must be evaluated graphically for different values of θ_2, the angle at which the spherical film ends. The complete table of values is shown below.

Angle θ^o	Integral (Rads)	$(\text{Integral})^{\frac{1}{2}}_{(\text{Rads})^{\frac{1}{2}}}$	$G/L^{\frac{1}{3}}$
6	0.0009	0.0301	0.0262
10	0.0035	0.0596	0.0518
15	0.0103	0.1016	0.0884
20	0.0221	0.1485	0.1292
25	0.0396	0.1990	0.1731
30	0.0637	0.2523	0.2195
35	0.0946	0.3076	0.2676
40	0.1324	0.3638	0.3165
45	0.1773	0.4211	0.3664
50	0.2295	0.4790	0.4167
55	0.2888	0.5374	0.4675
60	0.3544	0.5953	0.5179
65	0.4256	0.6524	0.5676
70	0.5020	0.7085	0.6164
75	0.5827	0.7634	0.6642
80	0.6664	0.8163	0.7102
85	0.7521	0.8673	0.7546
90	0.8388	0.9158	0.7967

Angle θ^o	Integral (Rads)	$(\text{Integral})^{\frac{1}{2}}_{(\text{Rads})^{\frac{1}{2}}}$	$G/L^{\frac{1}{3}}$
95	0.9255	0.9621	0.8370
100	1.0112	1.005	0.8744
105	1.0950	1.046	0.9100
110	1.1756	1.085	0.9440
115	1.2520	1.119	0.9735
120	1.3232	1.150	1.001
125	1.3888	1.179	1.026
130	1.4482	1.203	1.047
135	1.5004	1.225	1.066
140	1.5452	1.243	1.081
145	1.5831	1.258	1.094
150	1.6140	1.271	1.106
155	1.6380	1.280	1.114
160	1.6557	1.288	1.121
165	1.6673	1.291	1.123
170	1.6742	1.294	1.126
174	1.6768	1.295	1.127
180	1.6776	1.295	1.127

APPENDIX VII

THE EFFECT of the PRESENCE of a STAGNANT SURFACE on the FILM THICKNESS

The balance between viscous shear and gravity forces for the film leads to the equation

$$\mu \frac{\partial^2 u}{\partial z^2} = -\rho g \operatorname{Sin} \theta \qquad (1)$$

This can be solved for two cases.

(a) With no surface shear $u = 0$ at $z = 0$ (2)

$$\frac{du}{dz} = 0 \text{ at } z = F \qquad (3)$$

Integrating (1)

$$\mu \frac{\partial u}{\partial z} = -\rho g \operatorname{Sin} \theta \, z + A$$

and from (3) $A = \rho g F \operatorname{Sin} \theta$.

Integrating again

$$\mu u = -\rho g \operatorname{Sin}\theta \frac{z^2}{2} + \rho g F \operatorname{Sin} \theta \, z + B$$

and from (2) $B = 0$

whence $u = \frac{\rho g \operatorname{Sin} \theta}{\mu} \left(Fz - \frac{z^2}{2}\right)$ (4)

Now $L = 2\pi R \operatorname{Sin} \theta \int_0^F u \, dz$ (5)

and substituting (4) in (5) and integrating gives

$$F = \left(\frac{3\mu L}{2\pi R \operatorname{Sin}^2\theta \, \rho g}\right)^{\frac{1}{3}} \qquad (6)$$

(b) With zero surface velocity $u = 0$ at $z = 0$ (7)

$$u = 0 \text{ at } z = F^1 \qquad (8)$$

Integrating (1)

$$\mu \frac{\partial u}{\partial x} = -\rho g \operatorname{Sin} \theta \, z + A^1$$

and from (8) $A^1 = \rho g \operatorname{Sin} \theta \frac{F^1}{2}$

Integrating again

$$\mu u = -\rho g \operatorname{Sin} \theta \frac{z^2}{2} + \rho g \operatorname{Sin} \theta \frac{F^1}{2} z + B$$

and from (7) $B = 0$.

whence $u = \frac{\rho g \operatorname{Sin} \theta}{2\mu} (F^1 z - z^2)$.

$$L = 2\pi R \operatorname{Sin} \theta \int_0^{F^1} u \, dz$$

whence $F^1 = \left(\frac{6\mu L}{\pi R \rho g \operatorname{Sin}^2\theta}\right)^{\frac{1}{3}}$

The ratio of the two thicknesses

$$\frac{F^1}{F} = \left(\frac{6}{3/2}\right)^{\frac{1}{3}} = (4)^{\frac{1}{3}}$$

i.e. $F^1 = 1.587F$.

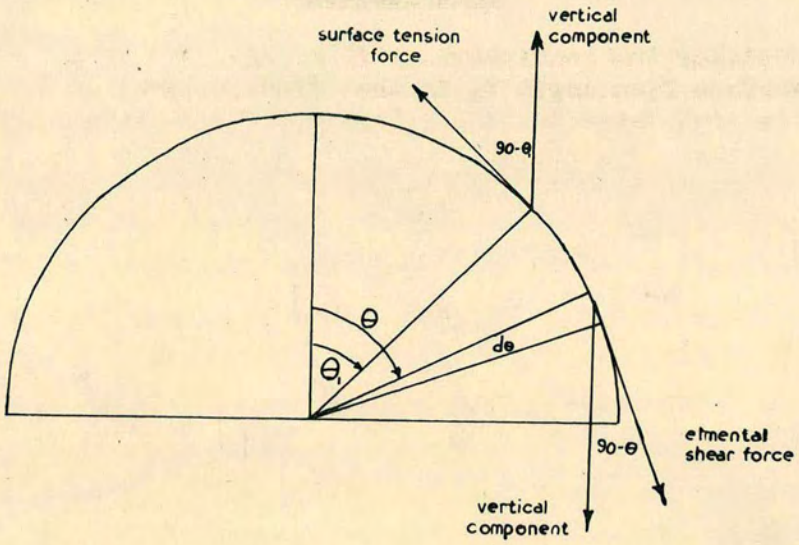
surface tension force
vertical component
90-θ
θ
θ1
dθ
90-θ
elmental shear force
vertical component

FIG. 23

APPENDIX VIII

A THEORETICAL ANALYSIS of the STAGNANT LAYER HEIGHT

Consider the hemispherical film (fig. 23) with a stagnant surface from angle θ_s to the off-take level at $\frac{\pi}{2}$ There is considered to be a balance of forces between the shear on the underside of this layer and the surface tension forces upwards at its upper extreme.

The stagnant surface zone has a velocity profile given by

$$u = \frac{\rho g \sin\theta}{2\mu}(F^1 z - z^2) \qquad \text{[Appendix VII]} \qquad (1)$$

$$\therefore \mu\frac{du}{dz} = \frac{\rho g \sin\theta}{2}(F^1 - 2x)$$

$$\text{Shear at the surface } S_{z=F'} = -\frac{\rho g F^1}{2}\sin\theta \qquad (2)$$

$$F^1 = \left(\frac{6\mu L}{\pi R \rho g \sin^2\theta}\right)^{\frac{1}{3}} \qquad \text{[Appendix VII]}$$

$$\therefore S = \left(\frac{3\mu L \rho^2 g^2 \sin\theta}{4\pi R}\right)^{\frac{1}{3}}$$

acting downwards on the layer.

Consider a small element $d\theta$ of the surface in the stagnant zone at angle θ.

Area of Element = $2\pi R^2 \sin\theta\, d\theta$.

Elemental shear force = $\left(\frac{3\mu L \rho^2 g^2 \sin\theta}{4\pi R}\right)^{\frac{1}{3}} 2\pi R^2 \sin\theta\, d\theta$.

Being tangential to the surface this force acts at $90 - \theta$ to the vertical.

$\therefore$ Vertical component of Elemental shear force

$$= \left(\frac{3\mu L \rho^2 g^2 \sin\theta}{4R}\right)^{\frac{1}{3}} 2\pi R^2 \sin\theta\, d\theta \cos(90 - \theta)$$

$$= \left(\frac{3\mu L \rho^2 g^2}{4\pi R}\right)^{\frac{1}{3}} 2 R^2 \sin^{7/3}\theta\, d\theta.$$

$\therefore$ Total vertical component of shear force

$$= 2\pi R^2 \left(\frac{3\mu L \rho^2 g^2}{4\pi R}\right)^{\frac{1}{3}} \int_{\theta_s}^{\frac{\pi}{2}} \sin^{7/3}\theta\, d\theta. \qquad (3)$$

At the upper limit of the layer surface tension forces act upwards, the surface of the stagnant layer being covered with surface active agent and the moving surface being water.

Let the surface tension difference be $s_1 - s_2$

Circumference at $\theta_s = 2\pi R \sin\theta_s$

$$\text{Upwards force} = 2\pi R (s_1 - s_2)\sin\theta_s \qquad (4)$$

at $90 - \theta_s$ to the vertical

$$\therefore \text{Vertical component} = 2\pi R (s_1 - s_2)\sin^2\theta_s \qquad (5)$$

Equating equations (3) and (5)

$$\frac{\sin^2 \theta_s}{\int_{\theta_s}^{\pi/2} \sin^{7/3}\theta \, d\theta} = \left(\frac{3\mu L R^2 \rho^2 g^2}{4\pi (s_1 - s_2)^3}\right)^{\frac{1}{3}} \qquad (6)$$

Values μ = 0.0114 gms/cm sec ρ = 1.00 gms/cm^3

R = 3.81 cm. g = 981 cm/sec^2

$s_1 = s_2$ = 40 dynes/cm [approx.]

Using these values the following table has been constructed.

$\theta^\circ s$	$(90 - \theta)$	$\frac{\sin \theta_s}{\int_{\theta_s}^{\pi/2} \sin^{7/3}\theta d\theta}$	$L^{\frac{1}{3}}$ $(cc/sec)^{\frac{1}{3}}$	L cc/sec
0	90	0	0	0
10	80	0.041	0.018	0.000
20	70	0.161	0.190	0.007
25	65	0.249	0.294	0.025
30	60	0.355	0.419	0.064
35	55	0.481	0.567	0.188
40	50	0.630	0.744	0.411
45	45	0.804	0.949	0.854
50	40	1.013	1.198	1.72
55	35	1.269	1.496	3.34
60	30	1.592	1.880	6.64

APPENDIX IX

ABSORPTION into a FILM with a STAGNANT SURFACE

(a) The equation deduced by Ratcliffe and Reid (44) is

$$G_s = \frac{3}{2.68}(3 \times 1.68)^{\frac{2}{3}} \left(\frac{\pi^4 \rho}{6\mu} g\right) R^{14/9} D^{\frac{2}{3}} L^{1/9} (C_i - C_o) \qquad (1)$$

In this equation 1.68 is the value of the integral of $\text{Sin}^{5/3}\theta$ over the whole sphere. If the integral from 0^o to θ^o is represented by I the equation may be expressed as

$$G_s = 0.229 (C_i - C_o) I^{\frac{2}{3}} L^{1/9} \qquad (2)$$

where the values of the various constants are as before.

By comparison the equation for a normal film can be expressed

$$G_n = 0.461 (C_i - C_o) I^{\frac{1}{2}} L^{\frac{1}{3}} \qquad (3)$$

The ratio of the absorption for an entirely stagnant film to the absorption for a normal film is

$$G_s/G_n = \frac{.229}{.461} \quad \frac{I^{1/6}}{L^{2/9}} = \frac{.541}{L^{2/9}}$$

The ratio $G_s/G_n < 1$ if $L^{2/9} > .541$

i.e. $L > .063$ cc/sec

i.e. for all practical flow rates.

(b) Using the equation for the stagnant surface it is possible to make a rough calculation of the absorption in the presence of the end effect if it is assumed that

(1) The stagnant layer begins at latitude 50^o and does not vary with the flow rate - only approximately true as seen from figure 13.

(2) The film is mixed so that the concentration profile at the start of the stagnant layer is flat and has a value equal to the mean concentration at 50^o. This is not true but is a reasonable approximation to make an estimate of the absorption. The concentration will probably be greater in the surface layers in fact and this rough estimate will therefor be an over-estimate.

Thus

From $0^o - 50^o$ $\quad G_n = .417 L^{\frac{1}{3}}$

$50^o - 90^o$ $\quad I = .609$

$$C_o = \frac{.417 L^{\frac{1}{3}}}{L} = \frac{.417}{L^{2/3}}$$

$$\therefore G_s = .229 \left(1.888 - \frac{.417}{L^{2/3}}\right) (.609)^{\frac{2}{3}} L^{1/9}$$

$$= .163 \left(1.888 L^{1/9} - \frac{.417}{L^{5/9}}\right)$$

Thus

$$G_t = G_n + G_s$$

$$= 0.417\ L^{\frac{1}{3}} + 0.163\ (1.888\ L^{1/9} - \frac{0.417}{L^{5/9}})$$

$$\therefore G_t/L^{\frac{1}{3}} = 0.417 + 0.163\ (\frac{1.888}{L^{2/9}} - \frac{0.417}{L^{8/9}})$$

Values of this are as follows.

At L = 1.00 cc/sec	$G_t/L_1^{\frac{1}{3}} = 0.657$ mg/sec
L = 2.00 cc/sec	$G_t/L_1^{\frac{1}{3}} = 0.644$ mg/sec
L = 3.00 cc/sec	$G_t/L_1^{\frac{1}{3}} = 0.633$ mg/sec
L = 4.00 cc/sec	$G_t/L_1^{\frac{1}{3}} = 0.623$ mg/sec
L = 5.00 cc/sec	$G_t/L_1^{\frac{1}{3}} = 0.616$ mg/sec
L = 6.00 cc/sec	$G_t/L^{\frac{1}{3}} = 0.610$ mg/sec

These values apply only in the cases of water and Hexanol when the film is totally stagnant. They are of the correct order (compare with fig. 11) and also forecast the region of negative gradient at low flow rates.

TABLE I

Start-Up Measurements - Absorption versus Time after Starting Gas Flow

A. Inlet Meter Temperature 18.5°C) Absorbing Liquid 0.1 g/l
Outlet Meter Temperature 17.8°C) Lissapol.
Liquid Temperature 17.2°C) Liquid Rate, L = 3.75 cc/sec.

Inlet Gas Rate = 2.45 cc/sec (at 18.5°C) i.e. 4.520 mgs/sec

Time After Start (min)	Meter Time t (sec)	Outlet Gas Rate (mg/sec)	Absorption Rate (mg/sec)	%age of Final Rate
1.18	22.0	4.19	0.33	18.8
2.19	23.0	4.01	0.51	29.0
3.20	24.3	3.80	0.72	41.0
4.21	25.4	3.64	0.88	50.0
5.22	26.7	3.46	1.06	60.1
6.23	27.7	3.33	1.19	67.6
7.24	28.6	3.23	1.29	73.2
8.24	28.7	3.22	1.30	73.9
9.25	29.8	3.11	1.41	80.0
10.25	30.1	3.07	1.45	82.4
11.26	31.0	2.98	1.54	87.5
12.26	31.1	2.97	1.55	88.0
13.26	31.4	2.94	1.58	89.7
14.27	31.8	2.90	1.62	91.0
16.27	32.4	2.85	1.67	94.9
20.27	33.0	2.80	1.72	97.8
22.27	33.5	2.76	1.76	100.0
25.27	33.5	2.76	1.76	100.0
26.27	33.4	2.76	1.76	100.0
	33.0	2.76	1.76	100.0

B. Inlet Meter Temperature 18.7°C) Absorbing Liquid 0.1 g/l
Outlet Meter Temperature 18.5°C) Lissapol.
Liquid Temperature 17.5°C) Liquid Rate L = 1.78 cc/sec.

Inlet Gas Rate = .795 cc/sec (at 18.7°C) = 1.463 mgs/sec.

Time After Start (min)	Meter Time t (sec)	Outlet Gas Rate (mg/sec)	Absorption Rate (mg/sec)	%age of Final Rate
1.62	65.2	1.413	0.050	3.7
3.58	70.7	1.303	0.160	11.9
5.73	79.6	1.159	0.304	22.5
7.73	87.3	1.058	0.405	29.9
9.82	97.0	0.951	0.512	37.9
11.90	105.2	0.876	0.587	43.5
13.68	113.0	0.816	0.647	48.0
15.22	123.0	0.750	0.713	52.8
16.32	124.8	0.740	0.723	53.6
18.55	133.4	0.691	0.772	57.1
20.62	139.8	0.660	0.803	59.5
22.63	148.6	0.621	0.842	62.5
24.70	159.2	0.579	0.884	65.4
26.72	162.4	0.568	0.895	66.4
28.70	168.8	0.547	0.916	67.9
30.68	177.2	0.520	0.943	69.9
32.75	182.2	0.506	0.957	70.9
34.85	185.0	0.499	0.964	71.4
37.33	195.0	0.474	0.989	73.2
39.52	204.0	0.452	1.011	75.0
41.60	206.0	0.448	1.015	75.2
43.52	208.0	0.444	1.019	75.3
45.72	217.0	0.425	1.038	76.8
47.55	218.0	0.423	1.040	77.0
49.62	222.0	0.416	1.047	77.5
51.50	226.0	0.408	1.055	78.1
53.65	230.0	0.401	1.062	78.6
			1.350	100.0

TABLE II

Whole Sphere Absorption Rates for Water and Aqueous Solutions of Lissapol and n-Hexanol.

A. Water.

Flow Rate L cc/sec	Time to Absorb 50 ml t sec.	Temperature °C Meter	Temperature °C Absn. Liquid	Measured Absn. Rate G Mgs/sec	Temp. Corrected G	Fully Corrected G	G^3
1.12	73.0	17.0	13.0	1.267	1.242	1.265	2.024
1.25	69.8	17.0	13.0	1.325	1.299	1.322	2.310
1.43	66.6	17.0	13.0	1.389	1.361	1.385	2.657
1.45	67.0	17.8	13.5	1.377	1.356	1.380	2.628
1.85	60.0	17.8	13.0	1.537	1.506	1.533	3.603
2.00	57.0	16.7	13.0	1.624	1.592	1.621	4.259
2.13	56.5	17.6	12.5	1.634	1.593	1.622	4.267
2.24	54.3	17.5	13.5	1.700	1.675	1.705	4.956
2.40	52.0	16.3	13.0	1.783	1.747	1.778	5.621
2.52	49.5	17.5	12.5	1.865	1.818	1.851	6.342
2.83	46.8	17.0	13.0	1.976	1.936	1.971	7.657
3.25	44.0	16.4	13.5	2.106	2.047	2.084	9.051
3.54	42.0	15.4	13.0	2.214	2.170	2.209	10.78
3.84	39.6	17.3	12.5	2.333	2.275	2.316	12.42
4.03	39.0	17.2	13.0	2.370	2.323	2.365	13.23
4.22	38.3	16.2	13.0	2.421	2.373	2.416	14.10
4.24	38.0	17.1	13.0	2.434	2.385	2.428	14.31
4.50	37.6	17.2	13.0	2.458	2.409	2.452	14.74
4.80	36.2	17.8	13.0	2.542	2.491	2.536	16.31
5.08	35.0	18.2	13.0	2.632	2.579	2.625	18.09
5.35	35.2	18.5	13.0	2.614	2.562	2.608	17.74
5.87	34.8	18.1	13.0	2.648	2.595	2.642	18.44
6.20	34.5	18.8	13.0	2.664	2.611	2.658	18.78

B. 0.1 g/l Lissapol.

Flow Rate L cc/sec	Time to Absorb 50 ml t sec	Temperature °C Meter	Temperature °C Abspn. Liquid	Measured Abspn. G mg/sec	Temp. Corrected G	Fully Corrected G	G^3
0.93	90.0	18.0	17.5	1.024	1.053	1.072	1.232
1.23	79.6	18.0	17.5	1.158	1.190	1.211	1.776
1.49	70.9	17.9	15.0	1.300	1.300	1.323	2.316
1.84	65.7	18.0	15.0	1.403	1.403	1.428	2.912
1.89	67.9	18.0	17.5	1.357	1.395	1.420	2.863
2.04	63.3	18.0	15.0	1.456	1.456	1.482	3.255
2.23	63.0	18.0	17.5	1.463	1.504	1.531	3.589
2.59	59.4	18.0	17.5	1.552	1.595	1.624	4.283
2.70	57.8	18.0	17.5	1.595	1.640	1.670	4.657
2.94	56.8	18.0	17.5	1.623	1.668	1.698	4.896
3.31	54.3	18.4	18.0	1.695	1.753	1.785	5.687
3.49	53.4	18.4	17.5	1.724	1.772	1.804	5.871
3.77	51.0	16.0	14.0	1.820	1.802	1.834	6.169
4.12	50.7	18.4	17.5	1.815	1.866	1.900	6.859
4.44	48.7	18.0	17.0	1.893	1.935	1.970	7.645
4.72	48.0	18.0	17.0	1.920	1.962	1.997	7.964
5.40	45.4	18.0	17.0	2.030	2.075	2.112	9.421
5.86	44.0	18.0	17.0	2.095	2.141	2.180	10.36

C. 0.5 g/l Lissapol.

Flow Rate L cc/sec	Time to Absorb 50 ml t sec	Temperature °C Meter	Temperature °C Abspn. Liquid	Measured Abspn. G mg/sec	Temp. Corrected G	Fully Corrected G	G^3
1.22	87.5	16.4	16.0	1.059	1.071	1.090	1.292
1.26	84.7	16.9	17.0	1.093	1.117	1.137	1.470
1.40	81.7	17.8	18.0	1.128	1.166	1.187	1.672
1.44	81.6	16.9	17.0	1.134	1.159	1.180	1.643
1.61	77.4	16.4	16.0	1.197	1.210	1.232	1.870
1.71	75.8	16.3	16.0	1.223	1.236	1.258	1.991
1.78	74.6	18.0	18.0	1.237	1.279	1.302	2.207
2.01	72.3	17.5	18.0	1.277	1.320	1.344	2.428
2.01	72.3	16.3	16.0	1.281	1.295	1.318	2.290
2.10	70.7	16.3	16.0	1.308	1.322	1.346	2.439
2.25	68.6	16.2	16.0	1.351	1.366	1.391	2.691
2.34	68.0	16.2	16.0	1.363	1.378	1.403	2.762
2.46	66.7	18.0	18.0	1.380	1.427	1.453	3.068
2.50	64.6	16.3	16.0	1.420	1.436	1.462	3.125
2.50	66.2	16.1	16.0	1.399	1.414	1.439	2.980
2.55	66.7	17.9	18.0	1.380	1.427	1.453	3.068
2.79	63.5	16.9	16.0	1.459	1.475	1.502	3.389
2.91	63.0	17.0	16.0	1.463	1.479	1.506	3.416
2.93	62.8	16.1	16.0	1.476	1.492	1.519	3.505
2.93	62.8	17.3	18.0	1.469	1.519	1.546	3.695
2.94	62.6	18.3	18.0	1.469	1.519	1.546	3.695
3.26	59.8	15.9	16.0	1.547	1.564	1.592	4.035
3.27	60.0	17.1	16.0	1.537	1.554	1.582	3.959
3.32	59.6	16.7	17.0	1.552	1.586	1.615	4.212
3.49	58.3	16.2	16.0	1.588	1.605	1.634	4.363
3.63	57.8	17.1	16.0	1.600	1.618	1.647	4.468
3.64	57.3	16.6	16.0	1.615	1.633	1.662	4.591
3.80	56.8	16.9	16.0	1.629	1.647	1.677	4.716
3.95	56.0	17.1	16.0	1.652	1.670	1.700	4.913
3.99	55.7	17.7	16.0	1.660	1.678	1.708	4.983
4.13	54.3	17.0	16.0	1.703	1.722	1.753	5.387
4.34	53.7	17.2	16.0	1.721	1.740	1.771	5.555
4.40	53.4	18.1	18.0	1.730	1.789	1.821	6.039
4.56	53.0	18.1	16.0	1.750	1.769	1.801	5.842
4.63	52.8	17.3	16.0	1.752	1.771	1.803	5.861
4.63	53.0	16.7	17.0	1.748	1.786	1.818	6.009
4.90	51.6	16.7	17.0	1.791	1.830	1.863	6.466
5.47	49.2	16.7	17.0	1.880	1.921	1.956	7.484
5.95	47.8	16.7	17.0	1.938	1.981	2.017	8.206
6.27	47.1	16.7	17.0	1.965	2.008	2.044	8.540

D. 1.0 g/l Lissapol.

Flow Rate L cc/sec	Time to Absorb 50 ml t sec	Temperature °C Meter	Temperature °C Abspn. Liquid	Measured Abspn. G mg/sec	Temp. Corrected G	Fully Corrected G	G^3
0.96	90.0	15.5	15.0	1.033	1.033	1.052	1.164
1.15	83.7	15.5	15.0	1.110	1.110	1.130	1.443
1.35	78.9	15.5	15.0	1.178	1.178	1.199	1.724
1.52	76.3	15.2	15.0	1.220	1.220	1.242	1.916
1.65	74.3	15.5	15.0	1.251	1.251	1.274	2.068
1.78	72.3	15.0	15.0	1.289	1.289	1.312	2.258
1.86	71.9	15.5	15.0	1.292	1.292	1.315	2.274
1.98	70.3	15.5	15.0	1.322	1.322	1.346	2.439
2.13	67.9	15.0	14.5	1.372	1.365	1.390	2.686
2.15	68.5	15.5	15.0	1.358	1.358	1.382	2.640
2.22	67.8	17.9	15.5	1.361	1.369	1.394	2.709
2.32	66.6	15.5	15.0	1.396	1.396	1.421	2.869
2.57	63.6	17.8	15.0	1.450	1.450	1.476	3.216
2.59	63.5	15.5	15.0	1.463	1.463	1.489	3.301
2.69	62.7	16.4	15.5	1.478	1.487	1.514	3.470
2.88	61.3	15.5	15.0	1.518	1.518	1.545	3.688
2.93	61.1	15.2	15.0	1.524	1.524	1.551	3.731
3.06	60.0	16.3	15.0	1.546	1.546	1.574	3.900
3.20	58.6	14.3	14.0	1.593	1.581	1.609	4.166
3.23	57.8	16.0	14.5	1.607	1.599	1.628	4.315
3.24	58.4	15.2	15.0	1.597	1.597	1.626	4.299
3.34	57.8	13.4	14.0	1.620	1.604	1.633	4.355
3.51	57.0	16.2	15.0	1.628	1.628	1.657	4.550
3.58	56.0	15.9	15.0	1.658	1.658	1.688	4.810
3.59	57.0	15.3	15.0	1.635	1.635	1.664	4.607
3.63	56.6	16.0	15.0	1.639	1.639	1.669	4.649
3.77	55.8	16.0	15.0	1.664	1.664	1.694	4.861
3.91	54.8	15.4	15.0	1.700	1.700	1.731	5.187
4.08	54.3	15.5	15.0	1.712	1.712	1.743	5.295
4.27	53.0	15.1	15.0	1.758	1.758	1.790	5.735
4.45	52.3	15.6	15.0	1.778	1.778	1.810	5.930
4.65	52.0	15.0	15.0	1.792	1.792	1.824	6.068
4.78	51.0	16.0	15.0	1.820	1.820	1.853	6.362
5.00	50.2	16.0	15.0	1.849	1.849	1.882	6.666
5.11	49.9	16.0	15.0	1.860	1.860	1.893	6.783
5.15	49.9	15.0	15.0	1.869	1.869	1.903	6.892
5.33	49.4	16.0	15.0	1.880	1.880	1.914	7.012
5.55	48.6	16.0	15.0	1.909	1.909	1.943	7.335
5.71	48.2	16.0	15.0	1.924	1.924	1.959	7.518
5.95	47.5	16.0	15.0	1.955	1.955	1.990	7.881
6.10	46.8	16.0	15.0	1.985	1.985	2.021	8.255

E. 1.0 g/l n-Hexanol.

Flow Rate L cc/sec	Time to Absorb 50 ml t sec	Temperature °C		Measured Abspn. G mg/sec	Temp. Corrected G	Fully Corrected G	G^3
		Meter	Abspn. Liquid				
0.71	97.0	18.2	17.5	0.949	0.976	0.994	0.982
0.83	90.0	17.5	16.5	1.025	1.042	1.061	1.194
0.88	87.9	18.2	17.5	1.048	1.077	1.096	1.317
1.12	80.3	18.0	17.5	1.147	1.179	1.200	1.728
1.30	74.3	16.9	16.5	1.245	1.266	1.289	2.142
1.41	74.2	18.4	17.5	1.240	1.275	1.298	2.187
1.50	72.1	17.9	17.0	1.279	1.307	1.331	2.358
1.71	69.1	18.4	17.5	1.332	1.369	1.394	2.709
1.76	67.5	17.1	16.5	1.370	1.393	1.418	2.851
1.91	65.7	18.5	17.5	1.400	1.439	1.465	3.144
1.94	65.5	17.6	17.0	1.410	1.441	1.467	3.157
2.23	63.4	18.5	17.5	1.450	1.491	1.518	3.498
2.24	61.8	17.4	16.5	1.494	1.519	1.546	3.695
2.36	60.8	17.6	17.0	1.517	1.550	1.578	3.929
2.52	59.2	17.3	16.5	1.561	1.588	1.617	4.228
3.98	51.0	17.5	17.0	1.812	1.852	1.885	6.698
4.25	50.0	17.5	17.0	1.850	1.891	1.925	7.133
4.69	48.1	17.5	17.0	1.922	1.964	1.999	7.988

TABLE III

Whole Sphere Absorption Rates for Various Concentrations of Lissapol and n-Hexanol.

A.

Lissapol Concn. g/l	Measured Absorption G mg/sec	Temp. Abspn. Liquid °C	Temp. Corrected G	Fully Corrected G	Flow Rate L cc/sec	$G/L^{\frac{1}{3}}$
0	Mean of results around 2.00 cc/sec from Table IIA					1.270
0.025	1.465	18.5	1.524	1.551	2.18	1.197
0.100	Mean of results around 2.00 cc/sec from Table IIB					1.165
0.500	Mean of results around 2.00 cc/sec from Table IIC					1.046
0.750	1.270	17.5	1.306	1.329	2.00	1.055
1.00	Mean of results around 2.00 cc/sec from Table IID					1.073
1.50	1.325	17.5	1.362	1.486	1.92	1.115
2.00	1.372	16.5	1.395	1.420	1.90	1.146
3.00	1.503	13.0	1.472	1.498	2.01	1.188

B.

n-Hexanol Concn. g/l	Measured Absorption G mg/sec	Temp. Abspn. Liquid °C	Temp. Corrected G	Fully Corrected G	Flow Rate L cc/sec	$G/L^{\frac{1}{3}}$
0.100	1.459	16.0	1.475	1.501	2.00	1.191
0.500	1.475	15.0	1.475	1.501	2.00	1.191
1.00	Mean of Results around 2.00 cc/sec from Table IIE					1.167
2.00	1.465	15.0	1.465	1.490	2.00	1.183

TABLE IV

Absorption versus Latitude for 0.1 g/l Lissapol.

A. Flow Rate Range - 1.40-1.50 cc/sec.

Angle θ°	Measured G mgs/sec	Temp. Abspn. Liquid $^{\circ}C$	Temp. Corrected G	Fully Corrected G	Flow Rate L cc/sec	$G/L^{\frac{1}{3}}$
27	0.118	17.0	0.121	0.123	1.47	0.109
37	0.168	17.0	0.172	0.175	1.47	0.153
39	0.172	16.0	0.174	0.177	1.49	0.154
45	0.207	17.5	0.213	0.217	1.46	0.191
54	0.253	16.0	0.256	0.260	1.49	0.228
54	0.260	17.5	0.267	0.272	1.46	0.240
64	0.317	18.0	0.328	0.334	1.45	0.295
67	0.328	16.0	0.332	0.348	1.46	0.307
77	0.392	16.0	0.396	0.403	1.41	0.359
79	0.411	17.5	0.423	0.430	1.45	0.380
88	0.488	17.5	0.502	0.511	1.44	0.452
91	0.528	16.0	0.534	0.544	1.56	0.469
92	0.540	18.0	0.558	0.568	1.50	0.496
96	0.554	17.0	0.566	0.576	1.43	0.511
101	0.621	16.0	0.629	0.640	1.50	0.559
107	0.667	17.0	0.682	0.694	1.50	0.606
114	0.740	16.0	0.748	0.761	1.50	0.665
117	0.768	17.0	0.785	0.799	1.50	0.698
124	0.813	16.5	0.827	0.842	1.47	0.741
128	0.870	16.0	0.880	0.895	1.48	0.786
136	0.925	16.0	0.935	0.952	1.49	0.833

B. Flow Rate - 2.40 cc/sec.

Angle θ°	Measured G mg/sec	Temp. Abspn. Liquid $^{\circ}C$	Temp. Corrected G	Fully Corrected G	Flow Rate L cc/sec	$G/L^{\frac{1}{3}}$
16	0.097	17.0	0.099	0.101	2.39	0.076
33	0.148	17.0	0.151	0.153	2.39	0.115
40	0.193	17.0	0.197	0.200	2.40	0.150
47	0.236	17.0	0.241	0.246	2.40	0.184
56	0.292	17.0	0.298	0.303	2.40	0.226
60	0.305	17.0	0.312	0.318	2.39	0.238
67	0.365	16.5	0.371	0.378	2.40	0.283
75	0.430	17.0	0.439	0.447	2.40	0.334
85	0.535	16.5	0.544	0.553	2.40	0.414
95	0.647	16.5	0.658	0.670	2.40	0.500
102	0.725	16.5	0.737	0.750	2.40	0.560
107	0.790	16.5	0.803	0.818	2.39	0.612
114	0.867	16.5	0.882	0.897	2.39	0.671
121	0.933	16.5	0.949	0.966	2.39	0.722
126	1.010	16.5	1.028	1.046	2.40	0.782
137	1.100	16.5	1.119	1.139	2.40	0.851
153	1.175	17.0	1.201	1.222	2.40	0.913
166	1.244	17.0	1.271	1.293	2.40	0.966

C. Flow Rate - 3.40 cc/sec.

Angle θ^{o}	Measured G mg/sec	Temp. Abspn. Liquid ^{o}C	Temp. Corrected G	Fully Corrected G	Flow Rate L cc/sec	$G/L^{\frac{1}{3}}$
21	0.110	17.0	0.112	0.114	3.43	0.075
41	0.195	17.0	0.199	0.203	3.44	0.134
52	0.255	17.0	0.261	0.266	3.44	0.176
64	0.350	17.0	0.358	0.364	3.44	0.241
77	0.540	18.0	0.558	0.568	3.46	0.376
82	0.580	17.0	0.593	0.603	3.44	0.399
83	0.595	18.0	0.615	0.626	3.45	0.415
84	0.620	16.0	0.627	0.638	3.40	0.424
97	0.782	18.0	0.809	0.821	3.45	0.544
111	0.985	18.0	1.013	1.036	3.42	0.687
115	1.056	15.5	1.062	1.082	3.36	0.721
121	1.090	18.0	1.127	1.147	3.37	0.765
132	1.181	18.0	1.221	1.243	3.41	0.825
141	1.271	17.5	1.307	1.330	3.38	0.887
147	1.358	16.0	1.373	1.397	3.36	0.933
157	1.370	17.5	1.408	1.433	3.32	0.961
166	1.435	17.5	1.475	1.501	3.39	0.999

D. Various Flow Rates.

Angle θ^{o}	Measured G mgs/sec	Temp. Abspn. Liquid ^{o}C	Temp. Corrected G	Fully Corrected G	Flow Rate L cc/sec	$G/L^{\frac{1}{3}}$
79	0.534	16.0	0.540	0.550	3.20	0.373
84	0.535	16.0	0.541	0.550	2.56	0.403
98	0.810	17.0	0.828	0.483	3.24	0.569
109	0.960	16.0	0.971	0.988	3.21	0.670
115	1.030	17.0	1.053	1.072	3.21	0.726
121	1.125	16.5	1.144	1.164	3.56	0.762
124	0.905	17.0	0.925	0.942	1.92	0.757
132	0.982	17.0	1.004	1.021	1.87	0.829

TABLE V

Absorption versus Latitude for 1.0 g/l Lissapol.

Angle θ^{o}	Measured G mg/sec	Temp. Abspn. Liquid ^{o}C	Temp. Corrected G	Fully Corrected G	Flow Rate L cc/sec	$G/L^{\frac{1}{3}}$
35	0.175	17.5	0.180	0.182	2.45	0.135
46	0.243	18.0	0.251	0.255	2.46	0.189
51	0.298	18.5	0.310	0.316	3.66	0.206
56	0.333	18.0	0.344	0.351	2.46	0.259
60	0.377	17.5	0.388	0.395	2.45	0.293
66	0.435	18.0	0.450	0.458	2.45	0.340
69	0.473	17.5	0.486	0.494	2.45	0.367
77	0.556	18.0	0.575	0.586	2.44	0.435
78	0.583	17.5	0.599	0.610	2.41	0.454
84	0.635	18.0	0.657	0.669	2.44	0.497
87	0.680	18.0	0.703	0.715	2.45	0.530
90	0.715	18.0	0.739	0.752	2.44	0.558
94	0.758	18.0	0.784	0.797	2.46	0.590
99	0.830	18.0	0.858	0.873	2.41	0.651
99	0.820	18.0	0.848	0.863	2.47	0.637
107	0.885	18.0	0.915	0.931	2.48	0.687
110	0.940	18.5	0.978	0.995	2.42	0.741
123	1.077	19.0	1.125	1.145	2.46	0.848
131	1.126	19.0	1.177	1.197	2.26	0.913
136	1.190	18.5	1.238	1.259	2.45	0.934
140	1.210	18.5	1.258	1.280	2.45	0.950
144	1.230	18.5	1.279	1.301	2.43	0.967
151	1.253	19.5	1.318	1.341	2.53	0.985
152	1.247	18.5	1.297	1.320	2.44	0.981

TABLE VI

Difference between the Theoretical and Experimental Curves of G versus θ for two concentrations of Lissapol.

Angle θ°	Difference	
	0.1 g/l	1.0 g/l
40	0.178	0.165
50	0.227	0.210
60	0.271	0.231
70	0.295	0.241
75	0.310	0.242
80	0.320	0.244
85	0.329	0.244
90	0.334	0.240
95	0.336	0.234
100	0.325	0.225
105	0.318	0.215
110	0.305	0.207
115	0.300	0.197
120	0.280	0.181
130	0.245	0.144

TABLE VII

Absorption over the Upper 90° for Two Concentrations of Lissapol and One of Hexanol.

A. 0.1 g/l Lissapol.

Flow Rate L cc/sec	Measured Absorption G mg/sec	Temp. Abspn. Liquid °C	Temp. Corrected G	Fully Corrected G	$G/L^{\frac{1}{3}}$
1.05	0.449	18.5	0.467	0.475	0.467
1.57	0.508	18.5	0.528	0.537	0.462
1.65	0.510	18.0	0.527	0.536	0.453
2.08	0.551	18.0	0.570	0.580	0.454
2.11	0.558	18.5	0.580	0.590	0.460
2.63	0.600	19.5	0.631	0.642	0.465
3.05	0.634	19.0	0.663	0.675	0.465
3.16	0.646	19.5	0.680	0.692	0.472
3.17	0.665	17.5	0.684	0.696	0.474
3.53	0.687	18.0	0.713	0.722	0.474
3.55	0.679	18.5	0.706	0.719	0.471
3.60	0.713	17.5	0.733	0.746	0.486
3.89	0.715	18.5	0.744	0.757	0.482
3.91	0.733	18.0	0.758	0.771	0.489
4.05	0.728	18.5	0.757	0.770	0.483
4.23	0.760	18.5	0.790	0.804	0.498
4.28	0.753	18.5	0.783	0.797	0.490
4.52	0.772	18.5	0.803	0.818	0.494
4.70	0.774	19.5	0.814	0.828	0.494
4.75	0.789	19.0	0.825	0.840	0.500
4.91	0.868	18.0	0.898	0.914	0.538
5.04	0.810	19.5	0.852	0.867	0.506
5.35	0.910	19.5	0.957	0.974	0.556

B. 1.0 g/l Lissapol.

Flow Rate L cc/sec	Measured Absorption G mg/sec	Temp. Absp. Liquid °C	Temp. Corrected G	Fully Corrected G	$G/L^{\frac{1}{3}}$
0.68	0.510	19.0	0.533	0.543	0.618
0.91	0.557	19.0	0.582	0.592	0.612
1.35	0.615	19.5	0.647	0.658	0.596
1.43	0.625	19.5	0.658	0.670	0.594
1.69	0.648	19.5	0.682	0.694	0.583
1.87	0.674	19.5	0.709	0.721	0.586
1.98	0.680	19.5	0.715	0.727	0.579
2.26	0.708	19.5	0.745	0.758	0.578
2.32	0.710	19.5	0.747	0.760	0.575
2.46	0.725	19.5	0.763	0.777	0.575
2.90	0.775	19.5	0.815	0.829	0.582
3.10	0.784	18.5	0.815	0.829	0.569
3.28	0.815	19.5	0.857	0.872	0.587
3.29	0.803	18.5	0.835	0.850	0.572
3.63	0.842	18.0	0.871	0.887	0.577
3.68	0.825	19.5	0.868	0.884	0.572
3.76	0.826	19.5	0.869	0.885	0.569
3.92	0.865	18.0	0.894	0.910	0.578
3.96	0.852	19.5	0.896	0.912	0.577
4.22	0.875	19.0	0.914	0.930	0.576
4.26	0.887	18.0	0.917	0.933	0.575
4.50	0.900	19.0	0.941	0.957	0.580
5.11	0.955	19.5	1.005	1.022	0.593

C. 1.0 g/l n-Hexanol.

Flow Rate L cc/sec	Measured Absorption G mg/sec	Temp. Abspn. Liquid °C	Temp. Corrected G	Fully Corrected G	$G/L^{\frac{1}{3}}$
0.76	0.544	14.5	0.541	0.551	0.604
1.05	0.590	14.5	0.587	0.598	0.589
1.24	0.662	14.5	0.659	0.671	0.625
1.34	0.656	14.5	0.653	0.665	0.603
1.67	0.692	14.5	0.689	0.701	0.591
1.76	0.742	14.5	0.738	0.751	0.622
1.93	0.732	15.0	0.732	0.745	0.598
2.17	0.771	15.0	0.771	0.785	0.606
2.33	0.803	14.5	0.799	0.813	0.613
2.63	0.820	15.0	0.820	0.835	0.605
3.01	0.872	15.0	0.872	0.888	0.615
3.35	0.913	15.0	0.913	0.929	0.621
3.53	0.942	15.0	0.942	0.959	0.630
3.76	0.960	15.0	0.960	0.977	0.628
4.05	0.986	15.0	0.986	1.004	0.630
4.37	1.040	15.0	1.040	1.059	0.648
4.54	1.034	15.0	1.034	1.053	0.636
4.77	1.035	15.0	1.035	1.054	0.626

TABLE VIII

Absorption over the Upper 90° for Various Concentrations of Lissapol.

Lissapol Concn. g/l	Measured Absorption G mg/sec	Temp. Abspn. Liquid °C	Temp. Corrected G	Fully Corrected G	Flow Rate L cc/sec	$G/L^{\frac{1}{3}}$
0.025	0.530	19.0	0.554	0.564	2.04	0.445
0.050	0.556	19.0	0.581	0.591	2.27	0.450
0.100	0.551	18.0	0.570	0.580	2.08	0.455
0.250	0.574	19.0	0.600	0.611	2.05	0.480
0.500	0.591	19.5	0.622	0.633	2.05	0.498
0.750	0.640	19.5	0.673	0.785	1.96	0.547
1.000	0.680	19.5	0.715	0.727	1.98	0.578
1.360	0.742	19.5	0.781	0.794	2.11	0.619
1.650	0.738	19.0	0.771	0.785	1.91	0.632
2.000	0.797	19.5	0.838	0.853	2.12	0.664

TABLE IX

Stagnant Layer Heights - Measured in Degrees Upwards from the Equator.

Flow Rate L cc/sec	0.95	1.32	1.53	1.85	2.13
Layer Height, η	66	51	56	50	60

2.35	3.03	3.12	3.78	3.87
45	60	45	43	42

4.44	4.54	4.76	5.15	5.41
41	32	39	42	40

TABLE X

Film thickness at Equator for Water and aqueous solutions of Lissapol and Hexanol.

A - Water.

Flow Rate, L cc/sec	1.13	1.20	1.41	1.80	2.00	2.18
Thickness, F_1 cm x 10^2	1.30	1.32	1.35	1.45	1.48	1.52

2.28	2.50	2.59	2.71	2.94	3.26
1.52	1.65	1.65	1.70	1.73	1.83

3.33	3.58	3.71	3.80	4.11	4.44
1.78	1.80	1.98	1.96	1.96	2.00

B - 0.5 g/l Lissapol.

Flow Rate, L cc/sec	1.96	2.28	2.36	2.48	2.69	2.88
Thickness, F_1 cm x 10^2	1.73	1.85	1.85	1.88	1.93	1.96

3.02	3.15	3.39	3.46	3.82	4.02
1.98	2.01	2.08	2.08	2.16	2.18

C - 1.0 g/l Lissapol.

Flow Rate, L cc/sec	0.87	1.19	1.55	1.58	1.81	1.90
Thickness, F_1 cm x 10^2	1.32	1.42	1.55	1.55	1.62	1.63

2.18	2.27	2.52	2.60	2.91	2.96
1.65	1.70	1.78	1.80	1.85	1.83

3.21	3.26	3.51	3.52	3.84	4.08
1.90	1.88	1.96	1.93	2.01	2.01

4.14	4.36	4.39	4.52	4.55	4.64
2.03	2.08	2.06	2.08	2.11	2.11

4.80	4.89	5.08	5.13
2.11	2.11	2.16	2.24

D - 1.0 g/l n-Hexanol.

Flow Rate, L cc/sec	1.02	1.56	1.67	2.00	2.06	2.47
Thickness, F_1 cm x 10^2	1.17	1.37	1.37	1.42	1.45	1.52

2.84	3.17	3.36	3.40	3.54	3.85
1.62	1.68	1.70	1.72	1.75	1.80

3.91	4.03	4.35
1.85	1.85	1.90

TABLE XI

Film Thickness at the Equator for Various Concentrations of Lissapol and Hexanol.

A - Lissapol - Flow Rate 2.00 cc/sec.

Concentration g/l	0.05	0.10	0.25	0.50	0.70
Film thickness F_1 cm x 10^2	1.42	1.42	1.68	1.73	1.68
$F/L^{\frac{1}{3}}$	1.13	1.13	1.33	1.37	1.33

1.00	1.50	2.00
1.63	1.55	1.50
1.29	1.23	1.19

B - n-Hexanol - Flow Rate 2.00 cc/sec.

Concentration g/l	0.25	0.50	1.00	1.50	2.00
Film thickness F_1 cm x 10^2	1.42	1.42	1.42	1.37	1.37
$F/L^{\frac{1}{3}}$	1.13	1.13	1.13	1.09	1.09

TABLE XII

Film thickness versus Latitude for Water and an Aqueous Solution (1 g/l) of n-Hexanol.

A - Water - Flow Rate 2.00 cc/sec.

Latitude, θ°	19	26	31	40	58	72	90
Thickness, F cm x 10^2	2.99	2.47	2.38	1.94	1.64	1.58	1.48
Ratio F/F_1	2.02	1.67	1.61	1.31	1.11	1.07	1.00

B - Water - Flow Rate 1.20 cc/sec.

Latitude, θ°	41	90	118	131	137	145
Thickness, F cm x 10^2	1.72	1.32	1.49	1.60	1.74	1.89
Ratio, F/F_1	1.30	1.00	1.13	1.21	1.32	1.43

C - n-Hexanol - Flow Rate 2.50 cc/sec.

Latitude, θ°	19	26	33	37	45	69	75	90	105	116	130	134	145
Thickness, F cm x 10^2	3.25	2.66	2.28	2.16	1.95	1.60	1.57	1.57	1.57	1.68	1.90	1.96	2.31
Ratio F/F_1	2.07	1.69	1.45	1.38	1.24	1.02	1.00	1.00	1.00	1.07	1.21	1.25	1.47

TABLE XIII

Film thickness versus Latitude for Aqueous Solutions of Lissapol.

0.05 g/l Lissapol.

Latitude, θ^{o}		13	31	49	88	102
Thickness F cm x 10^{2}	L=2.00 cc/sec	3.36	2.24	1.75	1.35	1.45
	L=3.00 cc/sec	3.78	2.49	1.96	1.58	1.65

108	115	119	126	128
1.52	1.55	1.55	1.65	1.70
1.73	1.78	1.78	1.91	1.96

134	139	144	148	152
1.78	1.93	2.16	2.46	2.77
2.06	2.24	2.39	2.70	3.02

0.10 g/l Lissapol.

Latitude, θ°		10	15	21	27	35
Thickness	L=2.00 cc/sec	3.63	3.22	2.80	2.41	2.11
F cm x 10^2	L=3.00 cc/sec	4.26	3.50	3.07	2.69	2.36

42	52	56	59	68
1.93	1.70	1.70	1.52	1.55
2.18	1.96	1.93	1.78	1.78

75	81	89	95	108
1.52	1.42	1.42	1.44	1.52
1.75	1.65	1.63	1.60	1.73

112	119	131	140	144
1.55	1.73	2.03	2.28	2.41
1.70	1.85	2.24	2.62	2.80

147	154	159
2.59	2.94	3.05
3.02	3.56	3.56

0.25 g/l Lissapol.

Latitude, θ°		28	38	43	90
Thickness	L=2.00 cc/sec	2.28	2.03	1.96	1.68
F cm x 10^2	L=3.00 cc/sec	2.56	2.28	2.21	1.80

0.50 g/l Lissapol.

Latitude, θ^{o}		15	21	33	41	45
Thickness	L=2.00 cc/sec	3.61	3.08	2.44	2.24	2.06
F cm x 10^{2}	L=3.00 cc/sec	3.64	3.20	2.62	2.42	2.24

53	62	76	90	110
1.93	1.80	1.75	1.73	1.78
2.11	2.01	2.01	1.96	2.03

118	128	136	143	148
1.83	1.98	2.11	2.36	2.49
2.11	2.31	2.49	2.74	2.97

151	155
2.56	2.80
3.05	3.33

0.70 g/l Lissapol - L = 2.00 cc/sec.

Latitude, θ^{o}	11	21	28	38	50	60
Thickness, F cm x 10^{2}	4.55	3.38	2.90	2.36	2.06	1.91

70	89	103	118	127	144
1.75	1.68	1.75	1.78	1.86	2.23

150	155
2.44	2.59

1.00 g/l Lissapol.

Latitude θ^{o}		11	12	15	19	28
Thickness	L=2.00 cc/sec	5.33	4.75	4.52	3.76	2.95
F cm x 10^{2}	L=3.00 cc/sec	-	4.62	4.50	3.96	3.18

35	42	52	60	72
2.57	2.31	2.06	1.96	1.70
2.82	2.54	2.31	2.21	1.96

79	89	103	109	119
1.65	1.68	1.65	1.73	1.75
1.91	1.91	1.91	1.98	2.03

124	137	149	152	156
1.80	2.01	2.41	2.49	2.59
2.08	2.34	2.74	2.84	3.10

1.50 g/l Lissapol - L = 2.00 cc/sec.

Latitude, θ^{o}	13	19	28	34	39	47
Thickness, F cm x 10^{2}	5.28	4.24	3.20	2.64	2.54	2.24

53	61	70	78	89	102
1.98	1.85	1.65	1.52	1.55	1.57

114	120	131	135
1.60	1.68	1.83	1.85

2.00 g/l Lissapol.

Latitude, θ^{o}		12	22	26	31	40
Thickness	L=2.00 cc/sec	5.10	3.63	3.28	2.82	2.31
F cm x 10^2	L=3.00 cc/sec	5.46	4.09	3.70	3.18	2.62

46	54	59	63	73
2.11	1.93	1.83	1.78	1.65
2.38	2.16	2.11	2.06	1.93

82	90	99	105	110
1.55	1.50	1.52	1.45	1.55
1.83	1.75	1.78	1.73	1.80

116	121	129	137
1.57	1.62	1.75	1.93
1.85	1.90	2.01	2.21

3.00 g/l Lissapol - L = 2.00 cc/sec.

Latitude, θ^{o}	15	20	28	48	65	68
Thickness, F cm x 10^2	4.57	3.94	2.97	2.01	1.60	1.55

4.00 g/l Lissapol - L = 2.00 cc/sec.

Latitude, θ^{o}	24	40	50	56
Thickness, F cm x 10^2	3.25	2.08	1.80	1.70

TABLE XIV

Values of the Limits of the Region of Increased Film Thickness versus Lissapol Concentration.

Lissapol Concentration g/l	Point of Divergence		Point of Convergence	
	L = 2.00 cc/sec	L = 3.00 cc/sec	L = 2.00 cc/sec	L = 3.00 cc/sec
0.05	137	145	-	-
0.10	95	113	165	-
0.25	33	40	-	-
0.50	15	25	165	-
0.70	8	-	157	-
1.00	Entry	12	155	-
1.50	Entry	-	140	-
2.00	Entry	-	120	-
3.00	Entry	-	90	-
4.00	Entry	-	50	-

TABLE XV

Values of the Ratio α from Experimental Measurements of Film Thickness of Lissapol Solutions.

Angle θ^{o}	Values of					
	0.1 g/l	0.5 g/l	0.7 g/l	1.0 g/l	1.5 g/l	2.0 g/l
10	0.785	1.00	1.04	1.16	1.25	1.21
15	0.905	1.00	1.11	1.25	1.38	1.27
20	1.00	1.07	1.18	1.25	1.37	1.32
25	1.00	1.11	1.21	1.28	1.34	1.32
30	1.00	1.12	1.21	1.25	1.29	1.25
35	1.00	1.14	1.21	1.25	1.26	1.22
40	1.00	1.16	1.20	1.23	1.25	1.20
45	1.00	1.16	1.19	1.22	1.22	1.16
50	1.00	1.16	1.20	1.22	1.20	1.16
55	1.00	1.15	1.20	1.21	1.17	1.15
60	1.00	1.17	1.20	1.22	1.13	1.16
65	1.00	1.18	1.18	1.20	1.11	1.14
70	1.00	1.18	1.17	1.16	1.09	1.12
75	1.00	1.19	1.16	1.14	1.07	1.11
80	1.00	1.20	1.17	1.14	1.06	1.08
85	1.00	1.21	1.18	1.15	1.06	1.06
90	1.00	1.21	1.17	1.14	1.06	1.05
95	1.00	1.22	1.18	1.15	1.06	1.05
100	1.01	1.21	1.17	1.14	1.07	1.03
105	1.02	1.19	1.18	1.14	1.07	1.03
110	1.03	1.19	1.17	1.12	1.07	1.03
115	1.08	1.19	1.16	1.12	1.07	1.02
120	1.12	1.18	1.15	1.11	1.07	1.00
125	1.14	1.17	1.12	1.09	1.05	1.00
130	1.16	1.16	1.12	1.09	1.04	1.00
135	1.18	1.14	1.10	1.08	1.01	1.00
140	1.18	1.14	1.10	1.09	1.00	1.00
145	1.20	1.14	1.09	1.08	1.00	1.00
150	1.18	1.12	1.07	1.05	1.00	1.00
155	1.16	1.10	1.02	1.00	1.00	1.00
160	1.05	1.03	1.00	1.00	1.00	1.00
165	1.00	1.00	1.00	1.00	1.00	1.00

TABLE XVI

Values of Dynamic Surface Tension of Lissapol Solutions based on Experimental Values of α.

Angle θ°	Dynamic Surface Tension (dynes/cm)					
	0.1 g/l	0.5 g/l	0.7 g/l	1.0 g/l	1.5 g/l	2.0 g/l
10	72.0	72.0	71.9	71.6	71.5	71.4
15	72.0	72.0	71.5	70.7	70.1	70.3
20	72.0	71.8	70.7	69.4	68.3	68.8
25	72.0	71.2	69.6	68.0	66.5	67.1
30	72.0	70.5	68.3	66.4	64.7	65.5
35	72.0	69.6	67.0	64.9	63.1	64.0
40	72.0	68.6	65.6	63.3	61.5	62.6
45	72.0	67.4	64.3	61.8	59.9	61.4
50	72.0	66.3	62.9	60.3	58.4	60.2
55	72.0	65.1	61.4	58.7	57.0	59.1
60	72.0	63.9	60.0	57.1	55.9	57.9
65	72.0	62.5	58.5	55.6	54.9	56.7
70	72.0	61.1	57.1	54.2	54.1	55.6
75	72.0	59.7	55.8	53.0	53.4	54.7
80	72.0	58.1	54.5	51.8	52.8	53.9
85	72.0	56.5	53.1	50.6	52.3	53.3
90	72.0	54.9	51.7	49.5	51.8	52.8
95	72.0	53.2	50.3	48.3	51.3	52.3
100	72.0	51.6	48.9	47.1	50.7	52.0
105	71.8	50.0	47.5	45.9	50.1	51.7
110	71.6	48.5	46.2	44.9	49.5	51.4
115	71.1	47.1	44.9	43.9	48.9	51.2
120	70.3	45.7	43.6	43.0	48.3	51.1
125	69.3	44.3	42.6	42.2	47.8	51.1
130	68.2	43.1	41.7	41.5	47.4	51.1
135	66.9	42.0	40.8	40.8	47.2	51.1
140	65.7	41.0	40.1	40.2	47.2	51.1
145	64.4	40.0	39.4	39.5	47.2	51.1
150	63.2	39.1	38.8	39.1	47.2	51.1
155	62.1	38.4	38.5	38.9	47.2	51.1
160	61.5	38.0	38.4	38.9	47.2	51.1
165	61.3	37.9	38.4	38.9	47.2	51.1

TABLE XVII

Values of Time of Exposure of Lissapol Solutions based on Experimental Values of α.

Angle θ°	Values of Time of Exposure (sec)					
	0.1 g/l	0.5 g/l	0.7 g/l	1.0 g/l	1.5 g/l	2.0 g/l
5	0.01	0.01	0.01	0.01	0.01	0.01
10	0.03	0.03	0.03	0.03	0.04	0.04
15	0.05	0.05	0.05	0.07	0.10	0.08
20	0.07	0.08	0.09	0.12	0.17	0.13
25	0.10	0.11	0.13	0.17	0.24	0.20
30	0.13	0.15	0.18	0.22	0.31	0.26
35	0.16	0.19	0.23	0.28	0.37	0.31
40	0.19	0.23	0.28	0.34	0.43	0.36
45	0.23	0.28	0.33	0.39	0.49	0.41
50	0.26	0.33	0.38	0.45	0.54	0.46
55	0.29	0.37	0.44	0.51	0.59	0.51
60	0.33	0.43	0.49	0.56	0.64	0.56
65	0.37	0.48	0.55	0.62	0.69	0.61
70	0.40	0.53	0.60	0.68	0.73	0.65
75	0.44	0.59	0.66	0.73	0.78	0.70
80	0.48	0.65	0.71	0.78	0.82	0.75
85	0.51	0.71	0.77	0.83	0.86	0.79
90	0.55	0.77	0.82	0.88	0.90	0.83
95	0.59	0.83	0.88	0.93	0.95	0.87
100	0.63	0.89	0.93	0.98	0.99	0.91
105	0.66	0.95	0.99	1.03	1.03	0.95
110	0.70	1.01	1.04	1.08	1.07	0.99
115	0.74	1.06	1.09	1.13	1.12	1.03
120	0.79	1.12	1.15	1.18	1.16	1.07
125	0.83	1.17	1.19	1.22	1.20	1.10
130	0.88	1.22	1.24	1.26	1.24	1.14
135	0.93	1.27	1.28	1.30	1.27	1.17
140	0.98	1.31	1.32	1.34	1.31	1.20
145	1.03	1.36	1.36	1.38	1.34	1224
150	1.08	1.40	1.40	1.41	1.37	1.27
155	1.12	1.43	1.43	1.44	1.40	1.30
160	1.15	1.46	1.45	1.47	1.42	1.32
165	1.18	1.49	1.48	1.50	1.45	1.35
170	1.20	1.51	1.50	1.52	1.47	1.37
175	1.22	1.53	1.52	1.54	1.49	1.39

NOMENCLATURE

		Units
A and B	Constants of integration.	-
a	$\alpha^4 - \alpha$	-
C	Concentration of gas in liquid	mg/cc
C_i	Interfacial concentration	mg/cc
C	Saturation concentration (normally $C_i = C$)	mg/cc
C_o	Concentration in liquid at inlet	mg/cc
D	Diffusivity of gas in liquid	cm^2/sec
e	Time of exposure of gas to liquid	sec
F	Film thickness	cm
F_1	Equatorial film thickness	cm
F^1	Film thickness in stagnant zone	cm
f	Film thickness of a retarded film	cm
G	Gas Absorption Rate	mg/sec
G_a	Corrected experimental absorption rate	mg/sec
G_m	Experimentally measured absorption rate	mg/sec
G_n	Absorption rate of a normal film	mg/sec
G_r	Absorption rate of a retarded film	mg/sec
G_s	Absorption rate of a film with a stagnant layer	mg/sec
G_t	Total absorption rate of a film with a stagnant layer end effect	mg/sec
$G_{t.o.}$	Absorption rate of the liquid on the take-off tube	mg/sec
g	Acceleration due to gravity	cm/sec^2
h	Height of a wetted-wall column	cm
I	Integral of Sin θ	-
K	Constant of proportionality between G and $L^{\frac{1}{3}}$	mg/cm $sec^{\frac{2}{3}}$
k_s	Interface mass transfer coefficient (i.e. $1/k_s$ = Interfacial resistance)	cm/sec
L	Liquid flow rate	cc/sec
l	Length of take-off tube below the sphere	cm
P	Temperature correction factor	-
p	Series variable - defined with the series	-
Q	Atmospheric Pressure	m.m. Hg

Q_i	Pressure of gas at inlet meter	m.m. Hg
Q_o	Pressure of gas at outlet meter	m.m. Hg
q	Saturated water vapour pressure at atmospheric conditions	m.m. Hg
q_i	Saturated water vapour pressure at inlet meter	mm. Hg
q_o	Saturated water vapour pressure at outlet meter	m.m. Hg
R	Radius of sphere	cm.
r	Radius of wetted-wall column	cm.
S	Viscous shear	dynes/cm^2
s	Surface tension	dynes/cm
s_1	Surface tension above stagnant layer	dynes/cm
s_2	Surface tension of stagnant layer	dynes/cm
T	Temperature	^oK
T_i	Temperature of inlet meter jacket	^oK
T_o	Temperature of outlet meter jacket	^oK
t	Time for 50 mls of travel of soap film on outlet meter	sec
U	$\alpha - \frac{\alpha^4}{4}$	
u	Velocity of liquid in film	cm/sec
u_i	Interfacial velocity of a normal film	cm/sec
u_{i1}	Interfacial velocity of a normal film at the equator of the sphere	cm/sec
V_i	Inlet volume rate of gas	cc/sec
V_o	Outlet volume rate of gas	cc/sec
v	Interfacial velocity of a retarded film	cm/sec
x	Distance into film from liquid surface	cm
y	Ratio of x/F or x/f	-
z	Distance into film from solid surface	cm
α	Ratio f/F	-
β	Ratio v/u_i	-
η	Angle subtended by stagnant layer	Radians or degrees
θ	Latitude on sphere	Radians or degrees
θ_1 and θ_2	Limits of latitude on the sphere	Radians or degrees
θ_s	Latitude at which stagnant layer begins	Radians or degrees

μ	Liquid viscosity	gm/cm.sec
ρ	Liquid density	gm/cc
ϕ	A function of θ, defined where used	cm/sec^2

BIBLIOGRAPHY

(1)	Addison, C.C.	J. Chem. Soc. (1945) 103
(2)	Addison, C.C.	J. Chem. Soc. (1943) 535 (1944) 252, 477 (1945) 98,354
(3)	Beek, W.J. and Bakker, C.A.P.	App. Sci. Research Sect. A. Vol. X (1961) 241
(4)	Benjamin, T.B.	J. Fluid Mechs. 2(1957) 554
(5)	Binnie, A.M.	J. Fluid Mechs. 2(1957) 551
(6)	Brotz. W.	Chem. - Ing. - Tech. 26(1954) 470
(7)	Burcik, E.J.	J. Colloid Sci. 5(1950) 421 8(1953) 520
(8)	Burcick, E.J. and Newman, R.C.	J. Colloid Sci. 9(1954) 498
(9)	Burcik, E.J. and Vaughn, C.R.	J. Colloid Sci. 6(1951) 522
(10)	Chiang, S.H. and Toor, H.L.	Amer. Instn. Chem. Engrs. J 5(1959) 165
(11)	Cooper, C.M., Drew, T.B. and MacAdams, W.H.	Industr. Engng. Chem. 26(1934) 428
(12)	Cullen, E.J. and Davidson, J.F.	Chem. Engng. Sci. 6(1956) 49
(13)	Cullen, E.J. and Davidson, J.F.	Trans. Farady Soc. 53(1957) 113
(14)	Danckwerts, P.V. and Kennedy, A.M.	Trans. Instn. Chem. Engrs. Lond. 32(1954) S.53
(15)	Davidson, J.F. and Cullen, E.J.	Trans. Instn. Chem. Engrs. Lond. 35(1957) 51
(16)	Davidson, J.F., Cullen, E.J., Hanson, D. and Roberts, D.	Trans. Instn. Chem. Engrs. Lond. 37(1959) 122
(17)	Davies, J.T.	Trans. Instn. Chem. Engrs. Lond. 38(1960) 289.
(18)	Defay, R. and Hommeln, J.R.	J. Colloid Sci. 13(1958) 553
(19)	Defay, R. and Hommeln, J.R.	J. Colloid Sci. 14(1959) 411
(20)	Defay, R. and Hommeln, J.R.	J. Colloid Sci. 14(1959) 401
(21)	Dukler, A.E. and Bergelin, O.P.	Chem. Engng. Progr. 48(1952) 557
(22)	Emmert, R.E. and Pigford, R.L.	Chem. Engng. Progr. 50(1954) 87
(23)	Frumkin, A. and Levich, V.	J. Phys. Chem. U.S.S.R. 21(1947) 1183
(24)	Friedman, S.J. and Miller, C.O.	Indstr. Engng. Chem. 33(1941) 885

(25)	Garner, F.H. and Skelland, A.H.P.	Indstr. Engng. Chem. 48(1956) 51
(26)	Gibbons, J.H., Houghton, G. and Coull, J.	Amer. Instn. Chem. Engrs. J. 8(1962) 274
(27)	Grimley, S.S.	Trans. Instn. Chem. Engrs. London 23(1945) 228
(28)	"Handbookoof Chemistry and Physics"	1955-56, 37th Ed. (Cleveland, Ohio Chemical Rubber Publishing Co.)
(29)	Hansen, R.S.	J. Phys. Chem. 62(1958) 210
(30)	Hansen, R.S. and Wallace, T.C.	J. Phys. Chem. 63(1959) 1085
(31)	Harvey, E.A. and Smith, W.	Chem. Enging. Sci. 10(1959) 274
(32)	Higbie, R.	Trans. Amer. Inst. Chem. Engrs. XXXI(1935) 365
(33)	Jackson, M.L.	Amer. Instn. Chem. Engrs. J 1(1955) 231
(34)	Kirkbride, C.G.	Indstr. Engng. Chem. 26(1934) 425
(35)	Kuffner, R.J.	J. Colloid Sci. 16(1961) 497
(36)	Lynn, S., Straatemeier, J.R. and Kramers, H.	Chem. Engng. Sci. 4(1955) 58
(37)	Lynn, S., Straatemeier, J.R. and Kramers, H.	Chem. Engng. Sci. 4(1955) 63
(38)	Moilliet, J.L. Collie, B. and Black, W.	"Surface Activity" 1961 2nd Ed. 113-133 (London E. and F.N. Spon Ltd.)
(39)	Moll, C.A. and Polsky, J.W.	Tech. Pap. Pulp. Pab. Ind. New York 39(1956) 51
(40)	Nusselt, W.	Z ver Deut. Ing. 60(1961) 541, 569
(41)	Padday, J.F. and Russel, D.R.	J. Colloid Sci. 15(1960) 503
(42)	Perry, J.H. (Ed)	"Chemical Engineers Handbook" 1950, 3rd Ed. (London - McGraw - Hill Book Co. Inc.)
(43)	Raimondi, P. and Toor, H.L.	Amer. Instn. Chem. Engrs. J. 5(1959) 86
(44)	Ratcliffe, G.A. and Reid, K.J.	Trans. Instn. Chem. Engrs. Lond. 39(1961) 423
(45)	Rideal, E.K. and Sutherland, K.L.	Trans. Farady Soc. 48(1952) 1109.
(46)	Scriven, L.E. and Pigford, R.L.	Amer. Instn. Chem. Engrs. J. 4(1958) 439
(47)	Stephens, E.J. and Morris, G.A.	Chem. Engng. Progr. 47(1951) 232

(48)	Tailby, S.R. and Portalski, S.	Trans. Instn. Chem. Engrs. Lond. 38(1960) 324
(49)	Ternovskaya, A.N. and Belopolskii, A.P.	J. Phys. Chem. U.S.S.R. 24(1950) 43-57, 981-7, 26(1952) 1090-6, 1097-1102.
(50)	Vivian, J.E. and Peaceman, D.W.	Amer. Instn. Chem. Engrs.J. 2(1956) 437
(51)	Ward, A.F.H. and Tordai, L.	J. Chem. Phys. 14(1946) 453
(52)	Wilkie, C.R.	Chem. Engng. Progr. 45(1949) 218.
